Radius Bending: User Element Testing and Investigation on Effect of Stacking Sequence on Out-of-plane Failure

- MSc. Thesis -

J.J. van der Meijs

A new doubly-curved shell element (ThickS4 element) is presented and tested for flat and singly curved configurations. The benchmark tests show good correlation for the ThickS4 element with the Abaqus S4 shell element and with 3D FEM for flat and highly curved configurations ($R/t \geq 4$). For radius over thickness ratios smaller than 4 the element is not able to predict the correct behaviour. In order to give a good insight in the most critical radius over thickness ratios $1 \leq R/t \geq 8$ a stacking sequence investigation has been done making use of the Abaqus C3D8 element. An L-shaped structure has been tested for different load combinations of in-plane, out-plane and opening-moment loading. From the investigation a clear overview of best stacking sequences for all the different loading combinations were presented as well as the ratio of ILNS versus ILSS. The results can further be used as guidelines for the initial design of composite C-spars and stringers.

August 5, 2016

TU Delft INTALES

Radius Bending: User Element Testing and Investigation on Effect of Stacking Sequence on Out-of-plane Failure

- MSc. Thesis -

by

J.J. van der Meijs

to obtain the degree of Master of Science
at the Delft University of Technology,
to be defended publicly on Tuesday August 5, 2016 at 14:00 AM.

Student number:	4089146	
Project duration:	April 1, 2015 – August 5, 2016	
Thesis committee:	Dr. ir. M.O. Abdalla,	TU Delft, supervisor
	Dr. ir. C. Kassapoglou,	TU Delft
	Dr. ir. O.K. Bergsma,	TU Delft

This thesis is confidential and cannot be made public until August 5, 2026.

TU Delft INTALES

Preface

First of all I would like to thank Dr. Herbert Haller, Dipl.-Ing. and Hermann-Josef Starmans, Dipl.-Ing. from the company Intales GmbH Engeneering Solutions for giving me the opportunity to write this Master Thesis in collaboration with them. Furthermore I would like to thank them for the possibility to use their facilities in the time of the contract as well as when the contract had ended. Lastly I would like to thank them as well as the employees from Intales for the great time they have given me, at the company itself.

Secondly I would like to thank Dr. Robert G. Winkler, Dipl.-Ing. of the University of Innsbruck for helping out with the understanding of the Abaqus USER-element and for writing the element in the first place. I would also like to thank Dr. Mostafa Abdalla, MSc from Delft University of Technology for being my supervisor and giving feedback and steering where necessary.

Lastly I would like to thank M. Schmeetz for the mental support and helpful discussions throughout the entire thesis as well as my parents for the support during my stay abroad as well as during the study time in Delft.

J.J. van der Meijs
Delft, August 2016

Nomenclature

Abbreviations

Symbol	Description
2D	Two-dimensional
3D	Three-dimensional
CFRP	Carbon Fiber Reinforced Polymers
CLPT	Classical Laminated Plate Theory
FEM	Finite Element Method
GA	Genetic Algorithm
ILNS	Interlaminar Normal Stress
ILSS	Interlaminar Shear Stress
UEL	USER-element

Greek Symbols

Symbol	Description	Units
$[\alpha]$	inverse of the laminate A-matrix	[m/N]
$[\beta]$	inverse of the laminate B-matrix	[m/(N·m)]
β	anisotropic parameter	[–]
γ	shear strain	[–]
$[\delta]$	inverse of the laminate D-matrix	[m/(N·m^2)]
ε	normal strain	[–]
κ	curvatures	[m^{-1}]
ν	Poisson's ratio	[–]
ρ	radii ratio	[–]
σ	normal stress	[N/m^2]
τ	shear stress	[N/m^2]
θ	angular coordinate	[rad]
ϕ	angle between the local ply x-axis and global laminate 1-axis	[°]
ξ	element curved direction	[–]
ζ	transverse coordinate	[mm]

Roman Symbols

Symbol	Description	Units
$[A]$	laminate A-matrix	[N/m]
$[a]$	inverse of the laminate A-matrix for a symmetric and balanced laminate	[m/N]
a	natural element coordinate system at mid-plane	[mm]
a	inner radius	[m]
A', B', C', D'	arbitrary constants multilayer theory end force	[–]
A, B, C, D	arbitrary constants multilayer theory end force	[–]
$[B]$	laminate B-matrix	[N/m]
$[b]$	inverse of the laminate B-matrix for a symmetric and balanced laminate	[m/(N·m)]
b	outer radius	[m]
co	transformation vector	[–]
$[D]$	laminate D-matrix	[N/m]
$[d]$	inverse of the laminate D-matrix for a symmetric and balanced laminate	[m/(N·m^2)]
E	Young's modulus	[N/m^2]
e	error	[–]
f	failure mode function	[–]
F_i	fitness function	[–]
F_{ij}	ply failure stresses with (i, j = 1,2,3)	[MPa]
g	natural element coordinate system	[mm]
G	shear stiffness	[N/m^2]
H	shape functions	[–]
h	laminate thickness	[m]
k	anisotropic parameter	[–]
l	length of flat part	[mm]
M	resultant moment	[N·m/m]
n	vector with the element normal directions	[–]
N	resultant force	[N/m]
n_i	number of occurrences in roulette	[–]
N_{rate}	convergence rate	[–]
N_{tot}	total number	[–]
P	applied force	[N]
p	penalty for fitness function	[–]
Q_{ij}	stiffnesses in the local (ply) (x, y, s) coordinate system and global coordinate system (i, j = 1,2,6)	[N/m^2]

R	radius at mid-plane[m]	
r	radial coordinate	[m]
RF	reserve factor	[–]
S_{ij}	stress over failure stress ratio	[–]
t	Cartesian coordinate system	[mm]
t	thickness	[m]
tg	correction factor	[–]
u, v, w	global displacements in the x-, y- and z-direction respectively	[m]
V	transformation vector	[–]
w	width of beam/laminate	[m]
w_i	weight of individual	[–]
x	vector with the element coordinates	[mm]
x, y, z	global laminate/sandwich coordinate directions	

Subscripts

Symbol	Description
$(\,)_0$	properties at the mid-plane
$(\,)_{1,2,3}$	global laminate coordinates
$(\,)_3$	element normal direction
$(\,)_\alpha$	element directions, either 1 or 2
$(\,)_{avg}$	average
$(\,)_b$	element coordinates are curvilinear
$(\,)_c$	stress in compression
$(\,)_i$	individual of generation
$(\,)_{ISO}$	element coordinates are isoparametric
$(\,)_k$	ply counter
$(\,)_L$	longitudinal direction
$(\,)_r$	global laminate radial coordinate
$(\,)_t$	stress in tension
$(\,)_\theta$	global laminate angular coordinate
$(\,)_T$	transverse direction
$(\,)_{x,y,z}$	local (ply) coordinate directions or global laminate coordinates

Contents

1 Introduction **1**

2 Description of Laminate Theories and User Element **3**
2.1 Classical Laminated Plate Theory . . . 3
2.2 Analytical Curved Beam Solutions . . . 7
2.2.1 Lekhnitskii . . . 7
2.2.2 Multilayer Theory . . . 8
2.3 ThickS4 User Element Description . . . 13
2.3.1 Input . . . 15
2.3.2 Output . . . 15

3 Benchmark Tests for ThickS4 UEL Validation **17**
3.1 Descriptions of Benchmark Models . . . 17
3.1.1 Cantilever Beam Subjected to an End Load . . . 17
3.1.2 Curved Beam Subjected to End Load & End Moment . . . 19
3.2 Benchmark Test Results . . . 22
3.2.1 Cantilever Beam . . . 22
3.2.2 Lekhnitskii End Load . . . 24
3.2.3 Lekhnitskii End Moment . . . 30
3.2.4 Multilayer Theory . . . 33
3.3 Conclusions on Performance and Working Range of ThickS4 UEL . . . 47
3.3.1 Seperate Conclusions . . . 47
3.3.2 Final conclusion . . . 48

4 Genetic Algorithms **49**
4.1 Permutation Algorithms . . . 49
4.1.1 Permutation Algorithm Literature . . . 49
4.1.2 New Permutation Algorithm . . . 52
4.1.3 Fitness Function . . . 53
4.1.4 Comparison and Selection . . . 53
4.2 Standard Genetic Algorithm . . . 55
4.2.1 Crossover . . . 55
4.2.2 Mutation . . . 56
4.2.3 Fitness Function . . . 56
4.2.4 Parameter Selection . . . 57

5 Design Space Exploration **59**
5.1 FEM-Model . . . 59
5.2 Mesh Used . . . 61
5.3 Results Extraction . . . 61
5.4 Optimisation Setup . . . 62
5.5 Optimisation Results . . . 64
5.5.1 Permutation Algorithm Results . . . 64
5.5.2 Standard Genetic Algorithm Results . . . 68
5.5.3 Shear Stress Versus Normal Stress . . . 71
5.6 Concluding Remarks . . . 73

6 Conclusions and Recommendations **75**
6.1 Element Validation . . . 75
6.2 Stacking Sequence Investigation . . . 75

A Excel Input Sheet **77**

B Matrix Equations for Boundary Conditions for Multilayer Theory **79**

C Optimisation Distribution **81**
C.1 Asymmetric 81
C.2 Symmetric 83

D Optimum Layup Combined Loading **85**

Bibliography **87**

1 Introduction

In many industrial fields conventional materials such as metals are replaced with light-weight materials such as composite materials. The most important material used in these fields are the carbon-fiber reinforce polymers (CFRP) due to their high specific strength and the ability to tweak the properties of the material to the desired need.

In industrial projects such as projects in the aerospace industry finite element method (FEM) calculations are widely used. For such calculations lots of different elements can be used depending on what application. However two-dimensional (2D) shell elements are used by the company Intales GmbH and Airbus to reduce the computing costs.

In these industrial projects, one could imagine that not all structures are simple shapes as flat plates. In many of these projects, curved structures are used. These curvatures in the structure lead to out-of-plane stresses also known as interlaminar stresses [15]. In the conventional shell element formulations (Kirchoff-Love [9] or Mindlin-Reissner [11, 13]), the stress state is underestimated when analysing these curved structures with a geometry ratio of radius over thickness smaller than 100 (R/t<100). Despite the fact that the through the thickness stresses are usually at least one order of magnitude lower than the in-plane stresses, they are of crucial meaning for composite materials as the allowables for out-of-plane stresses are also at least one order of magnitude lower [10, 14].

In addition, a conventional shell element does not have a full three-dimensional (3D) stress state, which means that it can only determine the in-plane stresses. As told before, these out-of-plane stresses are of crucial meaning for composites, especially the interlaminar normal stresses (ILNS), also known as σ_{33} and the interlaminar shear stresses (ILSS), as these stresses lead to delaminations in the laminate, which effects the bending, buckling and vibration behaviour of the structure [14]. Though a 3D solid element analysis bypasses this drawback, these analyses are highly time consuming and thus expensive in big industrial projects.

For this reason a curved shell element has already been formulated [2] and translated to an USER-element in the Abaqus vicinity, called the ThickS4 USER-element. This element enables the user to get a full set of the 3D stress state.

The purpose of this thesis is to investigate the non-linear distributed stress over the laminate thickness in these highly curved structures. This will be done by first validating the in-house formulated Abaqus user-element written by Intales by comparing it to various analytical solutions and comparing the solution of the ThickS4 element with the solution of S4 Abaqus elements, of C3D8 Abaqus elements and of C3D27 Abaqus elements. The configurations for which the element is tested are a cantilever beam subjected to an end load and a curved beam subjected to an end moment or an end load. Only singly curved structures are compared as the doubly-curved models took too much effort to implement.

After the element has been validated a stacking sequence investigation will be designed in order to find a relation between the stacking sequence and the out-of-plane stress distribution over the thickness of the laminate. In this investigation the Abaqus C3D8 element is used in order to make sure that the results of the investigation are useful. The investigation is done for three different separate loading cases, being an in-plane force, an out-of-plane force and an applied moment as well as for combinations of these loading cases and doing optimisations for each of these loading cases.

Theories needed in order to be able to validate the in-house formulated Abaqus USER-element as well as a description of the element itself are given in chapter 2. This is followed by the actual validation of the

element itself in chapter 3 in which the tests itself are described, the results and a small conclusion regarding the element is given. With the knowledge of the performance of the ThickS4 element, a selection is made with what element the next phase will be done.

The second part of the thesis starts with the description of the different optimisers used in chapter 4 and is followed by the the description and results of the optimisation problem in chapter 5. The thesis is finalized by the conclusions and recommendations in chapter 6.

2

Description of Laminate Theories and User Element

This chapter discussed the laminate theories used and the analytical solutions used to validate the element. The selection of the laminate theory and the analytical solution follow from the literature survey done for this project. From the literature survey it followed that the classical laminated plate theory (CLPT) solution is enough to compare a simple flat structure to, as the ThickS4 element does not have a solution for the interlaminar stresses if there is no curvature present. Furthermore it was decided to only take singly curved structures into account as this simplifies the problem at hand and as the main highly curvatures found in the current aircraft design are singly curved. The chapter is finalised by a description of the ThickS4 user element.

2.1. Classical Laminated Plate Theory

This section is a review of the CLPT [5], which is partly needed for analytical solutions explained in subsection 2.2.2.

The equations for plain stress in matrix are the following

$$\begin{bmatrix} \sigma_{xx} \\ \sigma_{yy} \\ \tau_{xy} \end{bmatrix} = \begin{bmatrix} Q_{xx} & Q_{xy} & 0 \\ Q_{xy} & Q_{yy} & 0 \\ 0 & 0 & Q_{ss} \end{bmatrix} \begin{bmatrix} \varepsilon_x \\ \varepsilon_y \\ \gamma_{xy} \end{bmatrix}, \tag{2.1}$$

where σ_x, σ_y and τ_{xy} are the in-plane stresses, Q_{xx}, Q_{yy}, Q_{xy} and Q_{ss} are the stiffnesses and ε_x, ε_y and γ_{xy} are the in-plane strains. All variables are in the local ply coordinate system.

The stiffness are defined using the material properties as

$$Q_{xx} = \frac{E_L}{1 - \nu_{LT}\nu_{TL}}; \tag{2.2a}$$

$$Q_{yy} = \frac{E_T}{1 - \nu_{LT}\nu_{TL}}; \tag{2.2b}$$

$$Q_{xy} = \frac{\nu_{LT}E_T}{1 - \nu_{LT}\nu_{TL}} = \frac{\nu_{TL}E_T}{1 - \nu_{LT}\nu_{TL}}; \tag{2.2c}$$

$$Q_{ss} = G_{LT}, \tag{2.2d}$$

where E_L and E_T are the Young's moduli, ν_{LT} and ν_{TL} are the Poisson's ratios, and G_{LT} is the in-plane shear stiffness.

However in most cases not all plies are aligned in the main direction, therefore plies under an angle are defined in the following manner.

$$\begin{bmatrix} \sigma_{11} \\ \sigma_{22} \\ \tau_{12} \end{bmatrix}_k = \begin{bmatrix} Q_{11} & Q_{12} & Q_{16} \\ Q_{12} & Q_{22} & Q_{26} \\ Q_{16} & Q_{26} & Q_{66} \end{bmatrix}_k \begin{bmatrix} \varepsilon_{11} \\ \varepsilon_{22} \\ \gamma_{12} \end{bmatrix}, \tag{2.3}$$

where σ_{11}, σ_{22} and τ_{12} are the in-plane stresses, Q_{ij} are the transformed stiffnesses and ε_{11}, ε_{22} and γ_{12} are the in-plane strains in the global laminate coordinate system.

The stiffnesses in Equation (2.3) are transformed from the local ply coordinate system to the global laminate/sandwich coordinate system over an angle θ using

$$Q_{11} = m^4 Q_{xx} + 2m^2 n^2 \left(Q_{xy} + 2Q_{ss}\right) + n^4 Q_{yy}; \tag{2.4a}$$

$$Q_{22} = n^4 Q_{xx} + 2m^2 n^2 \left(Q_{xy} + 2Q_{ss}\right) + m^4 Q_{yy}; \tag{2.4b}$$

$$Q_{12} = m^2 n^2 \left(Q_{xx} + Q_{yy} - 4Q_{ss}\right) + \left(m^4 + n^4\right) Q_{xy}; \tag{2.4c}$$

$$Q_{16} = m^3 n \left(Q_{xx} - Q_{xy}\right) + mn^3 \left(Q_{xy} - Q_{yy}\right) - 2mn\left(m^2 - n^2\right) Q_{ss}; \tag{2.4d}$$

$$Q_{26} = mn^3 \left(Q_{xx} - Q_{xy}\right) + m^3 n \left(Q_{xy} - Q_{yy}\right) + 2mn\left(m^2 - n^2\right) Q_{ss}; \tag{2.4e}$$

$$Q_{66} = m^2 n^2 \left(Q_{xx} + Q_{yy} - 2Q_{xy} - 2Q_{ss}\right) + \left(m^4 - n^4\right) Q_{ss}, \tag{2.4f}$$

where $m = \cos(\phi)$ and $n = \sin(\phi)$.

When the stresses are integrated over the thickness of the laminate, the force and moment resultants are retrieved. The theory assumes that stresses are continuous within a ply, but can jump when going from ply to ply. This means that the force and moment resultants can be summed over all the plies in order to get the total resultants. The stresses are given in the laminate coordinate system

$$\begin{bmatrix} N_x \\ N_y \\ N_{xy} \end{bmatrix} = \int_{-h/2}^{h/2} \begin{bmatrix} \sigma_{11} \\ \sigma_{22} \\ \tau_{12} \end{bmatrix} dz = \sum_{k=1}^{N} \int_{z_{k-1}}^{z_k} \begin{bmatrix} \sigma_{11} \\ \sigma_{22} \\ \tau_{12} \end{bmatrix}_k dz; \tag{2.5a}$$

$$\begin{bmatrix} M_x \\ M_y \\ M_{xy} \end{bmatrix} = \int_{-h/2}^{h/2} \begin{bmatrix} \sigma_{11} \\ \sigma_{22} \\ \tau_{12} \end{bmatrix} z\, dz = \sum_{k=1}^{N} \int_{z_{k-1}}^{z_k} \begin{bmatrix} \sigma_{11} \\ \sigma_{22} \\ \tau_{12} \end{bmatrix}_k z\, dz, \tag{2.5b}$$

where N_x, N_y and N_{xy} are the resultant forces and M_x, M_y and M_{xy} are the resultant moments in the global laminate coordinate system, h is the laminate thickness, z is the through thickness coordinate, and z_{k-1} and z_k are through thickness coordinates at the bottom and top of ply k respectively.

Combining Equation (2.5a) with Equation (2.3) therefore yields the following equations.

$$\begin{bmatrix} N_x \\ N_y \\ N_{xy} \end{bmatrix} = \sum_{k=1}^{N} \int_{z_{k-1}}^{z_k} \begin{bmatrix} Q_{11} & Q_{12} & Q_{16} \\ Q_{12} & Q_{22} & Q_{26} \\ Q_{16} & Q_{26} & Q_{66} \end{bmatrix}_k \begin{bmatrix} \varepsilon_{11} \\ \varepsilon_{22} \\ \gamma_{12} \end{bmatrix} dz \tag{2.6}$$

In the standard plate theory it is assumed that strains vary linearly through the thickness

$$\varepsilon_{11} = \varepsilon_{11_0} - \frac{\partial^2 w}{\partial x^2} z = \varepsilon_{11_0} + z\kappa_{11}; \tag{2.7a}$$

$$\varepsilon_{22} = \varepsilon_{22_0} - \frac{\partial^2 w}{\partial y^2} z = \varepsilon_{22_0} + z\kappa_{22}; \tag{2.7b}$$

$$\gamma_{12} = \gamma_{12_0} - 2\frac{\partial^2 w}{\partial x \partial y} z = \gamma_{12_0} + z\kappa_{12}, \tag{2.7c}$$

where ε_{11_0}, ε_{22_0} and γ_{12_0} are the in-plane strains at the mid-plane, κ_{11}, κ_{22} and κ_{12} are the curvatures at the mid-plane, and w is the displacement in the z-direction of the global laminate coordinate system.

Substituting Equation (2.7) into Equation (2.6) yields the following

$$\begin{aligned} \begin{bmatrix} N_x \\ N_y \\ N_{xy} \end{bmatrix} &= \sum_{k=1}^{N} \int_{z_{k-1}}^{z_k} \begin{bmatrix} Q_{11} & Q_{12} & Q_{16} \\ Q_{12} & Q_{22} & Q_{26} \\ Q_{16} & Q_{26} & Q_{66} \end{bmatrix}_k \begin{bmatrix} \varepsilon_{11_0} + z\kappa_{11} \\ \varepsilon_{22_0} + z\kappa_{22} \\ \gamma_{12_0} + z\kappa_{12} \end{bmatrix} \\ &= \begin{bmatrix} A_{11} & A_{12} & A_{16} \\ A_{12} & A_{22} & A_{26} \\ A_{16} & A_{26} & A_{66} \end{bmatrix} \begin{bmatrix} \varepsilon_{11_0} \\ \varepsilon_{22_0} \\ \gamma_{12_0} \end{bmatrix} + \begin{bmatrix} B_{11} & B_{12} & B_{16} \\ B_{12} & B_{22} & B_{26} \\ B_{16} & B_{26} & B_{66} \end{bmatrix} \begin{bmatrix} \kappa_{11} \\ \kappa_{22} \\ \kappa_{12} \end{bmatrix}, \end{aligned} \tag{2.8}$$

where

$$A_{ij} = \sum_{k=1}^{N} \left(Q_{ij}\right)_k (z_k - z_{k-1}) \tag{2.9}$$

and

$$B_{ij} = \sum_{k=1}^{N} \left(Q_{ij}\right)_k \frac{z_k^2 - z_{k-1}^2}{2} \tag{2.10}$$

In a similar fashion, the equations for the resulting bending moment can be changed into

$$\begin{aligned} \begin{bmatrix} M_x \\ M_y \\ M_{xy} \end{bmatrix} &= \sum_{k=1}^{N} \int_{z_{k-1}}^{z_k} \begin{bmatrix} Q_{11} & Q_{12} & Q_{16} \\ Q_{12} & Q_{22} & Q_{26} \\ Q_{16} & Q_{26} & Q_{66} \end{bmatrix}_k \begin{bmatrix} \varepsilon_{11_0} + z\kappa_{11} \\ \varepsilon_{22_0} + z\kappa_{22} \\ \gamma_{12_0} + z\kappa_{12} \end{bmatrix} z \, dz \\ &= \begin{bmatrix} B_{11} & B_{12} & B_{16} \\ B_{12} & B_{22} & B_{26} \\ B_{16} & B_{26} & B_{66} \end{bmatrix} \begin{bmatrix} \varepsilon_{11_0} \\ \varepsilon_{22_0} \\ \gamma_{12_0} \end{bmatrix} + \begin{bmatrix} D_{11} & D_{12} & D_{16} \\ D_{12} & D_{22} & D_{26} \\ D_{16} & D_{26} & D_{66} \end{bmatrix} \begin{bmatrix} \kappa_{11} \\ \kappa_{22} \\ \kappa_{12} \end{bmatrix}, \end{aligned} \tag{2.11}$$

where

$$D_{ij} = \sum_{k=1}^{N} \left(Q_{ij}\right)_k \frac{z_k^3 - z_{k-1}^3}{3} \tag{2.12}$$

Combining Equations (2.8) and (2.11) gives the full relation between resultant forces and moments, and strains and curvatures as

$$\begin{bmatrix} N_x \\ N_y \\ N_{xy} \\ M_x \\ M_y \\ M_{xy} \end{bmatrix} = \begin{bmatrix} A_{11} & A_{12} & A_{16} & B_{11} & B_{12} & B_{16} \\ A_{12} & A_{22} & A_{26} & B_{12} & B_{22} & B_{26} \\ A_{16} & A_{26} & A_{66} & B_{16} & B_{26} & B_{66} \\ B_{11} & B_{12} & B_{16} & D_{11} & D_{12} & D_{16} \\ B_{12} & B_{22} & B_{26} & D_{12} & D_{22} & D_{26} \\ B_{16} & B_{26} & B_{66} & D_{16} & D_{26} & D_{66} \end{bmatrix} \begin{bmatrix} \varepsilon_{11_0} \\ \varepsilon_{22_0} \\ \gamma_{12_0} \\ \kappa_{11} \\ \kappa_{22} \\ \kappa_{12} \end{bmatrix}. \tag{2.13}$$

In many cases a loads are given/known and strains and stresses need to be determined, this conversion from loads to strains is given by

$$\begin{bmatrix} \varepsilon_{11_0} \\ \varepsilon_{22_0} \\ \gamma_{12_0} \\ \kappa_{11} \\ \kappa_{22} \\ \kappa_{12} \end{bmatrix} = \begin{bmatrix} \alpha_{11} & \alpha_{12} & \alpha_{16} & \beta_{11} & \beta_{12} & \beta_{16} \\ \alpha_{12} & \alpha_{22} & \alpha_{26} & \beta_{12} & \beta_{22} & \beta_{26} \\ \alpha_{16} & \alpha_{26} & \alpha_{66} & \beta_{16} & \beta_{26} & \beta_{66} \\ \beta_{11} & \beta_{12} & \beta_{16} & \delta_{11} & \delta_{12} & \delta_{16} \\ \beta_{12} & \beta_{22} & \beta_{26} & \delta_{12} & \delta_{22} & \delta_{26} \\ \beta_{16} & \beta_{26} & \beta_{66} & \delta_{16} & \delta_{26} & \delta_{66} \end{bmatrix} \begin{bmatrix} N_x \\ N_y \\ N_{xy} \\ M_x \\ M_y \\ M_{xy} \end{bmatrix}. \tag{2.14}$$

The new defined matrices α, β and δ are determined by

$$[\alpha] = [A]^{-1} + [A]^{-1}[B]\left([D] - [B][A]^{-1}[B]\right)^{-1}[B][A]^{-1}; \tag{2.15a}$$

$$[\beta] = -[A][B]\left([D] - [B][A]^{-1}[B]\right)^{-1}; \tag{2.15b}$$

$$[\delta] = \left([D] - [B][A]^{-1}[B]\right)^{-1}. \tag{2.15c}$$

For a symmetric and balanced laminate the $[B]$-matrix and two of the components of the $[A]$-matrix, A_{16} and A_{26} are zero. Renaming the inverse of the $[A]$-matrix by $[a]$, the inverse of the $[D]$-matrix by $[d]$ and the inverse of the $[B]$-matrix by $[d]$ leads to the following.

$$[a] = [A]^{-1}; \tag{2.16a}$$

$$[b] = \mathbf{0}; \tag{2.16b}$$

$$[d] = [D]^{-1}, \tag{2.16c}$$

The conversion from the in-plane stresses to the resultant forces and the other way around are then given by

$$\begin{bmatrix} N_x \\ N_y \\ N_{xy} \end{bmatrix} = \begin{bmatrix} A_{11} & A_{12} & 0 \\ A_{12} & A_{22} & 0 \\ 0 & 0 & A_{66} \end{bmatrix} \begin{bmatrix} \varepsilon_{11_0} \\ \varepsilon_{22_0} \\ \gamma_{12_0} \end{bmatrix}; \tag{2.17a}$$

$$\begin{bmatrix} \varepsilon_{11_0} \\ \varepsilon_{22_0} \\ \gamma_{12_0} \end{bmatrix} = \begin{bmatrix} a_{11} & a_{12} & 0 \\ a_{12} & a_{22} & 0 \\ 0 & 0 & a_{66} \end{bmatrix} \begin{bmatrix} N_x \\ N_y \\ N_{xy} \end{bmatrix}, \tag{2.17b}$$

where its components are defined as

$$a_{11} = \frac{A_{22}}{A_{11}A_{22} - A_{12}^2}; \tag{2.18a}$$

$$a_{22} = \frac{A_{11}}{A_{11}A_{22} - A_{12}^2}; \tag{2.18b}$$

$$a_{12} = \frac{-A_{12}}{A_{11}A_{22} - A_{12}^2}; \tag{2.18c}$$

$$a_{66} = \frac{1}{A_{66}}. \tag{2.18d}$$

The resultant forces have units force per unit width, and are defined as

$$N_x = h\bar{\sigma}_{11}; \tag{2.19a}$$

$$N_y = h\bar{\sigma}_{22}; \tag{2.19b}$$

$$N_{xy} = h\bar{\tau}_{12}, \tag{2.19c}$$

where $\bar{\sigma}_{11}$, $\bar{\sigma}_{22}$ and $\bar{\tau}_{12}$ are the average stresses and h is the laminate thickness.

Substituting Equation (2.19) into Equation (2.17b) gives

$$\begin{bmatrix} \varepsilon_{11_0} \\ \varepsilon_{22_0} \\ \gamma_{12_0} \end{bmatrix} = h \begin{bmatrix} a_{11} & a_{12} & 0 \\ a_{12} & a_{22} & 0 \\ 0 & 0 & a_{66} \end{bmatrix} \begin{bmatrix} \bar{\sigma}_{11} \\ \bar{\sigma}_{22} \\ \bar{\tau}_{12} \end{bmatrix}, \tag{2.20}$$

which can be compared to the following stress-strain relations for an orthotropic homogeneous material under in-plane loading

$$\begin{bmatrix} \varepsilon_{11} \\ \varepsilon_{22} \\ \gamma_{12} \end{bmatrix} = h \begin{bmatrix} 1/E_{11} & -\nu_{12}/E_{11} & 0 \\ -\nu_{21}/E_{22} & 1/E_{22} & 0 \\ 0 & 0 & 1/G_{12} \end{bmatrix} \begin{bmatrix} \sigma_{11} \\ \sigma_{22} \\ \tau_{12} \end{bmatrix}. \tag{2.21}$$

Comparing Equation (2.20) to Equation (2.21) gives the relations for the effective engineering constants of the complete laminate as

$$E_{11} = \frac{1}{ha_{11}}; \tag{2.22a}$$

$$E_{22} = \frac{1}{ha_{22}}; \tag{2.22b}$$

$$\nu_{12} = \frac{-a_{12}}{a_{11}}; \tag{2.22c}$$

$$\nu_{21} = \frac{-a_{12}}{a_{22}}; \tag{2.22d}$$

$$G_{12} = \frac{1}{ha_{66}}. \tag{2.22e}$$

2.2. Analytical Curved Beam Solutions

This section describes the analytical solutions found for a singly curved beam. Two analytical solutions were found, one for a uni-direction plied laminate subjected to an end moment and end load as described by Lekhnitskii in [8]. The second is a multilayer theory which is able to handle different layups, also applied to a curved beam subjected to an end moment and end load as described by Ko and Jackson [6]. The analytical solution from Lekhnitskii is described in subsection 2.2.1 and the multilayer theory by Ko and Jackson is described in subsection 2.2.2.

2.2.1. Lekhnitskii

The lekhnitskii solution is the oldest solution for the problem of a singly curved beam. It defines an analytical solution for a curved beam subjected to an end moment, as described in subsubsection 2.2.1.1, as well as for a curved beam subjected to an end load, as described in subsubsection 2.2.1.2.

2.2.1.1. End Moment

The analytical solutions for a curved beam with unidirectional plies subjected to an end moment are given in Equations (2.23) to (2.25).

$$\sigma_r(r) = -\frac{M}{b^2 w g}\left[1 - \frac{1-\rho^{k+1}}{1-\rho^{2k}}\left(\frac{r}{b}\right)^{k-1} - \frac{1-\rho^{k-1}}{1-\rho^{2k}}\rho^{k+1}\left(\frac{b}{r}\right)^{k+1}\right] \tag{2.23}$$

$$\sigma_\theta(r) = -\frac{M}{b^2 w g}\left[1 - \frac{1-\rho^{k+1}}{1-\rho^{2k}}k\left(\frac{r}{b}\right)^{k-1} - \frac{1-\rho^{k-1}}{1-\rho^{2k}}\rho^{k+1}k\left(\frac{b}{r}\right)^{k+1}\right] \tag{2.24}$$

$$\tau_{r\theta} = 0 \tag{2.25}$$

where b outer radius of the curved beam, r is the radial coordinate, w is the width of the curved beam, M the applied moment on the curved beam, σ_r the radial stress, σ_θ the tangential stress and $\tau_{r\theta}$ the out-of-plane shear stress and

$$g = \frac{1-\rho^2}{2} - \frac{k}{k+1}\frac{\left(1-\rho^{k+1}\right)^2}{1-\rho^{2k}} + \frac{k\rho^2}{k-1}\frac{\left(1-\rho^{k-1}\right)^2}{1-\rho^{2k}}, \tag{2.26}$$

the anisotropic parameter k is

$$k = \sqrt{\frac{E_\theta}{E_r}} \tag{2.27}$$

and the ratio of the inner radius over the outer radius ρ as

$$\rho = \frac{a}{b} \tag{2.28}$$

furthermore a is inner radius of the curved beam.

2.2.1.2. End Force

The analytical solutions for a curved beam with unidirectional plies subjected to an end load are given in Equations (2.29) to (2.31).

$$\sigma_r(r,\theta) = \frac{P}{r w g_1}\left[\left(\frac{r}{b}\right)^\beta + \rho^\beta\left(\frac{b}{r}\right)^\beta - 1 - \rho^\beta\right]\sin\theta \tag{2.29}$$

$$\sigma_\theta(r,\theta) = \frac{P}{r w g_1}\left[(1+\beta)\left(\frac{r}{b}\right)^\beta + (1-\beta)\left(\frac{b}{r}\right)^\beta \rho^\beta - 1 - \rho^\beta\right]\sin\theta \tag{2.30}$$

$$\tau_{r\theta}(r,\theta) = \frac{P}{r w g_1}\left[\left(\frac{r}{b}\right)^\beta + \rho^\beta\left(\frac{b}{r}\right)^\beta - 1 - \rho^\beta\right]\cos\theta \tag{2.31}$$

where w width of the curved bar, r radial coordinate, θ tangential coordinate, σ_r radial stress, σ_θ tangential stress, $\tau_{r\theta}$ shear stress, and

$$g_1 = \frac{2}{\beta}\left[1-\rho^{\beta}\right] + \left[1+\rho^{\beta}\right]\ln\rho \tag{2.32}$$

and the anisotropic parameter β is defined as

$$\beta = \sqrt{1 + \frac{E_\theta}{E_r}(1-2\nu_{\theta r}) + \frac{E_\theta}{G_{\theta r}}} \tag{2.33}$$

where E_θ is modulus of elasticity in tangential direction, E_r modulus of elasticity in radial direction, $G_{\theta r}$ shear modulus, and $\nu_{\theta r}$ Poisson's ratio.

2.2.2. Multilayer Theory

The analytical solution described in this section is the solution as described by Ko and Jackson [6]. For bending a linearly elastic continuous curved bar with cylindrical anisotropy, the Airy stress function F, written in cylindrical coordinate system, takes on the following functional forms [8]

for end forces P

$$F = \left[Ar^{1+\beta} + Br^{1-\beta} + Cr + Dr\ln r\right]\sin\theta \tag{2.34}$$

for end moments M

$$F = A' + B'r^2 + C'r^{1+k} + D'r^{1-k} \tag{2.35}$$

where (A,B,C,D) and $\left(A',B',C',D'\right)$ are arbitrary constants that must be determined from the boundary conditions, r is the radial coordinate through the thickness and θ is the angle of how much the beam is curved. The two anisotropic β and k are defined as for the Lekhnitskii solutions by Equations (2.27) and (2.33) respectively and are for the case of an isotropic material, $\beta = 2$ and $k = 1$.

Stresses in the cylindrically anisotropic body may be expressed in terms of the stress function F as

$$\sigma_r = \frac{1}{r}\frac{\partial F}{\partial r} + \frac{1}{r^2}\frac{\partial^2 F}{\partial\theta^2} \tag{2.36}$$

$$\sigma_\theta = -\frac{\partial^2 F}{\partial r^2} \tag{2.37}$$

$$\tau_{r\theta} = -\frac{\partial^2}{\partial r\partial\theta}\left(\frac{F}{r}\right) \tag{2.38}$$

where σ_r is the normal stress in radial direction, σ_θ the normal stress in tangential direction and $\tau_{r\theta}$ the out-of-plane shear stress. The stress-strain relationships for the plane stress case are given by

$$\varepsilon_r = \frac{1}{\sigma_r}\sigma_r - \frac{\nu_{\theta r}}{E_\theta}\sigma_\theta \tag{2.39}$$

$$\varepsilon_\theta = -\frac{\nu_{r\theta}}{E_r}\sigma_r + \frac{1}{E_\theta}\sigma_{\sigma_\theta} \tag{2.40}$$

$$\gamma_{r\theta} = \frac{1}{G_{r\theta}}\tau_{r\theta} \tag{2.41}$$

where ε_r is the normal strain in radial direction, ε_θ is the normal strain in tangential (hoop) direction and $\gamma_{r\theta}$ is the out-of-plane shear strain. In this equation the E_θ, the Young's modulus in tangential direction, for each ply is determined by the relation given in Equation (2.22a). E_r, the Young's modulus in radial direction, is not dependent on the angle of the plies. $\nu_{\theta r}$, the out-of-plane Poisson's ratio, is estimated for each ply by using Equation (2.22c). The reciprocity relationship is given by

$$\frac{\nu_{r\theta}}{E_r} = \frac{\nu_{\theta r}}{E_\theta} \tag{2.42}$$

The strains are related to the displacements through the following formulae:

$$\epsilon_r = \frac{\partial u_r}{\partial r} \tag{2.43}$$

$$\epsilon_\theta = \frac{1}{r}\frac{\partial u_\theta}{\partial \theta} + \frac{u_r}{r} \tag{2.44}$$

$$\gamma_{r\theta} = \frac{1}{2}\left(\frac{1}{r}\frac{\partial u_r}{\partial \theta} + \frac{\partial u_\theta}{\partial r} - \frac{u_\theta}{r}\right) \tag{2.45}$$

In these equations the u_r is the displacement in radial direction and u_θ is the displacement in tangential direction.

2.2.2.1. Stresses

Substitution of Equations (2.34) and (2.35) into Equations (2.36) to (2.38) yields the following stress equations for end forces P

$$\sigma_r(r,\theta) = \left[A\beta r^{\beta-1} - B\beta r^{-\beta-1} + \frac{D}{r}\right]\sin\theta \tag{2.46}$$

$$\sigma_\theta(r,\theta) = \left[A\beta(1+\beta) r^{\beta-1} - B\beta(1+\beta) r^{-\beta-1} + \frac{D}{r}\right]\sin\theta \tag{2.47}$$

$$\tau_{r\theta}(r,\theta) = -\left[A\beta r^{\beta-1} - B\beta r^{-\beta-1} + \frac{D}{r}\right]\cos\theta \tag{2.48}$$

for end moments M

$$\sigma_r(r) = 2B' + C'(1+k) r^{k-1} + D'(1-k) r^{-k-1} \tag{2.49}$$

$$\sigma_\theta(r) = 2B' + C'(1+k) r^{k-1} - D'(1-k) r^{-k-1} \tag{2.50}$$

$$\tau_{r\theta} = 0 \tag{2.51}$$

It must be noted that the magnitudes of σ_r and $\tau_{r\theta}$ for the case of end forces P are identical, but are out of phase in the θ direction by $\frac{\pi}{2}$. Furthermore, one must notice that if these equations are solved for a laminate with unidirectional plies one will end up with the equations as already given in subsection 2.2.1.

2.2.2.2. Displacements

Using Equations (2.39) to (2.42) and (2.46) to (2.51) , the displacements u_r (Equation (2.43)) and u_θ (Equation (2.44)) can be integrated to give the following forms, neglecting the rigid body motion terms:

for end forces P

$$\begin{aligned} u_r(r,\theta) = \Bigg\{ & Ar^\beta\left[\frac{1}{E_r} - (1+\beta)\frac{\nu_{\theta r}}{E_\theta}\right] + Br^{-\beta}\left[\frac{1}{E_r} - (1-\beta)\frac{\nu_{\theta r}}{E_\theta}\right] \\ & + D(\ln r)\left(\frac{1}{E_r} - \frac{\nu_{\theta r}}{E_\theta}\right)\Bigg\}\sin\theta \end{aligned} \tag{2.52}$$

$$\begin{aligned} u_\theta(r,\theta) = \Bigg\{ & Ar^\beta\left[\frac{1}{E_r} - \beta(1+\beta)\frac{1}{E_\theta} - \frac{\nu_{\theta r}}{E_\theta}\right] + Br^{-\beta}\left[\frac{1}{E_r} + \beta(1-\beta)\frac{1}{E_\theta} - \frac{\nu_{\theta r}}{E_\theta}\right] \\ & + D\left[(\ln r)\left(\frac{1}{E_r} - \frac{\nu_{\theta r}}{E_\theta}\right) - \left(\frac{1}{E_\theta} - \frac{\nu_{\theta r}}{E_\theta}\right)\right]\Bigg\}\sin\theta \end{aligned} \tag{2.53}$$

for end moments M

$$\begin{aligned} u_r(r) = & B'\left[2r\left(\frac{1}{E_r} - \frac{\nu_{\theta r}}{E_\theta}\right)\right] + C'\left[(1+k) r^k\left(\frac{1}{k}\frac{1}{E_r} - \frac{\nu_{\theta r}}{E_\theta}\right)\right] \\ & - D'\left[(1-k) r^{-k}\left(\frac{1}{k}\frac{1}{E_r} + \frac{\nu_{\theta r}}{E_\theta}\right)\right] \end{aligned} \tag{2.54}$$

$$u_\theta(r,\theta) = B'\left[2r\left(\frac{1}{E_\theta} - \frac{1}{E_r}\right)\right]\theta \tag{2.55}$$

2.2.2.3. Boundary Conditions

At each interface between layers i and $i+1$ ($i = 1,2,\dots N-1$), the following boundary conditions for the continuities of stresses and displacements must hold (no sliding between layers).

for end forces P

at $r = a_i$:

$$\sigma_r^{(i)}(a_i,\theta) = \sigma_r^{(i+1)}(a_i,\theta) \tag{2.56}$$

$$\tau_{r\theta}^{(i)}(a_i,\theta) = \tau_{r\theta}^{(i+1)}(a_i,\theta) \tag{2.57}$$

$$u_r^{(i)}(a_i,\theta) = u_r^{(i+1)}(a_i,\theta) \tag{2.58}$$

$$u_\theta^{(i)}(a_i,\theta) = u_\theta^{(i+1)}(a_i,\theta) \tag{2.59}$$

The boundary conditions at the traction-free inner surfaces ($i-1=0$) and outer surface ($i=N$) of the curved bar are

at $r = a_0 = a$:

$$\sigma_r^{(1)}(a,\theta) = 0 \tag{2.60}$$

$$\tau_{r\theta}^{(1)}(a,\theta) = 0 \tag{2.61}$$

at $r = a_N = b$:

$$\sigma_r^{(N)}(b,\theta) = 0 \tag{2.62}$$

$$\tau_{r\theta}^{(N)}(b,\theta) = 0 \tag{2.63}$$

for end moments M

at $r = a_i$:

$$\sigma_r^{(i)}(a_i) = \sigma_r^{(i+1)}(a_i) \tag{2.64}$$

$$u_r^{(i)}(a_i) = u_r^{(i+1)}(a_i) \tag{2.65}$$

$$u_\theta^{(i)}(a_i) = u_\theta^{(i+1)}(a_i) \tag{2.66}$$

at $r = a_0 = a$:

$$\sigma_r^{(1)}(a) = 0 \tag{2.67}$$

at $r = a_N = b$:

$$\sigma_r^{(N)}(b) = 0 \tag{2.68}$$

For each loading case, each set of the previous boundary conditions will give $2+3(N-1) = 3N-1$ equations for determining the $3N$ unknowns A_i, B_i, D_i ($i = 1,2,\dots N$) for the case of an end force P, or $3N$ unknowns B_i', C_i', D_i' ($i = 1,2,\dots N$) for the case of an end moment M.

The last equation needed for each loading case is the condition that the end force P or the end moment M is balanced by the stresses in the curved bar:

for end forces P

$$-P = \sum_{i=1}^{N} \int_{a_{i-1}}^{a_i} \tau_{r\theta}^{(i)}(r,0)\,dr \quad ; \quad \theta = 0 \tag{2.69}$$

for end moments M

$$-M=\sum_{i=1}^{N}\int_{a_{i-1}}^{a_i}(r-r_0)\,\sigma_\theta(r)\,dr \tag{2.70}$$

where the negative signs in front of P and M are to increase the radius of curvature of the curved bar, and r_0 is the unknown radial location where $\sigma_\theta = 0$. For pure bending we have

$$\sum_{i=1}^{N}\int_{a_{i-1}}^{a_i}\sigma \tag{2.71}$$

Therefore, Equation (2.70) becomes:

$$-M=\sum_{i=1}^{N}\int_{a_{i-1}}^{a_i}r\sigma_\theta(r)\,dr \tag{2.72}$$

2.2.2.4. Boundary Conditions in Final Forms

After substitution of stress and displacement expressions given respectively in Sections 2.2.2.1 and 2.2.2.2 into the boundary conditions given in Section 2.2.2.3, the following final forms of the boundary conditions are obtained:

for end forces P

for $\sigma_r^{(1)}$

$$A_1\beta_1 a^{\beta_1}-B_1\beta_1 a^{-\beta_1}+D_1=0 \tag{2.73}$$

for $\sigma_r^{(i)}$

$$A_i\beta_i a_i^{\beta_i}-B_i\beta_i a_i^{-\beta_i}+D_i-A_{i+1}\beta_{i+1}a_i^{\beta_{i+1}}+B_{i+1}\beta_{i+1}a_i^{-\beta_{i+1}}-D_{i+1}+0 \tag{2.74}$$

for $\sigma_r^{(N)}$

$$A_N\beta_N a_N^{\beta_N}-B_N\beta_N a_N^{-\beta_N}+D_N=0 \tag{2.75}$$

for $u_r^{(i)}$:

$$\begin{aligned}&A_i a_i^{\beta_i}\left[\frac{1}{E_r^{(i)}}-\left(1+\beta_i\right)\frac{\nu_{\theta r}^{(i)}}{E_\theta^{(i)}}\right]+B_i a_i^{-\beta_i}\left[\frac{1}{E_r^{(i)}}-\left(1-\beta_i\right)\frac{\nu_{\theta r}^{(i)}}{E_\theta^{(i)}}\right]\\&+D_i(\ln a_i)\left(\frac{1}{E_r^{(i)}}-\frac{\nu_{\theta r}^{(i)}}{E_\theta^{(i)}}\right)-A_{i+1}a_i^{\beta_{i+1}}\left[\frac{1}{E_r^{(i+1)}}-\left(1+\beta_{i+1}\right)\frac{\nu_{\theta r}^{(i+1)}}{E_\theta^{(i+1)}}\right]\\&-B_{i+1}a_i^{-\beta_{i+1}}\left[\frac{1}{E_r^{(i+1)}}-\left(1-\beta_{i+1}\right)\frac{\nu_{\theta r}^{(i+1)}}{E_\theta^{(i+1)}}\right]-D_{i+1}(\ln a_i)\left(\frac{1}{E_r^{(i+1)}}-\frac{\nu_{\theta r}^{(i+1)}}{E_\theta^{(i+1)}}\right)=0\end{aligned} \tag{2.76}$$

for $u_\theta^{(i)}$:

$$\begin{aligned}&A_i a_i^{\beta_i}\frac{\beta_i}{E_\theta^{(i)}}\left[\left(1+\beta_i\right)-\nu_{\theta r}^{(i)}\right]-B_i a_i^{\beta_i}\frac{\beta_i}{E_\theta^{(i)}}\left[\left(1-\beta_i\right)-\nu_{\theta r}^{(i)}\right]\\&+D_i\frac{1}{E_\theta^{(i)}}\left(1-\nu_{\theta r}^{(i)}\right)-A_{i+1}a_i^{\beta_{i+1}}\frac{\beta_{i+1}}{E_\theta^{(i+1)}}\left[\left(1+\beta_{i+1}\right)-\nu_{\theta r}^{(i+1)}\right]\\&+B_{i+1}a_i^{\beta_{i+1}}\frac{\beta_{i+1}}{E_\theta^{(i+1)}}\left[\left(1-\beta_{i+1}\right)-\nu_{\theta r}^{(i+1)}\right]+D_{i+1}\frac{1}{E_\theta^{(i+1)}}\left(1-\nu_{\theta r}^{(i+1)}\right)=0\end{aligned} \tag{2.77}$$

for P

$$\sum_{i=1}^{N}\left[A_i\left(a_i^{\beta_i}-a_{i-1}^{\beta_i}\right)+B_i\left(a_i^{\beta_i}-a_{i-1}^{-\beta_i}\right)+D_i(\ln a_i-\ln a_{i-1})\right]=P \tag{2.78}$$

for end moments M
for $\sigma_r^{(1)}$

$$2B_1' + C_1' (1+k_1)\, a^{k_1-1} + D'1\,(1-k_1)\, a^{-k_1-1} = 0 \tag{2.79}$$

for $\sigma_r^{(i)}$

$$\begin{aligned} &2B_i' + C_i' (1+k_i)\, a_i^{k_i-1} + D_i' (1-k_i)\, a_i^{-k_i-1} \\ &-2B_{i+1}' - C_{i+1}' (1+k_{i+1})\, a_i^{k_{i+1}-1} + D_{i+1}' (1-k_{i+1})\, a_i^{-k_{i+1}-1} = 0 \end{aligned} \tag{2.80}$$

for $\sigma_r^{(N)}$

$$2B_N' + C_N' (1+k_N)\, a^{k_N-1} + D_N' (1-k_N)\, a^{-k_N-1} = 0 \tag{2.81}$$

for $u_r^{(i)}$:

$$\begin{aligned} &B_i' \left[2a_i \left(\frac{1}{E_r^{(i)}} - \frac{\nu_{\theta r}^{(i)}}{E_\theta^{(i)}} \right) \right] + C_i' \left[(1+k_i)\, a_i^{k_i} \left(\frac{1}{k_i} \frac{1}{E_r^{(i)}} - \frac{n u_{\theta r}^{(i)}}{E_\theta^{(i)}} \right) \right] \\ &- D_i' \left[(1-k_i)\, a_i^{-k_i} \left(\frac{1}{k_i} \frac{1}{E_r^{(i)}} + \frac{n u_{\theta r}^{(i)}}{E_\theta^{(i)}} \right) \right] - B_{i+1}' \left[2a_i \left(\frac{1}{E_r^{(i+1)}} - \frac{\nu_{\theta r}^{(i+1)}}{E_\theta^{(i+1)}} \right) \right] \\ &- C_{i+1}' \left[(1+k_{i+1})\, a_i^{k_{i+1}} \left(\frac{1}{k_{i+1}} \frac{1}{E_r^{(i+1)}} - \frac{n u_{\theta r}^{(i+1)}}{E_\theta^{(i+1)}} \right) \right] + D_{i+1}' \left[(1-k_{i+1})\, a_i^{-k_{i+1}} \left(\frac{1}{k_{i+1}} \frac{1}{E_r^{(i+1)}} + \frac{n u_{\theta r}^{(i+1)}}{E_\theta^{(i+1)}} \right) \right] = 0 \end{aligned} \tag{2.82}$$

for $u_\theta^{(i)}$

$$B_i' \left[2a_i \left(\frac{1}{E_\theta^{(i)}} - \frac{1}{E_r^{(i)}} \right) \right] - B_{i+1}' \left[2a_i \left(\frac{1}{E_\theta^{(i+1)}} - \frac{1}{E_r^{(i+1)}} \right) \right] = 0 \tag{2.83}$$

for M

$$\sum_{i=1}^{N} \left[B_i' \left(a_i^2 - a_{i-1}^2 \right) + C_i' k_i \left(a_i^{k_i+1} - a_{i-1}^{k_i+1} \right) - D_i' k_i \left(a_i^{-k_i+1} - a_{i-1}^{-k_i+1} \right) \right] = -M \tag{2.84}$$

An example of the equations to solve in order to get the arbitrary constants can be found in Appendix B. In the appendix the equations for an end load (Equation (B.1)) and for an end moment (Equation (B.2)) can be found for the case of three layers, i.e. $N = 3$.

2.3. ThickS4 User Element Description

The thickS4 USER-element (UEL) is a user subroutine written in Fortran for the Abaqus user subroutine environment. The element is a four node, curved shell element which is able to predict out-of-plane stresses. The element is produced to get the curvature of a structure in the element and the stifness matrix. The element is visualised in Figure 2.1. However the element itself is not as it consists of only 4 nodes and therefore actually looks as in Figure 2.2.

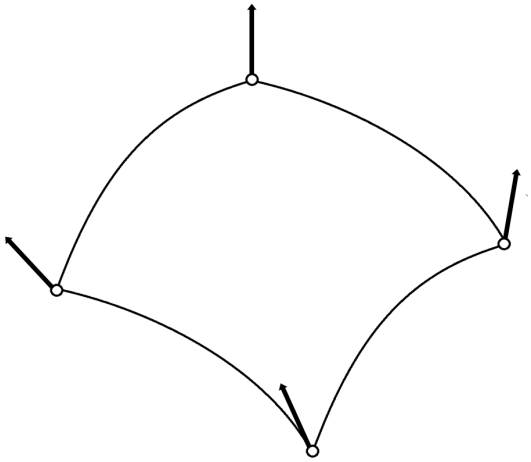

Figure 2.1: Structure of the curved element.

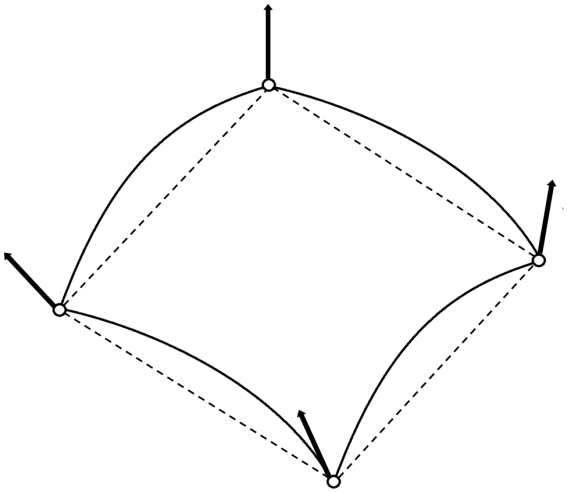

Figure 2.2: Structure of the curved element along with the projected real modeled element.

One could imagine that giving an input of only the locations of the nodes does not give enough information about the curvature of the element. Therefore in order to get the correct information of the curvature of the element a SQLite database is created for each model where the information of the model is stored. In order to access this data, a SQLite database connection is used for the loop of each element, the normal directions of the nodes are retrieved from the model database.

The isoparametric coordinate system $\mathbf{a}_{\alpha_{ISO}}$ is determined by multiplying the coordinates of the element with the derivatives of the shape functions. As can be seen in the following equation.

$$\mathbf{a}_{\alpha_{ISO}} = \mathbf{x} \cdot \mathrm{d}\mathbf{H} \tag{2.85}$$

The isoparametric coordinate system $\mathbf{t}_3$ is determined by multiplying the normals of the nodes by the shape functions.

$$\mathbf{t}_{3_{ISO}} = \mathbf{n} \cdot \mathbf{H} \tag{2.86}$$

However when an average is taken of the normals the resulting vector is not normalised, which it needs to be in order to make the coordinate system transformation, therefore the resulting vector is normalised again in the equation below.

$$\mathbf{t}_3 = \frac{\mathbf{t}_\alpha}{\|\mathbf{t}_\alpha\|} \tag{2.87}$$

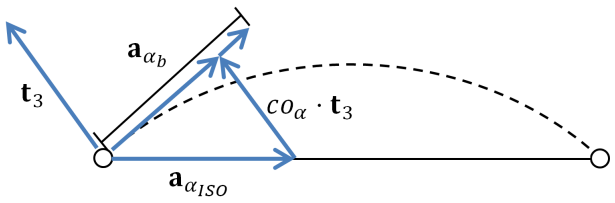

Figure 2.3: Visualisation of the transformation to the curvilinear coordinates.

In order to get the curvature into the element a transformations needs to be done. The isoparametric coordinate system $\mathbf{a}_{\alpha_{ISO}}$ needs to be transformed to the curvilinear coordinate system $\mathbf{a}_{\alpha_b}$. The transformation is visualised in Figure 2.3 and the equations of the transformation will be discussed below. The first coefficient needed is co and is determined in the following manner.

$$co_\alpha = \mathbf{t}_3 \cdot \mathbf{a}_{\alpha_{ISO}} \tag{2.88}$$

The coefficient co together with the normalised $\mathbf{t}_3$ are used to get make the transformation as can be seen in Figure 2.3 and in the equation below.

$$\mathbf{a}_{\alpha_{transformed}} = \mathbf{a}_{\alpha_{ISO}} - co_\alpha \cdot \mathbf{t}_3 \tag{2.89}$$

However as can be seen, $\mathbf{a}_{\alpha_{transformed}} \neq \mathbf{a}_{\alpha_b}$ and needs to be corrected with a certain factor. For the correction factor the vector $\mathbf{V}_\alpha$ which is orthogonal to both $\mathbf{t}_3$ and $\mathbf{a}_{\alpha_{ISO}}$ is used and is determined by taking the cross product of the two.

$$\mathbf{V}_\alpha = \mathbf{t}_3 \times \mathbf{a}_{\alpha_{ISO}} \tag{2.90}$$

When $\mathbf{V}_\alpha$ is known the correction factor becomes the following.

$$tg_\alpha = \frac{co_\alpha^2}{\mathbf{V}_\alpha^2} \tag{2.91}$$

Writing the final equation for the curvilinear coordinate system yields the following.

$$\mathbf{a}_{\alpha_b} = tg2_\alpha \cdot \left(\mathbf{a}_{\alpha_{ISO}} - co_\alpha \cdot \mathbf{t}_3\right) \tag{2.92}$$

For the ease of it, will the curvilinear coordinate system further be written as $\mathbf{a}_\alpha$. The curvilinear coordinate system is shown in both Figures 2.4 and 2.5.

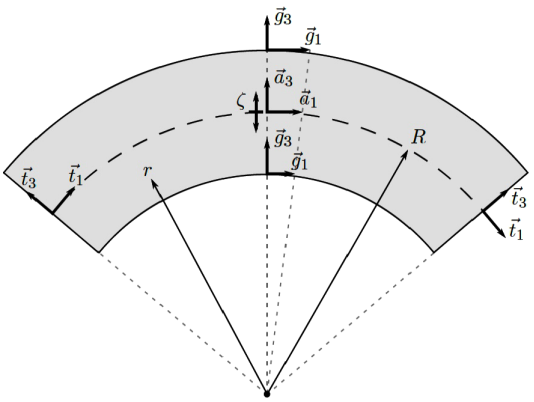

Figure 2.4: Cross-sectional representation of the coordinate systems and the correlation between the $\mathbf{a}_\alpha$ and $\mathbf{g}_\alpha$ coordinate systems.

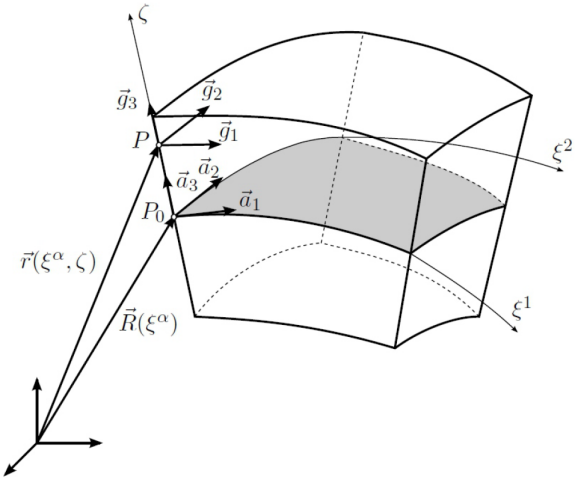

Figure 2.5: Three-dimensional representation of the natural coordinate system and the curvilinear coordinate system $\mathbf{a}_\alpha$.

In these figures the other coordinate systems are also shown, namely the natural (skew) coordinate system with the covariant base vectors $\mathbf{g}_1$, $\mathbf{g}_2$ and $\mathbf{g}_3$ and the Cartesian coordinate system with the orthonormal base vectors $\mathbf{t}_1$, $\mathbf{t}_2$ and $\mathbf{t}_3$. As can be seen the previously defined curvilinear coordinate system is the natural coordinate system taken at the mid-surface. The natural coordinate system is dependent on the transverse coordinate ζ. The in-plane vectors for the natural coordinate system can be written in the following form.

$$\mathbf{g}_\alpha = \frac{\partial \mathbf{r}}{\partial \xi^\alpha} = \mathbf{r}_{,\alpha} \tag{2.93}$$

The contravariant base vectors are defined in the following manner.

$$\mathbf{g} = \frac{\partial \xi^{\alpha}}{\partial \mathbf{r}} \tag{2.94}$$

The previously defined curvilinear coordinate system can also be written in the following manner (taking the mid-surface $\zeta = 0$ of the natural coordinate system).

$$\mathbf{a}_{\alpha} = \frac{\partial \mathbf{R}}{\partial \xi^{\alpha}} = \mathbf{R}_{,\alpha} \tag{2.95}$$

With the according contravariant base vectors.

$$\mathbf{a}^{\alpha} = \frac{\partial \xi^{\alpha}}{\partial \mathbf{R}} \tag{2.96}$$

The transverse component of the coordinate systems are all the same, written as follows.

$$\mathbf{t}_3 = \mathbf{g}_3 = \mathbf{a}_3 = \mathbf{t}^3 = \mathbf{g}^3 = \mathbf{a}^3 \tag{2.97}$$

From Figure 2.5 it can be seen that the position vector $\mathbf{r}$ can be expressed using the vector of the mid-surface $\mathbf{R}$ and the transverse component $\mathbf{a}_3$ as can be seen below.

$$\mathbf{r}\left(\xi^{\alpha}, \zeta\right) = \mathbf{R}\left(\xi^{\alpha}\right) + \zeta \mathbf{a}^3 \tag{2.98}$$

When combining this equation to the ones previously given the in-plane natural coordinate system vectors can be written in the following manner.

$$\mathbf{g}_{\alpha} = \mathbf{a}_{\alpha} + \zeta \mathbf{a}_{3,\alpha} \tag{2.99}$$

In this equation the last part $\zeta \mathbf{a}_{3,\alpha}$ is the change in length of the in-plane vector $\mathbf{g}_{\alpha}$ due to the curvature, i.e. the difference in the direction of the normal vector. In the element this change due to the curvature is determined in the following manner.

$$\mathbf{a}_{3,\alpha_{ISO}} = \mathbf{n} \cdot \mathrm{d}\mathbf{H} \tag{2.100}$$

This however is again without curvature and therefore needs to be transformed to the curvilinear coordinate system.

$$\mathbf{a}_{3,\alpha_b} = \frac{\mathbf{a}_{3,\alpha_{ISO}} - \left(\mathbf{t}_3 \cdot \mathbf{a}_{3,\alpha_{ISO}}\right) \cdot \mathbf{t}_3}{\|\mathbf{t}_{3_{\mathbf{ISO}}}\|} \tag{2.101}$$

In this equation, it can be seen that the transformation is similar as for $\mathbf{a}_{\alpha}$, in this case the correction is done by dividing by the norm of the transverse vector $\mathbf{t}_{3_{ISO}}$.

2.3.1. Input

The input for the element is an array with all the needed parameters. These parameters consist of the coordinates for two points A and B in order to determine the global direction of the element. The next input is the choice between retrieving the local (ply direction) or the global (element wise) stresses. Next are all the material properties needed for the determination of the stresses as well as for the determination of the failure criteria. These are the thickness of the plies t_{ply}, the E-moduli E_{11}, E_{22} and E_{33}, the Poisson's ratios ν_{21}, ν_{31} and ν_{32}, the shear-moduli G_{12} and G_{23}, and the failure stresses F_{11_t}, F_{11_c}, F_{22_t}, F_{22_c}, F_{33_t}, F_{33_c}, F_{12}, F_{13} and F_{23}. The last input to the element is an array with the fiber orientations, also known as the stacking sequence of the element.

2.3.2. Output

A few of the output variables were already mentioned, being the stresses and the failure criteria. The output stresses include the in-plane stresses σ_{11}, σ_{12} and σ_{22}, as well as the out-of-plane stresses σ_{33}, τ_{13} and τ_{23}. The failure criteria determined are described in subsubsection 2.3.2.1.

In order to have a proper way to access the results of the element, a results SQLite database is created in which the output is stored into different tables. It was chosen to do it in this way as the stresses and section forces cannot be retrieved via the Abaqus .odb file. Next to these previously mentioned output variables, the degrees of freedom and the section forces and moments are also written to this results SQLite database.

Furthermore extra output can be written such as the earlier mentioned failure criteria, such that no further post-processing is required to get the necessary information.

2.3.2.1. Failure Criteria

This section gives the four failure criteria as were implemented into the Abaqus USER-element. Four different failure criteria are written to the SQLite database. Two of these criteria are in-plane failure criteria and are the Yamada-Sun criterion and the Hashin criterion. The third criterion is an out-of-plane failure criterion in the form of the Kim & Soni failure criterion. The final criterion is a combination of the in-plane transverse stress direction and the out-of-plane stresses which is the Tsai-Wu failure criterion.

- Yamada-Sun

$$f_{yasu} = \begin{cases} \frac{\sigma_{11}^2}{F_{11_t}^2} + \frac{\tau_{12}^2}{F_{12}^2} & \text{if } \sigma_{11} > 0 \\ \frac{\sigma_{11}^2}{F_{11_c}^2} + \frac{\tau_{12}^2}{F_{12}^2} & \text{else} \end{cases} \tag{2.102}$$

- Hashin

$$f_{hash} = \begin{cases} \frac{\sigma_{22}^2}{F_{22_t}^2} + \frac{\tau_{12}^2}{F_{12}^2} & \text{if } \sigma_{22} > 0 \\ \frac{\sigma_{22}^2}{F_{22_c}^2} + \frac{\tau_{12}^2}{F_{12}^2} & \text{else} \end{cases} \tag{2.103}$$

- Kim & Soni

$$f_{kimson} = \begin{cases} \frac{\sigma_{33}^2}{F_{33_t}^2} + \frac{\tau_{13}^2}{F_{13}^2} + \frac{\tau_{23}^2}{F_{23}^2} & \text{if } \sigma_{33} > 0 \\ \frac{\sigma_{33}^2}{F_{33_c}^2} + \frac{\tau_{13}^2}{F_{13}^2} + \frac{\tau_{23}^2}{F_{23}^2} & \text{else} \end{cases} \tag{2.104}$$

  The failure criterion shown above is not really the failure criterion from Kim & Soni, however it is a failure criterion derived from the out of-plane failure criterion from Brewer and Lagace [1]. The difference with the Kim & Soni failure criterion is that this criterion does not take into account the fact that a compressive stress gives a delay of the delamination. The difference with the Brewer Lagace criterion is that the Brewer and Lagace criterion uses averaged stresses which won't be used in this element. This criterion will be further referenced as the Kim & Soni failure criterion.

- Tsai-Wu

$$\begin{aligned} f_{tsaiwu} = \frac{\sigma_{22}^2}{F_{22_t} S_{22_c}} + \frac{\sigma_{33}^2}{F_{33_t} F_{33_c}} - \sqrt{\frac{1}{F_{22_t} F_{22_c}} \frac{1}{F_{33_t} F_{33_c}}} \sigma_{22} \sigma_{33} \\ + \left(\frac{1}{F_{22_c}} - \frac{1}{F_{22_t}} \right) \sigma_{22} + \left(\frac{1}{F_{33_c}} - \frac{1}{F_{33_t}} \right) \sigma_{33} + \frac{\tau_{23}^2}{F_{23}} \end{aligned} \tag{2.105}$$

3

Benchmark Tests for ThickS4 UEL Validation

This chapter will discuss the validation of the ThickS4 user element. In order to make a good validation, benchmark tests need to be performed. For these benchmark tests FEM-models are needed which are explained in section 3.1. In this section the different components of the tests are also given as well as materials used. Following the descriptions of the benchmark tests the results of the tests are given in section 3.2. The chapter is finalised by a conclusion regarding the validation of the ThickS4 element and a recommendation on how to continue with the rest of the project in section 3.3.

3.1. Descriptions of Benchmark Models

In order to test, explore the limits and determine the performance of the ThickS4 UEL, three benchmark tests are performed. The first benchmark is a cantilever laminated beam subjected to an end load. The second and third benchmark are a curved laminated beam subjected to an end load and an end moment respectively. This section will give a detailed description about each of the individual benchmarks, the way they are modelled in Abaqus and to what analytical model the benchmark is compared. The three benchmarks are all modelled with four different kinds of finite elements: being the ThickS4 UEL and the three Abaqus elements S4, C3D8 and C3D27.

For all benchmarks there are certain layups to be modelled with a certain number of plies. This procedure is different for the 2D and 3D elements. In the 2D elements, also known as the shell elements, the element is assigned a certain stacking sequence and material. Each ply or layer in the element is then given a certain number of integration points, which for the current case is three. Three is a sufficient number of integration points as with three integration points a parabolic shape can be made. For the 3D elements, each ply in the laminate is given an own layer of elements to which then material properties and the direction of the ply/layer are given.

For the creation of the Abaqus models, scripts were written which are able to receive an excel sheet with all the necessary information as input. A screen shot of an example of such an input file can be seen in Appendix A in Figure A.1. This input is then used to create the Abaqus model by writing the model to an Abaqus input file. In this way it is easy to change certain parameters within the model. This also helps to create an easy flow between the input given and the output received as all information is known by the script at every stage of the analysis.

3.1.1. Cantilever Beam Subjected to an End Load

The first benchmark is about a cantilever beam subjected to a transverse end load. This is the most simple benchmark to compare the ThickS4 UEL with. The benchmark consists of the classical laminated plate theory as analytical solution. This simple solution is used to compare the element in the most simple configuration. For this benchmark only comparisons can be done for displacement and the in-plane stresses as the ThickS4 UEL does not have a solution for the out-of-plane stresses when the element has no curvature. Furthermore it is known that due to assumptions taken in the CLPT, the out-of-plane stresses are not present. The configuration can be seen in Figure 3.1.

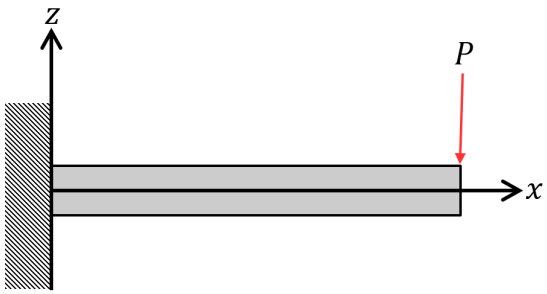

Figure 3.1: Cantilever Beam subjected to a transverse end load.

Figure 3.1 shows that the load is introduced at the end of the beam. However the element has to be modelled in 3D in Abaqus and therefore the point load at the end is changed to a distributed edge load. The 3D models of the cantilever beam can be seen in Figure 3.2 and Figure 3.3.

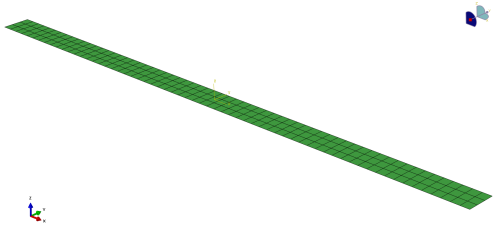

Figure 3.2: Cantilever beam modelled in Abaqus using S4 shell elements.

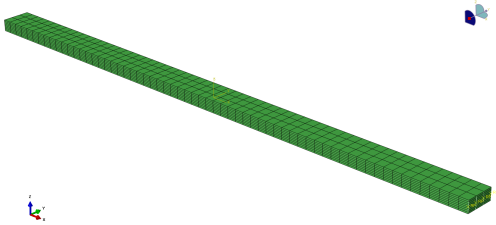

Figure 3.3: Cantilever beam modelled in Abaqus using C3D8 and C3D27 solid elements.

In the user element definition from Abaqus an edge load cannot be introduced, therefore the edge load is transferred to the nodes on the edge concerned. This is done by dividing the point load by the amount of elements and distributing this load between the nodes of each element. If more than one element is used at an edge, the elements will share nodes. The point loads applied to the separate element are in this case added up. In this manner the corner nodes of the edge will get half the load compared to the enclosed nodes as is shown in Figure 3.4(b). This is a bit different for the C3D27, as for the C3D27 element, there is an element in the middle of the edge as well. A distributed load on a C3D27 element is distributed as follows: the outer nodes both get a sixth of the load where the middle node gets two-third. When this is converted to multiple elements over an edge, this will result in the corner nodes having a sixth of the load per element, the middle nodes two-thirds and the joint nodes a third as can be seen in Figure 3.4(c).

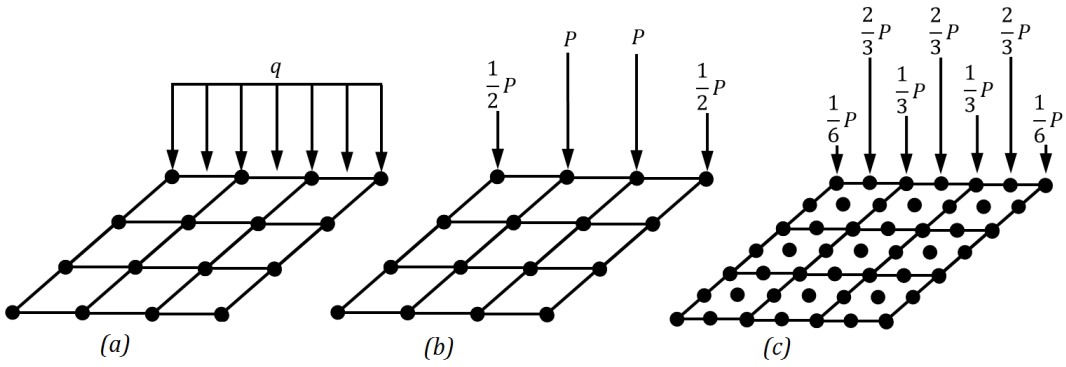

Figure 3.4: (a): Distributed load along the edge. (b): Distributed edge load converted to nodal loads for S4 & C3D8 elements. (c): Distributed edge load converted to nodal loads for C3D27 element.

To Introduce the load to the entire edge of the 3D elements is not that easy. Therefore in order to introduce the entire load to all the elements, rigid body elements were used which connect all the nodes in vertical direction. An RB3D2 Abaqus element is used between every node in vertical direction and a reference node

Table 3.1: Materials used as specified by the company intales, the thickness is given in mm, the moduli in GPa and the Young's moduli are dimensionless.

	Tape
t	0.254
E_1	1.54e+05
E_2	8.50e+03
E_3	8.50e+03
G_{12}	4.20e+03
G_{13}	4.20e+03
G_{23}	3.36e+03
ν_{12}	0.33
ν_{13}	0.33
ν_{23}	0.33

created at the mid-plane of the beam. This trick is visualised in Figure 3.5. Though the figure shows that the reference point is slightly to the right, in the model it is actually on the plane of the edge, however shown like this in order to make it clear. This is done for each vertical row of nodes and each row of RB3D2 elements are then combined to create a rigid body. What this looks like in the FEM model can be seen in Figure 3.6. The main reason the loads are applied in this way is not due to this benchmark test, however due to the curved beam subjected to an end moment, however this will be explained in subsection 3.1.2. The nodal loads are then applied to these created reference nodes making use of CLOADs, which are concentrated loads in Abaqus. As one can see, the end cross-section is only constrained vertically, this is done in order to keep the possibility for the elements to move in the depth direction, also known as the y-direction.

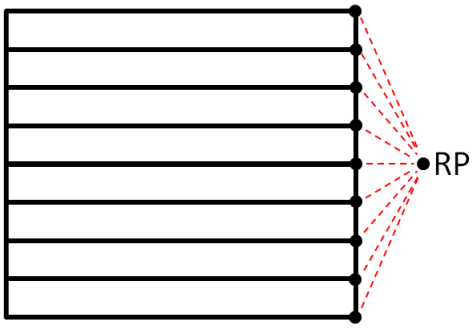

Figure 3.5: Schematic representation of rigid body element connections for the load introduction for C3D8 elements.

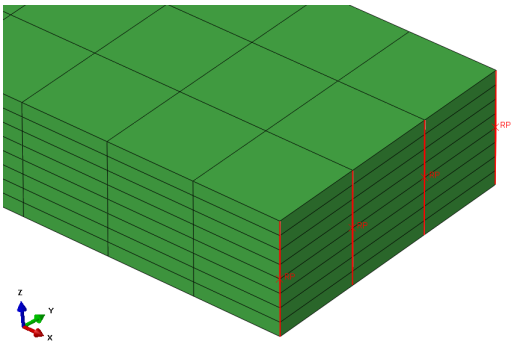

Figure 3.6: Rigid body connection for the load introduction for a FEM-model with C3D8 elements.

The clamped boundary condition is not made into a full clamped condition. All nodes are constrained in the x and z direction, however only the first row of nodes is constrained in the y-direction. Again to make sure that the elements can still expand and contract in the y-direction in order to minimize the effect of the boundary conditions.

The analytical solution used for this benchmark is the CLPT as described in section 2.1. The dimensions used for the cantilever beam are 1000 mm by 20 mm and the layup considered is $[45,-45,0,90]_s$. The properties of the material used can be seen in Table 3.1.

The analysis done for this benchmark is a convergence test comparing the different Abaqus elements and the ThickS4 element to the analytical solution for the displacement and the maximum value for the σ_{11}. This should give a good estimation about the performance of the element in this simple case. Furthermore a comparison for the distribution of the σ_{11}, σ_{22} and the σ_{12}, for a dense enough mesh. These values will be compared at the elements exactly in the middle of the beam, as this keeps the effect of the boundary conditions and load introduction as far away as possible.

3.1.2. Curved Beam Subjected to End Load & End Moment

This section describes the second and third benchmark tests as the structure to which the loads are applied are the same. The structure considered in these benchmark tests is a C-section as can be seen in Figure 3.7

subjected to both an end load and an end moment.

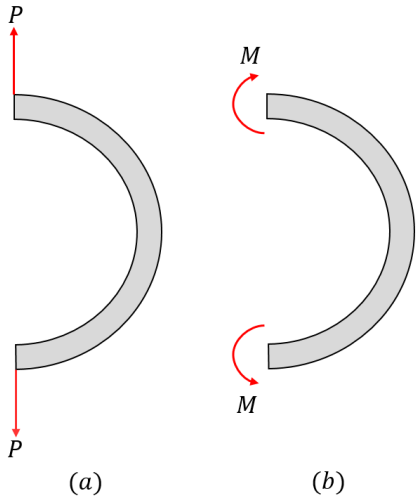

Figure 3.7: C-section to be modelled subjected to (a) end loads and (b) end moments.

However due to symmetry reasons it suffices to take only half the structure, in this case symmetry conditions have to be applied. These symmetry conditions are applied at the place where the structure has been cut. The boundary condition applied for the three-dimensional case is that at this location the movement in z-direction has been constrained all together. As was the case for the cantilever beam, also for this model the constraint for the movement in the y-direction is limited to the first row only, again to minimize the effect of the boundary conditions. For the two-dimensional case the same boundary conditions as for the 3D case are applied, however for the 2D model the rotation around the x-axis needs to be set to zero for the nodes at the symmetry plane.

The second set of boundary conditions is applied at the location where the load is introduced. The structure is constrained at the mid-plane of the laminate, making use of the same rigid bodies as were used in the cantilever beam. These reference nodes of the rigid bodies are constrained in the x-direction and again only in the y-direction for the first reference node. However for this boundary condition, the structure in case of the shell elements is not constrained for rotations. The structure is now able to bend outward as well as inward, depending on what load is applied. The sketch of the curved beam with its boundary conditions can be seen in Figure 3.8.

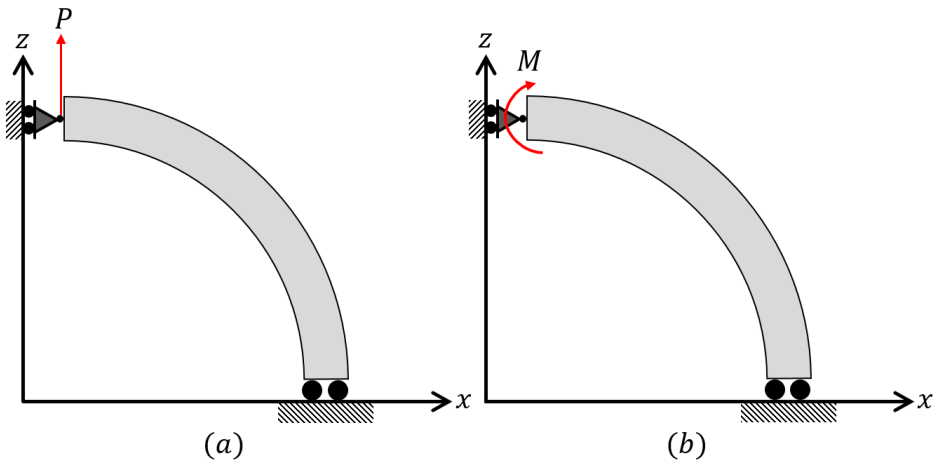

Figure 3.8: C-section to be modelled subjected to (a) end loads and (b) end moments.

For the load introduction and the second boundary condition, the Abaqus rigid body elements RB3D2 are used again. This gives the possibility to have the load applied exactly in the mid-plane of the laminate and still being able to apply the boundary condition. The 2D model in Abaqus can be seen in Figure 3.9 and the 3D model in Figure 3.10.

The main reason rigid body elements were used is that rotations cannot be applied to three dimensional elements. Three dimensional elements can only be constrained in the x, y and z-directions and not in any rotations. Therefore in order to bring the rotations, i.e. moments, into the model, extra nodes need to be made. These new nodes need to be connected to the nodes of the structure. This can be done through kinematic coupling or with the use of extra elements to connect the nodes. However with kinematic coupling, there is the problem that when applying boundary conditions to the reference nodes, the entire face of the structure is also constrained in that direction, which makes the rotation of the structure impossible. Therefore it was chosen to use rigid bodies instead as this solution still allows the structure to rotate as can be seen in Figure 3.11.

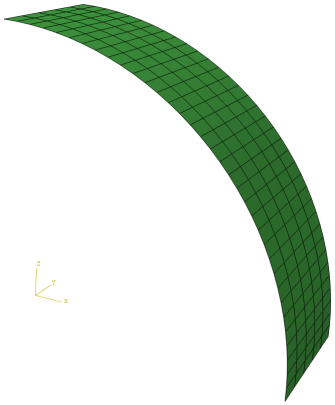

Figure 3.9: Curved beam modelled in Abaqus using S4 shell elements.

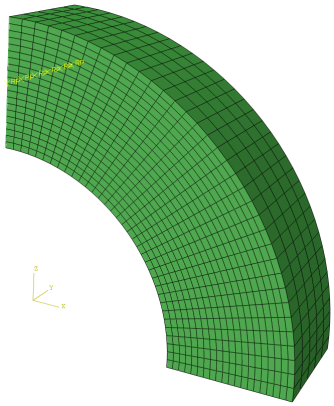

Figure 3.10: Curved beam modelled in Abaqus using C3D8 and C3D27 solid elements.

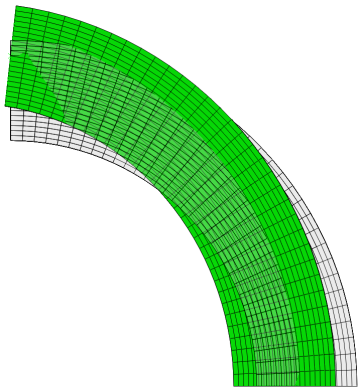

Figure 3.11: Curved beam in deformed configuration.

The finite element model for these two benchmarks will be compared to two analytical solutions. The first analytical solution is the Lekhnitskii's theory for anisotropic plates, as described in subsection 2.2.1. The same material properties will be used as were used for the cantilever beam given in Table 3.1.

The lekhnitskii solution will be used for the analysis of laminates with plies only in one direction as well as cross-ply laminates. In case of the cross-ply laminate the lekhnitskii solution is used in the multilayer theory developed by Ko and Jackson [6]. This is considered to be the second analytical solution. For the multilayer theory, the developers themselves have made a test already with the properties as given in Table 3.2.

These benchmarks will include a few scenarios. First of all the experiments as they are described in the papers earlier mentioned will be regenerated such that there is a good validation. In order to this properly a mesh convergence will be performed for which the convergence of the out of plane stresses σ_{33} and τ_{x3} and the in-plane stress σ_{11} will be analysed, as for these stresses an analytical solution is known. This is concluded by a thorough comparison of these stresses at a dense enough mesh. After this stage has been completed, other stacking sequences than the ones stated in the papers will be analysed. This will be done for a few stacking sequences commonly used.

Table 3.2: Benchmark Multilayer Theory Data

Variable	Metric	Imperial
a	2.1590 [cm]	0.85 [inch]
b	2.9724 [cm]	1.17022 [inch]
h	2.54 [cm]	1 [inch]
δ	0.01506 [cm]	0.00593 [inch]
E_L	17.2369e+10 [N/m^2]	25e+6 [lb/inch^2]
E_T	0.8274e+10 [N/m^2]	1.2e+6 [lb/inch^2]
G_{LT}	0.4137e+10 [N/m^2]	0.6e+6 [lb/inch^2]
ν_{LT}	0.33	
ν_{TL}	0.01584	

The next step is a check will be done regarding the radius over thickness ratio. For this check two parameters will be checked for two different set ups. The first set up is the case of only unidirectional plies and the second set up is with different layups. The two parameters to be changed are a constant radius while varying the thickness and a constant thickness, i.e. stacking sequence, while changing the radius for the Lekhnitskii solution. For the multilayer theory only the radius will be varied as the number of plies cannot be varied due to having plies in different directions.

Furthermore a stacking sequence investigation is done. For the stacking sequence investigation four different stacking sequences are used. Two of these stacking sequences are symmetrical and the other two are both asymmetric. The different stacking sequences are tested for three different radius over thickness ratios, being $R/t = 1$, $R/t = 4$ and $R/t = 8$. The four different stacking sequences are given in Table 3.3.

Table 3.3: Stacking sequences used for the distribution investigation.

Layup nr.	Stacking Sequence
1	$[(45,-45)_3, 0_3, 90_3]_s$
2	$[45,-45,0_3,90_3,(45,-45)_2]_s$
3	$[45,-45,0_4,90,0_2,(45,-45)_3,45,90,-45,90_4,-45,45]$
4	$[45,-45,90_4,-45,90,(45,-45)_3,45,0_2,90,0_4,-45,45]$

As can be seen, the in-plane properties of the stacking sequences are kept constant, i.e. the number of plies in each direction is kept constant. Furthermore it can be noticed that for the asymmetric stacking sequences, the layup is reversed in order to see how the ThickS4 element reacts to those two extreme cases. These two extreme cases being all zero plies towards the inner radius and almost all zero plies (respecting the maximum of four the same plies in a row as described in subsubsection 4.2.3.2) towards the outer radius.

3.2. Benchmark Test Results

In this section the benchmark test results will be given and described. It starts with the results for the cantilever beam subjected to an end load in subsection 3.2.1. This is followed by the results for a uni-directional curved beam subjected to an end load also known as the Lekhnitskii solution in subsection 3.2.2. Next are the results for the same uni-directional curved beam, but subjected to an end moment in subsection 3.2.3. Next the results of a curved beam with a cross-ply stacking sequence are discussed, which are compared to the multilayer theory in subsection 3.2.4 and the values of the article by Martin and Jackson [6]. The section is finalised by the results for a curved beam with different stacking sequences by using the multilayer theory as well.

3.2.1. Cantilever Beam

As was described in the description of the benchmarks, the first benchmark is the cantilever beam. For this simple case a mesh convergence with respect to the in-plane stress and the displacement, as well as a comparison of the stress distribution.

3.2.1.1. Mesh Convergence

The mesh convergence is done for the element in the middle of the beam, in this manner the results have the least influence of the boundary conditions on either the clamped side or the free side of the beam (where

the load is introduced). The convergence of the element has been checked for the in-plane stress σ_{11} as well as for the displacement as these variables are considered the most important for the cantilever beam. The results of the stresses are shown in the global coordinate system. The starting mesh of the mesh convergence is a mesh with five elements through the length and one element through the width. The N_{rate} in the graphs relate to the refinement of the starting mesh.

The results for the σ_{11} stress can be seen in Figure 3.12 and the results for the displacement w can be seen in Figure 3.14. As the convergence of the C3D8 Abaqus element is relatively slow the results are also given without the C3D8 element in the graph in Figure 3.13 and Figure 3.15.

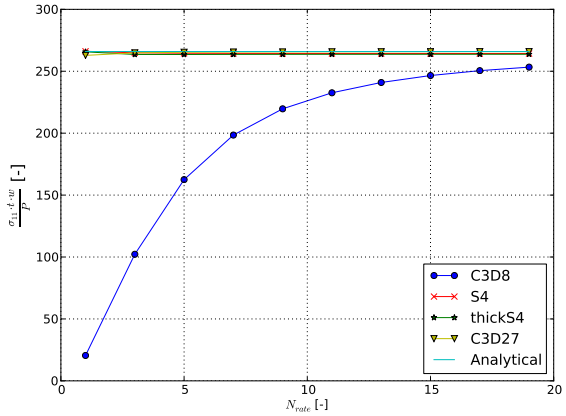

Figure 3.12: Mesh convergence of σ_{11} at the middle of the beam.

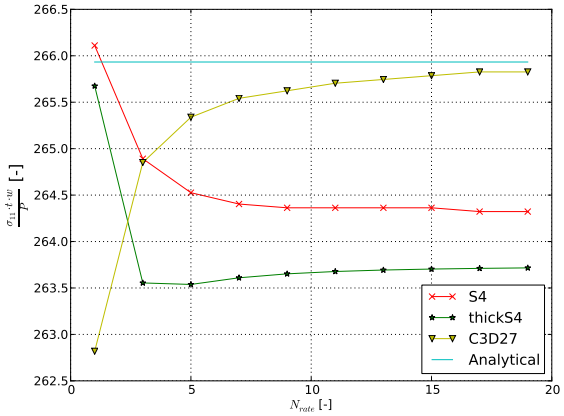

Figure 3.13: Mesh convergence of σ_{11} at the middle of the beam, without the C3D8 Abaqus element.

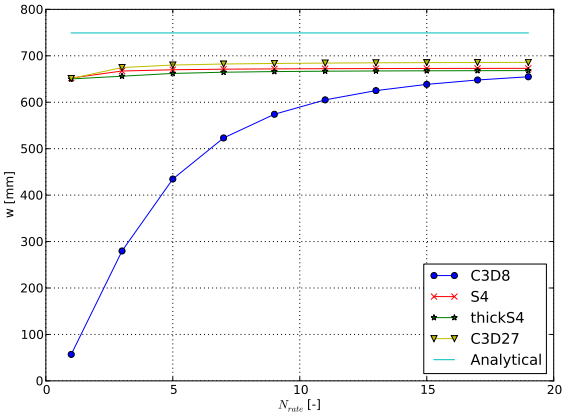

Figure 3.14: Mesh convergence of w at the tip of the beam.

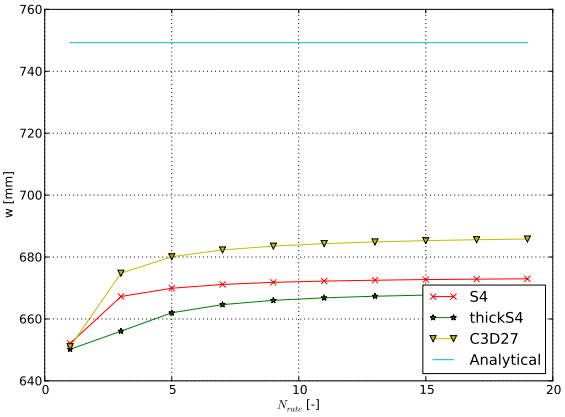

Figure 3.15: Mesh convergence of w at the tip of the beam, without the C3D8 Abaqus element.

The solution of the element is said to be converged when the change in stress for a next refinement is less than 1%. If this is considered, the C3D8 Abaqus element does not converge with respect to σ_{11} in the range of the analyses done. However the other elements are already converged at a convergence of three elements through the width. However when looking at the distribution of the graph itself one could say that the solution of the ThickS4 element is converged first and the solution of the C3D27 Abaqus element last, however as said before the difference the solutions still change is minor and for all of them less than the stated 1%. This can also be seen in the mesh convergence for the displacement w in Figures 3.14 and 3.15.

For the determination of the accuracy of the element the most dense mesh is taken to compare them. For the stress σ_{11} this results in the smallest error of $e = -0.0004$ for the C3D27 Abaqus element and when excluding the C3D8 Abaqus element the largest error is that of the ThickS4 element and is $e = -0.0083$. For the displacement it can be seen that the analytical solution is off from the displacement of the elements, this is because the standard classical laminate theory is not accurate with respect to displacement. This means that

the accuracy for the displacement cannot be taken with respect to the analytical solution. However, when taken with respect to the C3D27 Abaqus element (as this element is the most accurate for σ_{11}), the error for the ThickS4 element is $e = -0.00026$.

3.2.1.2. Distribution Comparison

In the stress mesh convergence check each time only the maximum stress was taken into account, it is however also interesting to see if the distribution over the thickness of the different elements are similar. These comparisons can be seen in Figures 3.16 to 3.19. For the distribution comparison, the finest mesh from the mesh convergence was used, being 95 elements through the length and 19 elements through the width.

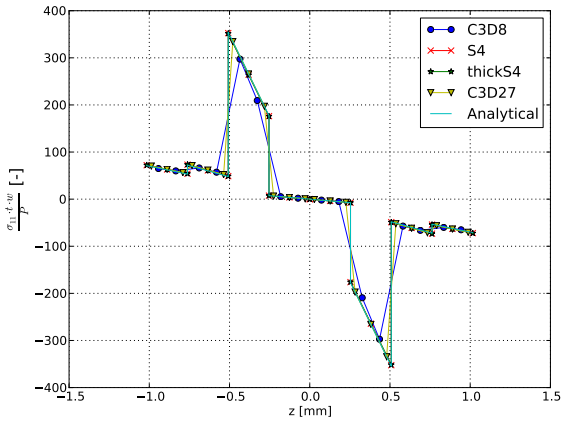

Figure 3.16: Comparison of the distribution of σ_{11} of the different elements with the analytical solution.

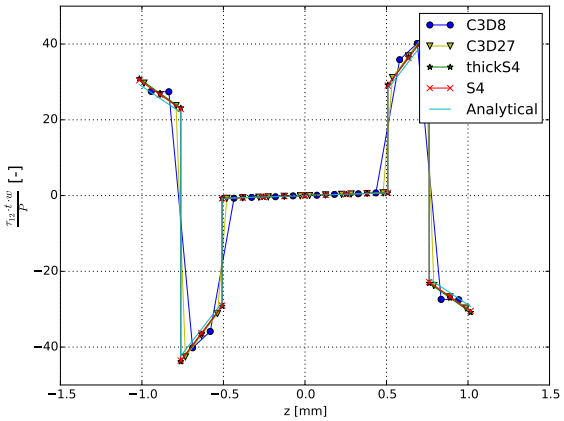

Figure 3.17: Comparison of the distribution of τ_{12} of the different elements with the analytical solution.

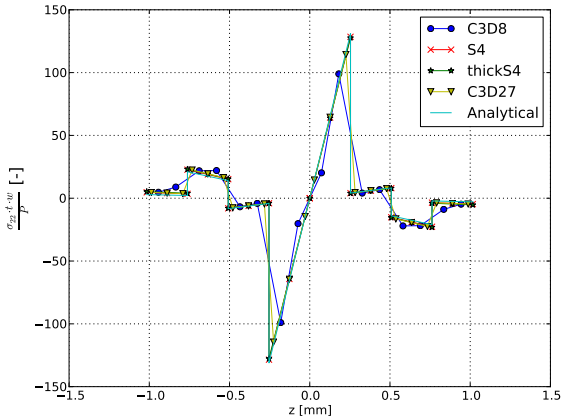

Figure 3.18: Comparison of the distribution of σ_{22} of the different elements with the analytical solution.

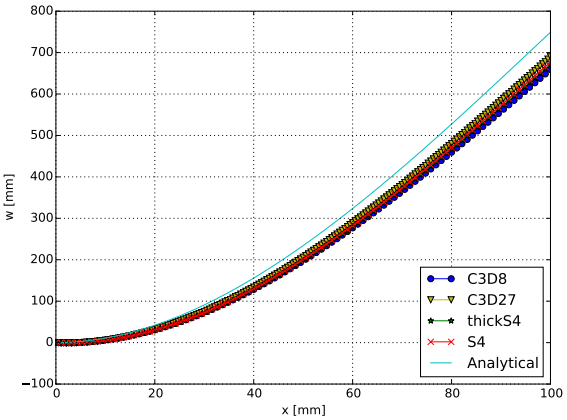

Figure 3.19: Comparison of the distribution of w of the different elements with the analytical solution.

From these figures it can be seen that in all cases the ThickS4 is able to follow the analytical solution near to perfect. The behaviour of the Abaqus C3D8 element in the mesh convergence can be seen that it is a bit off in all cases, which could be due to the special boundary conditions. However the C3D27 element has the same boundary conditions and is able to follow the distribution. From the graph for the displacement it can be seen that the analytical solution is much higher than the displacement for the different elements due to the reason given in the mesh convergence.

3.2.2. Lekhnitskii End Load

As was told before, the Lekhnitskii solution for an end load considers a curved beam with only uni-directional plies in the zero direction, therefore it does not matter whether the stresses are taken in the element coordinate system or the individual ply coordination. For the Lekhnitskii End Load, a mesh and radius convergence

are done. First the results for the mesh convergence are described followed by the radius convergence. The benchmark will be concluded by a distribution comparison of a few of the interesting cases following the radius convergence.

3.2.2.1. Mesh Convergence

The mesh convergence will be done for the three most important stresses σ_{11}, σ_{33} and τ_{13} and the displacement w and can be seen in Figures 3.20 to 3.23 respectively. The starting mesh for the mesh convergence is a mesh with three elements in the curved direction and one element through the depth direction also known as the y-direction. The N_{rate} is the same as in the cantilever beam, the refinement of the total mesh, and thus shows the number in the depth direction.

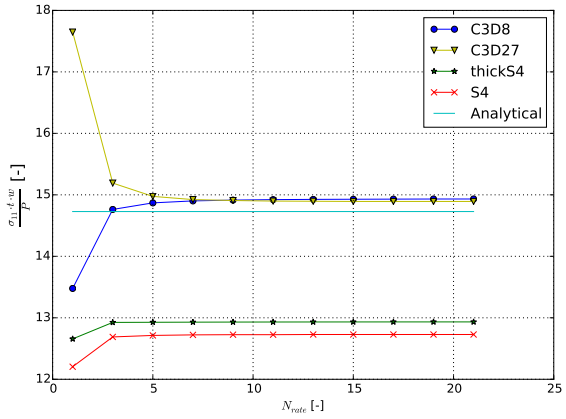

Figure 3.20: Mesh convergence of σ_{11} at the middle of the beam.

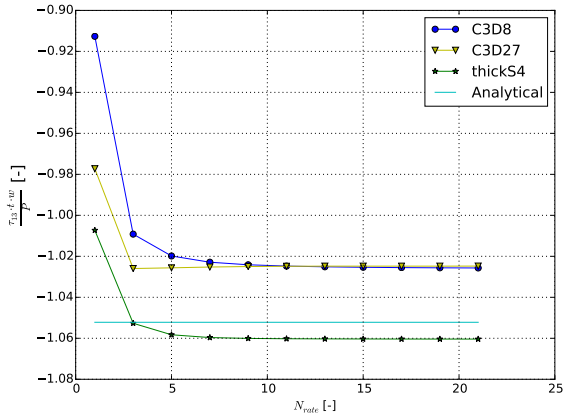

Figure 3.21: Mesh convergence of τ_{13} at the middle of the beam.

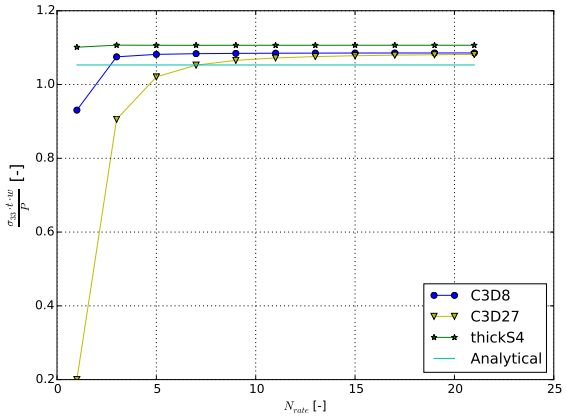

Figure 3.22: Mesh convergence of σ_{33} at the middle of the beam.

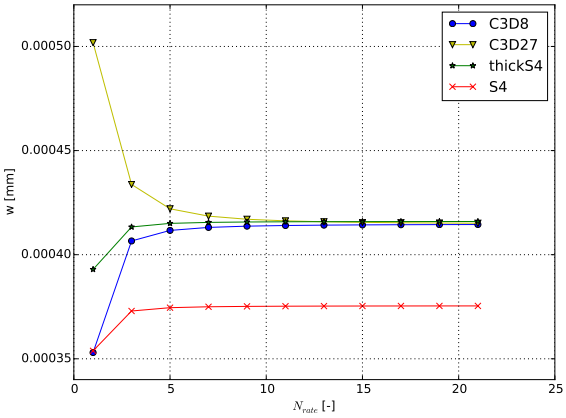

Figure 3.23: Mesh convergence of w at the tip of the beam.

If the convergence is considered the same as before, than the solution of the ThickS4 element converges the quickest for all the stresses. For σ_{11} and τ_{13} convergence is reached for three elements through the width and for σ_{33} already for three elements through the width. The slowest element to converge for this model is the C3D27 Abaqus element, which for the case of σ_{33} does not converge until nine elements through the width. However the C3D27 Abaqus element is faster to converge for the interlaminar shear stress τ_{13} than the other elements. When considering the displacement, all elements are relatively quickly converged with the ThickS4 and the S4 being the quickest.

However when looking at the accuracy of the element after convergence with respect to the analytical solution, it can be seen that for all the elements, the C3D27 Abaqus element is the most accurate for two out of the three stresses, with an error of $e = 0.0116$ for σ_{11}, $e = -0.0261$ for τ_{13} and $e = 0.0271$ for σ_{33}. As can be noticed, in the plots for the out-of-plane stresses, the S4 Abaqus element is not present, as this element is not able to compute out-of-plane stresses. The least accurate element for this case is the S4 Abaqus element for

the in-plane stress σ_{11} with an error of $e = -0.1358$. For the interlaminar normal stress the ThickS4 element is the least well performing with respect to accuracy, though it is the most accurate for the maximum of the interlaminar shear stress τ_{13}. The errors of the ThickS4 are $e = 0.1219$ for σ_{11}, $e = 0.0078$ for τ_{13} and $e = 0.0508$ for σ_{33}. For the displacement it can be seen that the ThickS4 element converges to almost the exact same value as the Abaqus 3D elements, in this case the S4 element has a big difference.

3.2.2.2. Radius Convergence

The radius convergence comparison for the lekhnitskii solution is one of the most important results as this result shows in what range the element can be used. The radius convergence check is done for the case where the thickness is kept constant, as can be seen in Figures 3.24, 3.26, 3.28 and 3.30, and for the case where the radius is kept constant and the thickness is varied as can be seen in Figures 3.25, 3.27, 3.29 and 3.31. The stresses for the convergence are taken at the middle of the curved beam in order to have the least effect of the boundary conditions. The mesh used for the radius convergence is a mesh with 49 elements through the curved direction and 7 element through the width/depth direction.

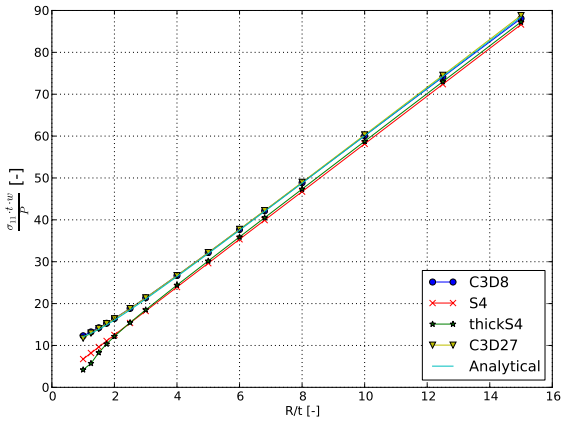

Figure 3.24: Radius convergence of σ_{11} at the middle of the beam with constant thickness.

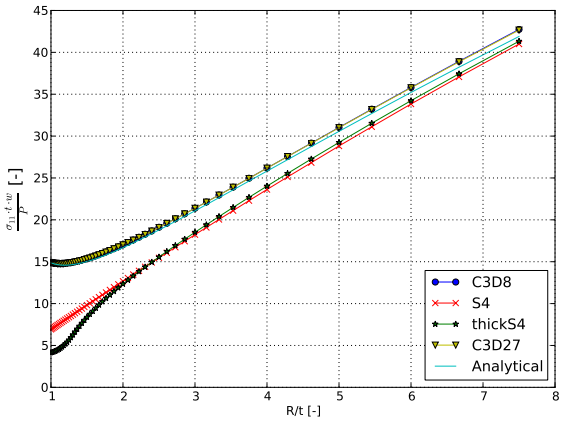

Figure 3.25: Radius convergence of σ_{11} at the middle of the beam with constant radius.

There are a few interesting points to the radius convergence for the in-plane stress σ_{11}. First of all there is the big difference at the most extreme case where $R/t = 1$. In this case, the ThickS4 element is furthest off of all the elements, even further then the regular S4 Abaqus element. This difference of 65% will be shown in the distribution comparison for this case in Figure 3.32 where it will also be explained. The second interesting point on the graph is the point where the line of the ThickS4 element crosses the line of the Abaqus S4 element. This is the radius over thickness ratio from which the ThickS4 element predicts the σ_{11} stress better than the S4 Abaqus element. This is for a radius over thickness ratio of around 2.5 for both convergence cases.

The difference between the two convergence cases can be seen towards the beginning and end of the graph for the convergence with a constant radius. At a low radius over thickness ratio for the constant radius case the graph flattens out for the 3D Abaqus elements and the analytical solution, whereas this does not happen for the S4 Abaqus element and the ThickS4 element. Where the constant thickness case had a difference of 65% for a radius over thickness ratio of $R/t = 1$, the case with a constant radius has a larger difference of 72%. This is probably due to the fact that for the analysis of radius convergence for a constant radius, a larger number of plies is used and thus the element becomes relatively thick.

The second difference is at the largest R/t ratio, where for a constant thickness the 3D Abaqus elements stay close to the analytical solution, which is not the case for a constant radius. For the radius convergence with constant radius, the solutions of the 3D Abaqus elements slowly diverge away from the analytical solution, which is probably due to the fact that for these cases the number of elements through the thickness is reduced and as every ply layer gets assigned one layer of elements, the solution may not be fully converged yet.

Figures 3.28 and 3.29 show the plots for the maximum absolute shear stress τ_{13}. An interesting phenomena can be seen for both the cases of a constant thickness and a constant radius, the solution of the ThickS4 element outperforms the three-dimensional Abaqus elements already for a radius over thickness ratio bigger than $R/t > 2.25$. For the case of a constant thickness, the solution for the ThickS4 element stays almost the

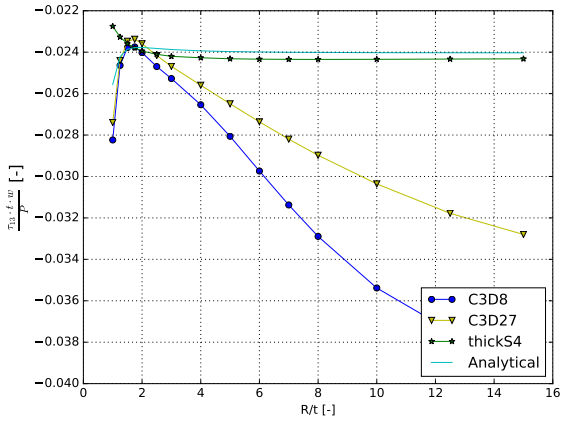

Figure 3.26: Radius convergence of σ_{13} at the middle of the beam with constant thickness.

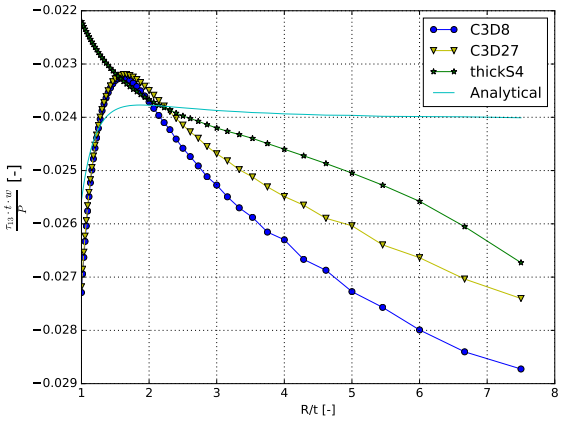

Figure 3.27: Radius convergence of σ_{13} at the middle of the beam with constant radius.

same as the analytical solution and is only about 1.4% off, whereas the solution of the C3D8 is off by 60% for the biggest radius over thickness ratio. In the distribution comparison, the location of the absolute maximum shear stress τ_{13} is discussed.

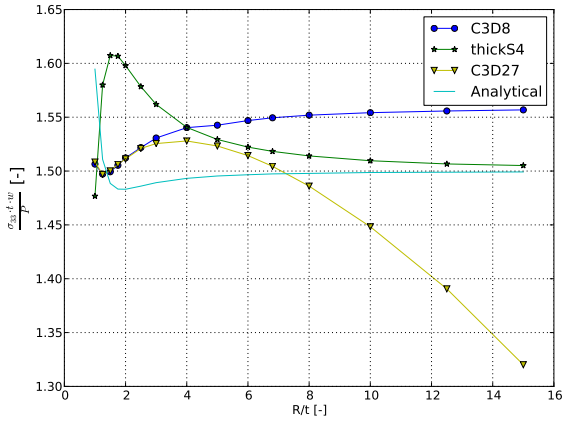

Figure 3.28: Radius convergence of σ_{33} at the middle of the beam with constant thickness.

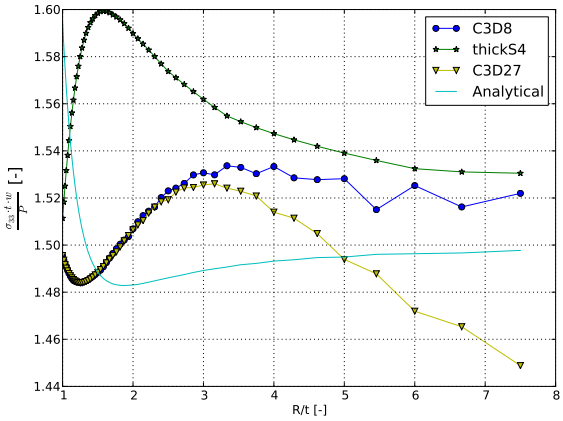

Figure 3.29: Radius convergence of σ_{33} at the middle of the beam with constant radius.

The plots for the maximum σ_{33} stress show that for all R/t ratios the maximum stress is always within 10% of the analytical solution and converges toward to analytical solution as the R/t ratio gets bigger. From these plots it can also be seen that for bigger R/t ratios, the ThickS4 performs better when predicting the maximum σ_{33} than the 3D Abaqus elements for the case of a constant thickness. The Abaqus C3D27 element even diverges away when the R/t ratio gets bigger. This however could be because the number of elements for this analysis is kept constant, therefore when increasing the radius the element size grows and therefore the solution of the C3D27 Abaqus element might not be fully converged yet.

For the case of a constant radius in Figure 3.29 it can be seen that the solution of the C3D8 element in this case seems to be more accurate towards the higher radius over thickness ratios. However as was said before for the in-plane stress σ_{11} it must be noted that due to the fact that there is only one layer of elements for every ply layer, the solution might not be fully converged through the thickness.

Though the maximum σ_{33} is relatively close to the analytical solution and sometimes even better than the 3D Abaqus element, the location of this maximum is not, as can be seen in Figures 3.30 and 3.31. These graphs show that again especially for small R/t ratios the location of the maximum is off by more than 50%. If this factor is taken into account for the working range of the element, and if the location for outperforming one of the 3D Abaqus elements is taken as the criteria than the lower range for the element would be a radius over thickness ratio of 6 (for the case of constant thickness). For the case of a constant radius, this would be

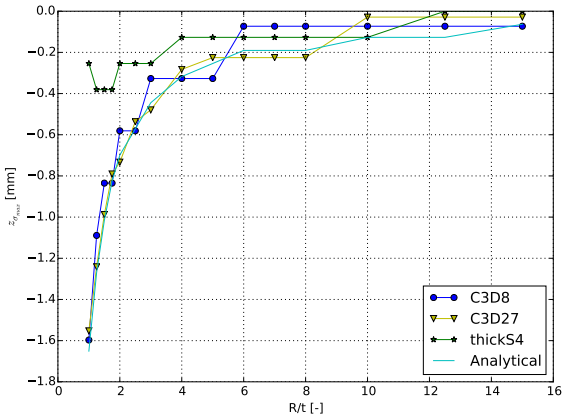

Figure 3.30: Radius convergence of $loc_{\sigma_{33}}$ at the middle of the beam with constant thickness.

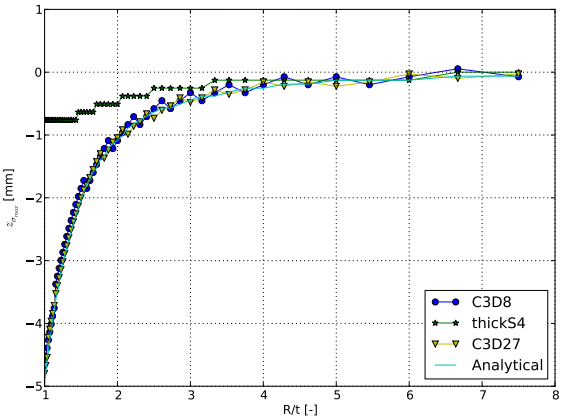

Figure 3.31: Radius convergence of $loc_{\sigma_{33}}$ at the middle of the beam with constant radius.

around a radius over thickness ratio of about $R/t = 5$, as for this ratio the solutions for ThickS4 and analytical show the same maximum location.

3.2.2.3. Distribution Comparison

In this section the distribution comparison of the different elements with respect to the analytical will be shown. These comparisons will be made for the three discussed situations in the radius convergence being $R/t = 1.00$, $R/t = 2.50$ and $R/t = 6.00$, and will be shown in Figures 3.32 and 3.33, Figures 3.34 and 3.35 and Figures 3.36 and 3.37 respectively. The section is finalised by a comparison of the shear stress $\tau 13$ for the radius over thickness ratios of $R/t = 1.00$ and $R/t = 6.00$. For the distribution comparison the same mesh was used as in the radius convergence, thus a 49 by 7 element mesh.

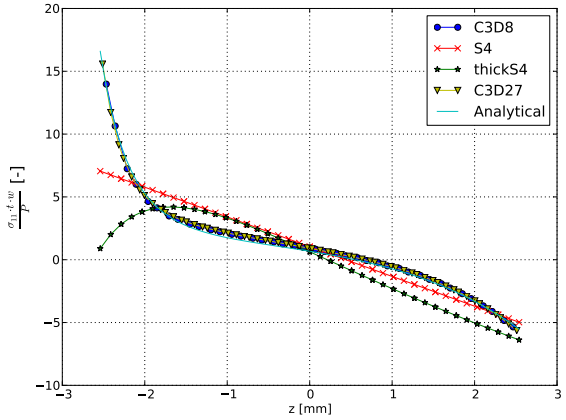

Figure 3.32: Distribution of σ_{11} at the middle of the beam for $R/t = 1.00$.

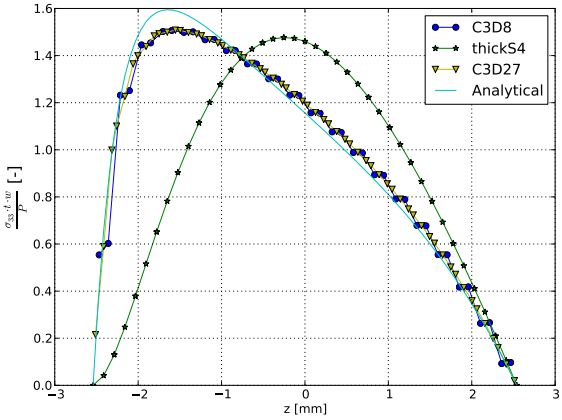

Figure 3.33: Distribution of σ_{33} at the middle of the beam for $R/t = 1.00$.

From Figure 3.32 it can be seen that instead of the expected behaviour of the element to have a peak for σ_{11} at the location of the inner radius, it shows an opposite behaviour. This is considered the biggest disadvantage of the element at the most extreme case of $R/t = 1.00$. Though it was said that the maximum in-plane stress σ_{11} was off by 65%, in Figure 3.32 it can however be seen that this difference is not taken at the same reference location. If it would be, the difference is even higher with a percentile difference of 83%. The same behaviour can be seen in Figure 3.33 where the peak of the graph should be located towards the inner radius, instead it is located near the middle of the laminate. This behaviour could already be seen in Figures 3.30 and 3.31 in the last section. The location of the peak is off by 6 plies. From Figures 3.32 and 3.33 it can be seen though, that for this extreme case, the two 3D Abaqus elements are able to follow the analytical solution quite accurately, though not reaching its maximum σ_{33}.

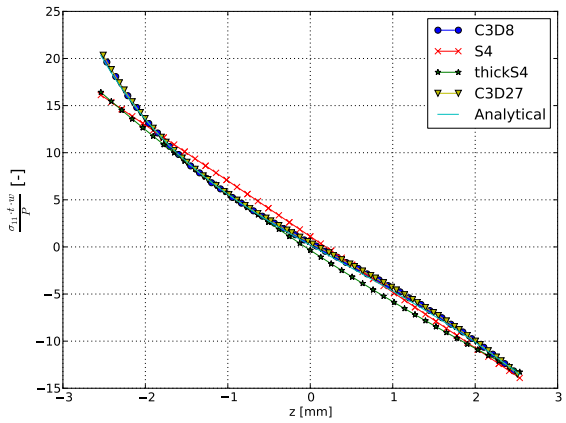

Figure 3.34: Distribution of σ_{11} at the middle of the beam for $R/t =$ 2.50.

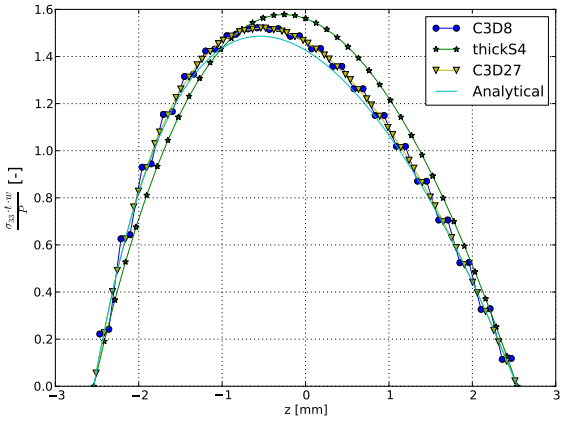

Figure 3.35: Distribution of σ_{33} at the middle of the beam for $R/t =$ 2.50.

As said before, $R/t = 2.50$ is the case where for σ_{11} the ThickS4 element outperforms the S4 Abaqus element. This can be seen in Figure 3.34, however as can be seen, it only just outperforms the S4 Abaqus element and only for the maximum σ_{11}. Also for the minimum σ_{11}, the ThickS4 element predicts the stress better, though the S4 Abaqus element is more conservative and the difference between the two is relatively small, about 5%. If the σ_{33} is considered (Figure 3.35), the distribution of ThickS4 element is still quite off, the location where the maximum should happen is for example still off by 2 plies, though getting closer to the value it should be.

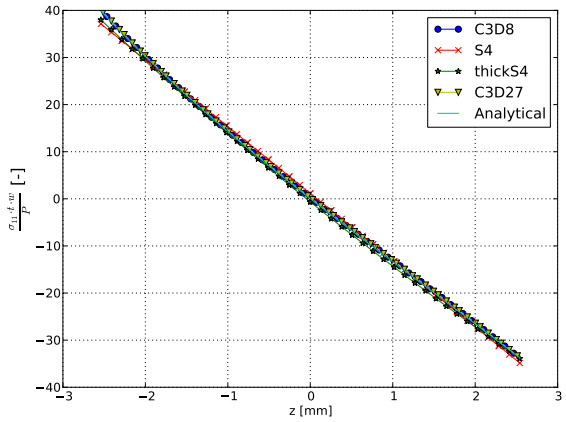

Figure 3.36: Distribution of σ_{11} at the middle of the beam for $R/t =$ 6.00.

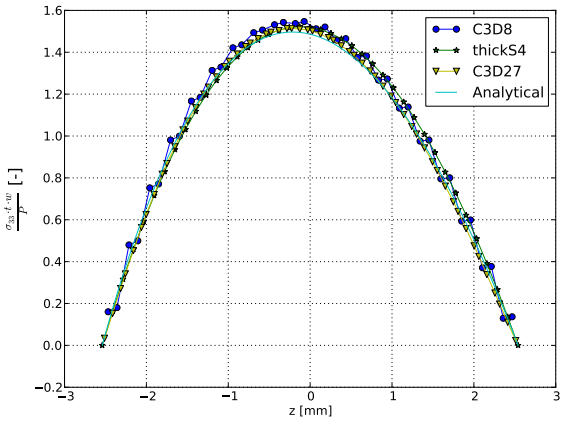

Figure 3.37: Distribution of σ_{33} at the middle of the beam for $R/t =$ 6.00.

The case of $R/t = 6.00$ is the case where the ThickS4 is able to predict the σ_{33} better for the first time than one of the 3D Abaqus elements, in this case the C3D8 Abaqus element as can be seen in Figure 3.37. This is mainly due to the fact that the distribution of the stresses in each C3D8 element is linear and thus not able to give the peak of the highest σ_{33} in the right element. Furthermore the large effect of the curved beam is in this situation not present anymore, the curvature only causes an error for the S4 Abaqus element in σ_{11} of $e = -0.0687$ as can be seen in Figure 3.36. This effect of the curvature decreases even more when increasing the radius over thickness ratio even further as was seen in the section for the radius convergence.

The final distribution comparison for the Lekhnitskii solution due to an end load is the comparison for the interlaminar shear stress τ_{13} and can be seen in Figures 3.38 and 3.39 for the radius over thickness ratios of $R/t = 1.00$ and $R/t = 6.00$ respectively. From the radius convergence it is known that for the smallest radius over thickness ratio, the three-dimensional Abaqus elements were better performing with respect to the maximum absolute τ_{13} for very low radius over thickness ratios and for higher radius over thickness ratios the ThickS4 element was performing better. This can indeed be seen in the distribution comparisons.

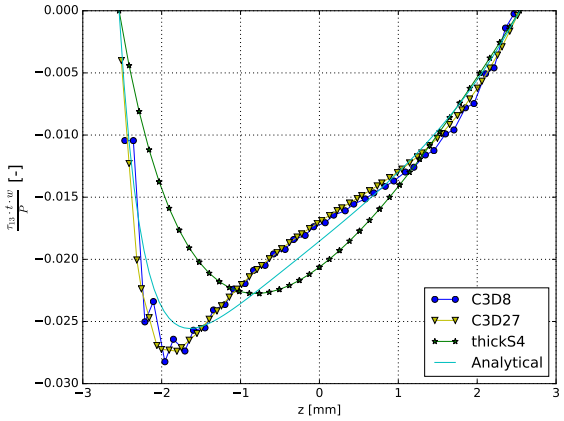

Figure 3.38: Distribution of τ_{13} at the middle of the beam for $R/t =$ 1.00.

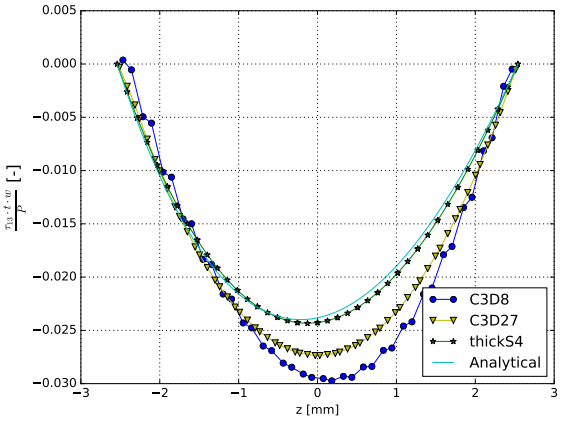

Figure 3.39: Distribution of τ_{13} at the middle of the beam for $R/t =$ 6.00.

In Figure 3.38 the three-dimensional elements are able to follow the analytical solution, though not completely. It can be seen that the peak value is off in both magnitude and location, though not much. Furthermore it can be seen that the ThickS4 is not able to show the expected peak close to the inner radius, though showing a more inward peak than before for the interlaminar normal stress σ_{33}.

For the larger radius over thickness ratio of $R/t = 6.00$, it can be seen that in Figure 3.39 the ThickS4 is able to follow the analytical solution quite accurately, whereas the three-dimensional Abaqus elements are showing a peak which is off in both magnitude and location. The Abaqus elements are showing a peak which is exactly in the middle, or in case of the C3D8 even a bit towards the outer radius. However it must be said that the Abaqus elements are in this case only off by one ply.

3.2.3. Lekhnitskii End Moment

The Lekhnitskii end moment has a mesh convergence which is almost the same as the one for the Lekhnitskii end load and will therefore not be shown and discussed. For the Lekhnitskii subjected to an end moment the radius convergence will be shown, followed by a distribution comparison for the interesting cases following from the radius convergence.

3.2.3.1. Radius Convergence

As for the Lekhnitskii solution with an end load the radius convergence is done for the σ_{11} stress, the σ_{33} and for the location of the maximum σ_{33} stress. The σ_{13} is not checked as this stress is zero for the case of pure bending. Furthermore the cases of constant thickness and constant radius are both plotted again. The cases for the constant thickness in Figures 3.40, 3.42 and 3.44 and the case of constant radius in Figures 3.41, 3.43 and 3.45. The same mesh was taken as for the case of an end load.

The main difference with respect to the Lekhnitskii solution for an end load is that the analytical solution and the solutions of the Abaqus elements vary more or less linearly with the radius over thickness ratio as can be seen in Figures 3.40 and 3.41. The second difference is that instead of at a radius over thickness ratio of 2.5, the ThickS4 performs already better at a ratio of just above 2. Furthermore as was the case in the Lekhnitskii solution for an end load, the same behaviour can be seen towards the higher R/t ratio for the radius convergence with a constant radius. Also in the case of an end moment, the analytical solution tends to get closer to the ThickS4 element instead of the 3D Abaqus elements. The errors for σ_{11} for the most extreme case are for the case where the thickness is kept constant $e = -0.590$ for the ThickS4 and $e = -0.289$ for the S4 Abaqus element. For the case of a constant radius the errors are $e = -0.650$ and $e = -0.364$ for the ThickS4 and S4 Abaqus element respectively. The solution of the three dimensional elements remain within 5% of the analytical solution.

As was the case for the Lekhnitskii solution for an end load, the maximum stress σ_{33} of the ThickS4 element stays close to the analytical solution, for this case even within 5% as can be seen in Figures 3.42 and 3.43. The solution of the ThickS4 also converges towards the analytical solution for larger R/t ratios and outperforms the two 3D Abaqus elements when considering the maximum value of the σ_{33}. Also in the case of an end moment, the C3D27 diverges away from the analytical solution. This is probably again due to the fact

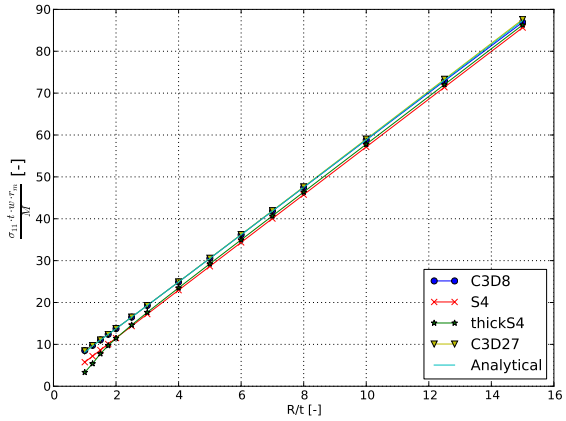

Figure 3.40: Radius convergence of σ_{11} at the middle of the beam with constant thickness.

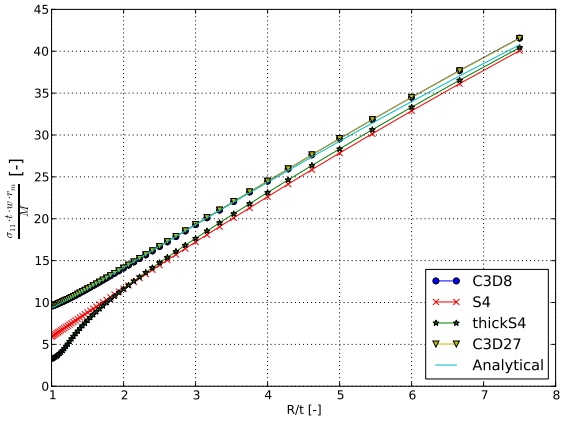

Figure 3.41: Radius convergence of σ_{11} at the middle of the beam with constant radius.

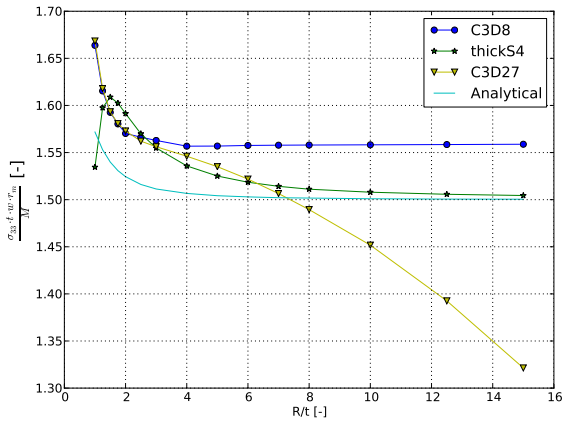

Figure 3.42: Radius convergence of σ_{33} at the middle of the beam with constant thickness.

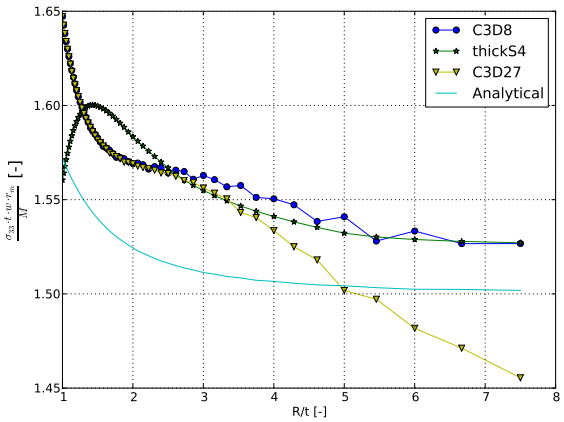

Figure 3.43: Radius convergence of σ_{33} at the middle of the beam with constant radius.

that the C3D27 element needs a denser mesh to have a converged solution and the size of the elements get bigger when taking a larger radius.

There is quite a difference between the radius convergence when the thickness is taken constant with the case where the radius is kept constant for the end moment benchmark. Though the two cases show the same behaviour at the beginning of the plots, the ThickS4 converges slower towards the analytical solution. Furthermore, the solutions of the Abaqus 3D elements show a different behaviour. The C3D27 Abaqus element diverges even quicker from the analytical solution, which is probably due to the fact that there are less elements through the thickness (no full convergence) as was the case for the Lekhnitskii solution to an end load. The C3D8 Abaqus element does not converge to a constant value, as was the case for a constant thickness, instead it decreases slowly, though getting closer to the analytical solution. This might be due to the fact that also for this case the solution is not fully converged.

Though the ThickS4 element outperforms the 3D Abaqus elements with respect to maximum σ_{33}, the location of where this maximum stress happens is far off from the Analytical solution. At the smallest radius over thickness ratio the error for the element is $e = -0.875$ for the case of constant thickness which can be seen in Figure 3.44. This error is equivalent to three plies. Even when taking a larger R/t ratio (except for $R/t = 7.00$ and $R/t = 8.00$) the ThickS4 is not quite able to predict the right location of the maximum stress.

For the case of a constant radius as can be seen in Figure 3.45, the differences are even bigger at the smallest radius over thickness ratio, which in this case means a thick laminate with 60 plies. The maximum location of the solution of ThickS4 element is off by 9 plies, where the Abaqus elements are only off by 1 ply. Even for bigger radius over thickness ratios the ThickS4 is not quite able to predict the right location, though getting closer.

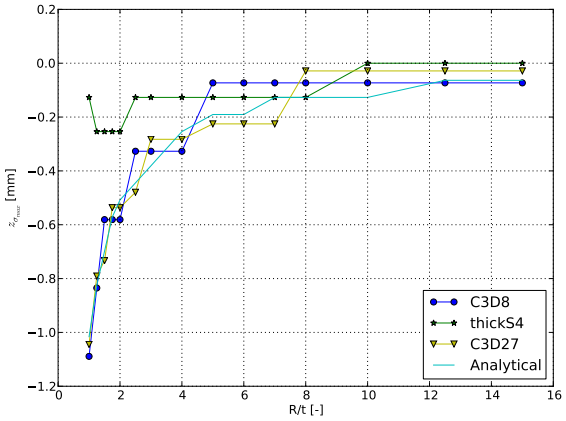

Figure 3.44: Radius convergence of $loc_{\sigma_{33max}}$ at the middle of the beam with constant thickness.

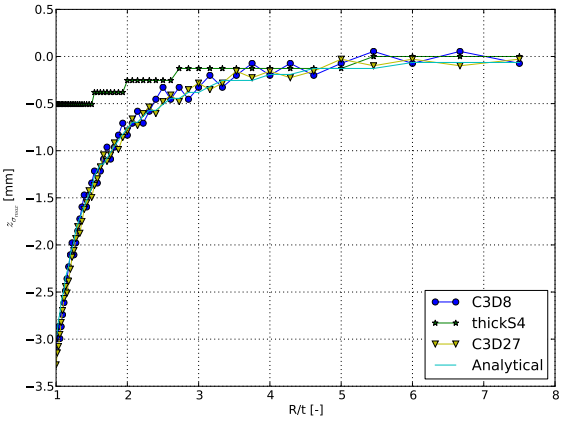

Figure 3.45: Radius convergence of $loc_{\sigma_{33max}}$ at the middle of the beam with constant radius.

3.2.3.2. Distribution Comparison

As for the case of the Lekhnitskii end load are the distributions of the σ_{33} and σ_{11} stresses over the thickness compared for the interesting cases as were specified in the radius convergence. The comparisons are done for $R/t = 1.00$, $R/t = 2.07$, and $R/t = 15.00$ and will be shown in Figures 3.46 and 3.47, Figures 3.48 and 3.49 and Figures 3.50 and 3.51 respectively.

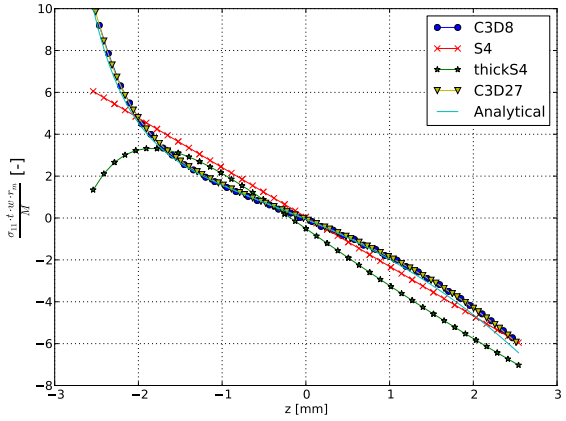

Figure 3.46: Distribution of σ_{11} at the middle of the beam for $R/t = 1.00$ (constant thickness).

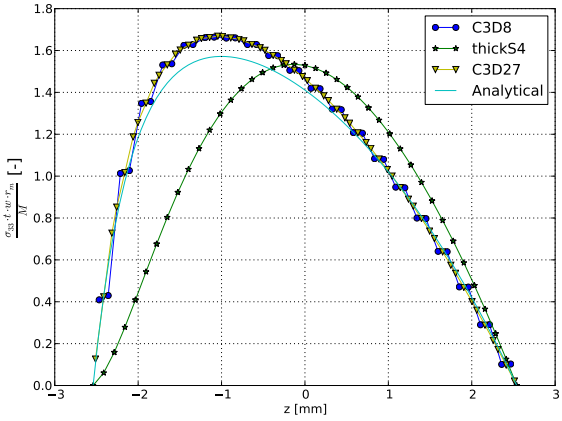

Figure 3.47: Distribution of σ_{33} at the middle of the beam for $R/t = 1.00$ (constant thickness).

The same behaviour as in the Lekhnitskii end load can be seen in the most extreme case where $R/t = 1.00$, the ThickS4 element does the opposite of what it is expected to do. Instead of showing a peak, the σ_{11} reduces towards the inner radius as can be seen in Figure 3.46. Also the graph for the σ_{33} is clearly off. Though the value of the maximum σ_{33} of the ThickS4 element only has an error of $e = -0.02374$, the location of this maximum is off by three plies, equivalent to an error of $e = -0.875$ as said in the radius convergence.

The plot for σ_{11} for a radius over thickness ratio of $R/t = 2.07$ as can be seen in Figure 3.48 shows the same behaviour as the plot did for the case of an end load in Figure 3.34. This is the point where the ThickS4 element starts to outperform the ThickS4 element with respect to predicting the maximum σ_{11}, though the differences are small. As for the σ_{33}, the solution for the ThickS4 is still off, both in maximum stress and in location of this maximum as can be seen in Figure 3.49.

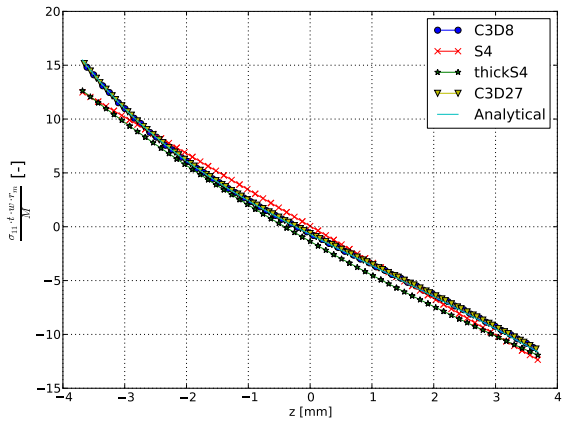

Figure 3.48: Distribution of σ_{11} at the middle of the beam for $R/t =$ 2.07 (constant radius).

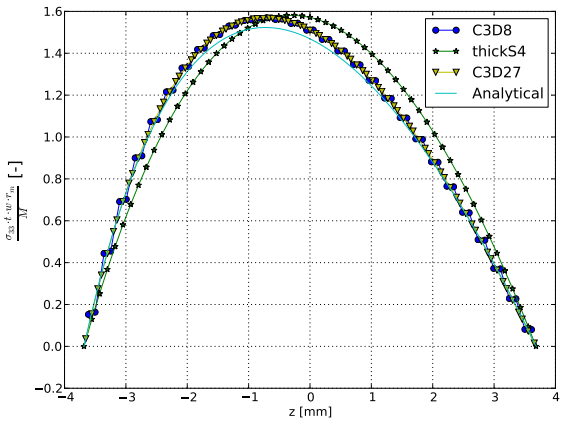

Figure 3.49: Distribution of σ_{33} at the middle of the beam for $R/t =$ 2.07 (constant radius).

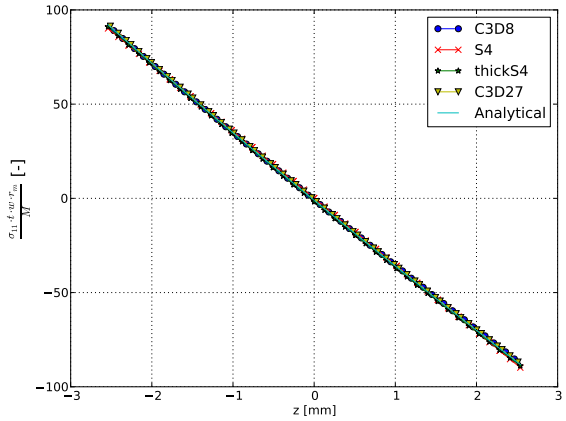

Figure 3.50: Distribution of σ_{11} at the middle of the beam for $R/t =$ 2.07 (constant radius).

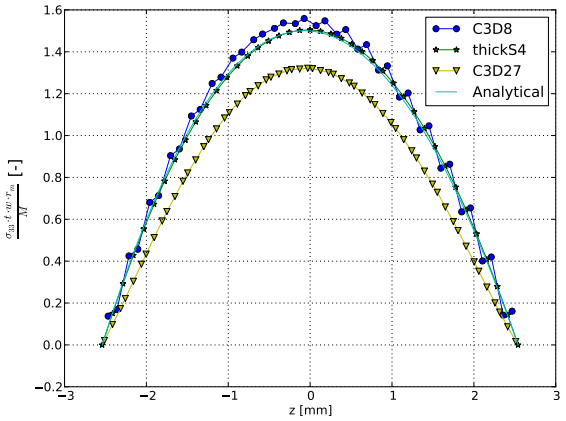

Figure 3.51: Distribution of σ_{33} at the middle of the beam for $R/t =$ 2.07 (constant radius).

In Figures 3.50 and 3.51 it can be seen that for very large radius over thickness ratios, the ThickS4 performs very good. Though for in-planes stresses the element does not outperform the Abaqus S4 element. The biggest benefit in this case is that it is able to give a full 3 dimensional stress state. It can also be seen that in Figure 3.51 the C3D8 element is still able to follow the Analytical solution quite well, whereas the C3D27 Abaqus element does not quite reach the maximum σ_{33} and has an error of $e = -0.1194$, which can however be due to the not fully converged state of the solution.

3.2.4. Multilayer Theory

For the next analytical solution, the Multilayer Theory by Ko and Jackson as described in subsection 2.2.2 is used. As stated earlier in the description of the benchmark test, the analysis will be done for the case as described in the article of Ko and Jackson as well as for a case of one of the cases for which the optimisation is done. The section is finalised by a short stacking sequence investigation in order to test a few extreme cases.

3.2.4.1. Article Ko and Jackson

The article of Ko & Jackson analyses a stacking sequence of $[0^\circ_{25}/+15^\circ/-15^\circ/-15^\circ/+15^\circ/0^\circ_{25}]$ and a curved beam structure as described in subsection 3.1.2. For this model a mesh convergence will be done, to see how the element performs with respect to the Abaqus elements. Furthermore the outcome of the mesh convergence is used to get the right element density for the comparison of the distribution of the stresses over the thickness.

Mesh Convergence

The mesh convergence for this structure is done for the three relevant stresses σ_{11}, τ_{13} and σ_{33} as well as for the displacement at the location where the load is introduced (the root of the beam). For the mesh convergence, the stresses are extracted at the middle row of elements of the beam in case of three dimensional elements or middle element of the beam in case of a two dimensional element. This is done in order to minimise the influence of the boundary conditions. The stresses extracted are the global element stresses as the analytical solution is in this same configuration. The plots for the mesh convergence for σ_{11}, τ_{13}, σ_{33} and w are shown in Figures 3.52 to 3.55 respectively. The mesh convergence is only shown for the case of an end load as the convergence for the case of an end moment is rather similar. The starting mesh of the mesh convergence is a three by one mesh, the N_{rate} shown in the plots refer to the amount of elements in the width direction, which is the y-direction in this case.

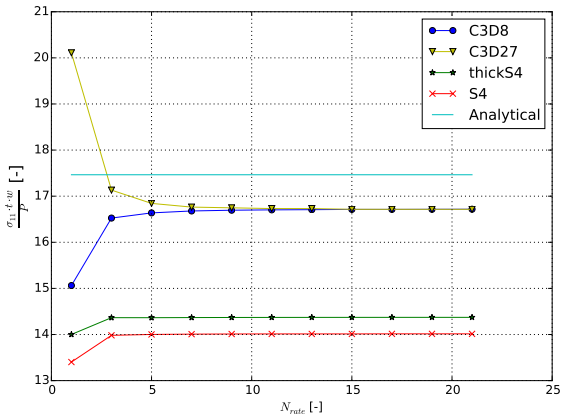

Figure 3.52: Mesh convergence of σ_{11} at the middle of the beam.

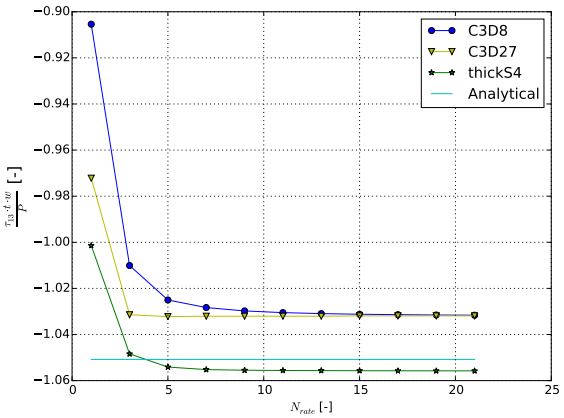

Figure 3.53: Mesh convergence of σ_{13} at the middle of the beam.

As in the previous benchmarks, if a denser mesh results in a change which is less than 1%, the solution is considered to be converged. Considering this, the solutions of all elements except for the Abaqus C3D27 element are converged for the σ_{11} with three elements through the width as can be seen in Figure 3.52. Though the differences are small, the ThickS4 element converges the quickest. For the case of the out-of-plane shear stress τ_{13}, as can be seen in Figure 3.53, the C3D27 Abaqus element outperforms the two other elements though the difference with the ThickS4 element is only minor. The solutions for the C3D27 Abaqus element and the ThickS4 element are already converged for three elements through the width whereas the C3D8 Abaqus element needs five elements.

Considering the accuracy and taking the analytical solution as a reference, the Abaqus 3D elements do perform the best with both an error of $e = -0.0429$ for σ_{11}. However, the ThickS4 element does outperform the Abaqus S4 element with errors of $e = -0.1771$ and $e = -0.1976$ respectively. If the stress τ_{13} is considered, the ThickS4 element is the most accurate in comparison with the analytical solution with an error after convergence of only $e = 0.0047$, the two Abaqus elements are a bit further off, though not much, having errors of $e = -0.0182$ and $e = -0.0180$ for the solutions of the Abaqus C3D8 and the C3D27 element respectively.

A similar behaviour as for the in-plane stress σ_{11} can be seen in Figure 3.54 for the σ_{33} stress as for the previous stresses, the solution of the C3D27 Abaqus element converges the slowest and requires nine elements through the width. The ThickS4 element is the quickest to converge with only one element through the width, whereas the Abaqus C3D8 element requires three elements. Not many differences can be seen when looking at the convergence of the displacement w in Figure 3.55, the two three dimensional Abaqus element need five elements through the width and the ThickS4 element and the Abaqus S4 element need three elements.

Though converging the slowest, the solution of the C3D27 Abaqus element is the most accurate with an error of $e = 0.0197$. However the differences are small with an error of $e = 0.0239$ for the Abaqus C3D8 elements and an error of $e = 0.0452$ for the ThickS4 element. For the displacement it can be seen that the two 3D Abaqus elements and the ThickS4 element are very accurate as they have an error of only $e = 0.0079$ for the solution of the C3D8 Abaqus element and $e = 0.0062$ for solutions the C3D27 Abaqus and the ThickS4 element. The error of the solution of the Abaqus S4 element is relatively large and found to be $e = -0.1047$.

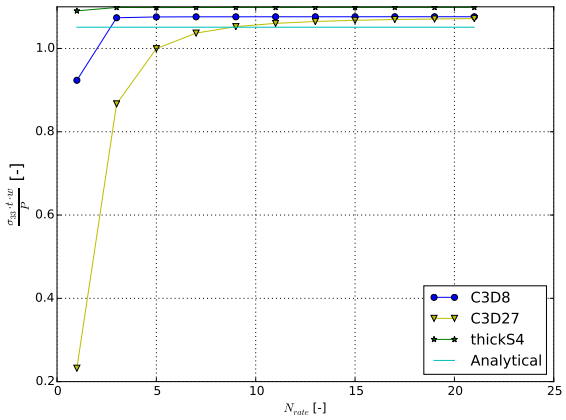

Figure 3.54: Mesh convergence of σ_{33} at the middle of the beam.

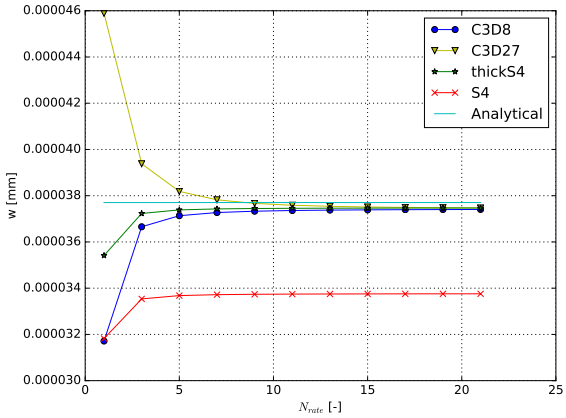

Figure 3.55: Mesh convergence of w at the beginning of the beam.

Distribution Comparison for End Load

For the distribution comparison a dense enough was used of 33 by 11 elements. The same variables will be checked as was done for the mesh convergence. Also in this case the element stresses are extracted at the middle of the beam at all integration points of the element. The plots of the stresses σ_{11}, τ_{13} and σ_{33} are shown in Figures 3.56, 3.58 and 3.60 respectively.

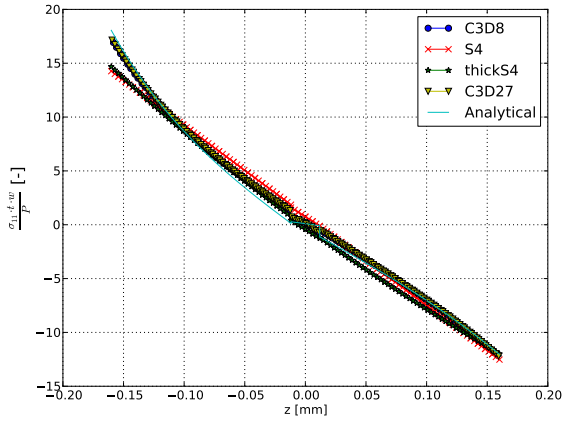

Figure 3.56: Distribution comparison of σ_{11} at the middle of the beam.

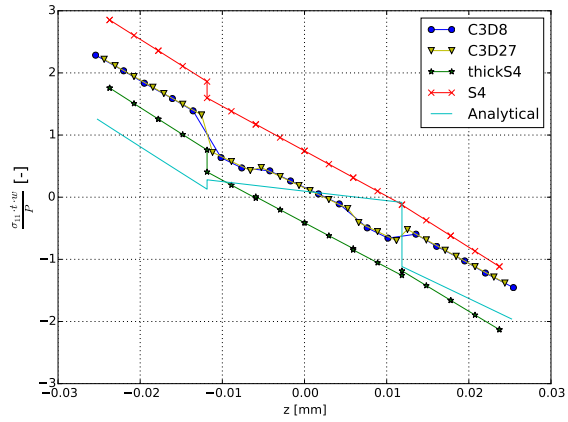

Figure 3.57: Close-up distribution comparison of σ_{11} at the middle of the beam.

In the distribution of σ_{11} over the thickness of the laminate it can be seen in Figure 3.56 that close to the inner radius the behaviour of a higher peak as seen before in the lekhnitskii is visible again. As was the case for the lekhnitskii benchmark, the ThickS4 and the Abaqus S4 element are not able to follow this behaviour, though the ThickS4 is able to follow the behaviour better than the Abaqus S4 element. The interesting zone is the middle of the laminate where the ±15 plies are located. A close-up of this section can be seen in Figure 3.57.

When looking at the zoomed in section, it can be seen that for this section and especially at the location ±15° plies, the analytical solution is quite off from the solution of the elements. Not only are the values off, also the slope of the solution in this point is very different. It could however be argued that this is a discrepancy in the analytical solution, as for a change of only 15° one would not expect such a big difference in the slope of the solution.

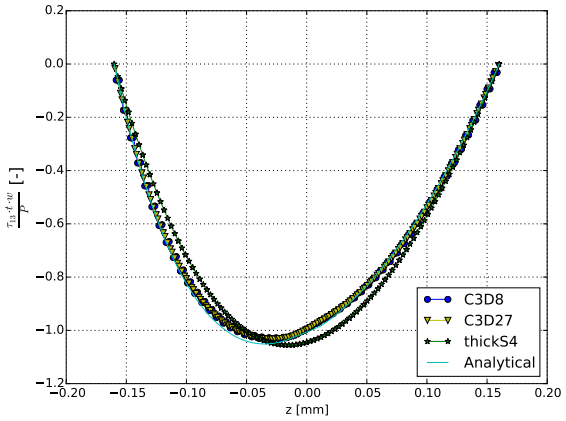

Figure 3.58: Distribution comparison of τ_{13} at the middle of the beam.

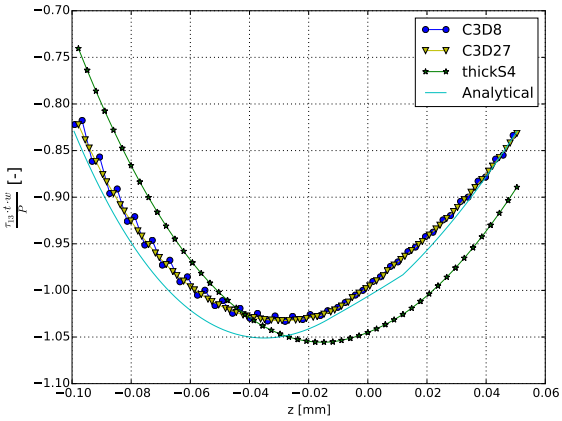

Figure 3.59: Close-up distribution comparison of τ_{13} at the middle of the beam.

For the shear stress τ_{13} the distribution of the thee dimensional elements are similar to the analytical solution as can be seen in Figure 3.58. It can also be seen that the ThickS4 element is quite off when it comes the location of the minimum τ_{13} though being quite correct when it comes to the magnitude of this minimum. Furthermore in the close-up section of τ_{13} as shown in Figure 3.59, it can be seen that indeed the general distribution of the Abaqus 3D elements are quite accurate, though not showing the same behaviour as the analytical solution when it comes to the location of the $\pm 15°$ plies. Neither can this behaviour been seen in the solution of the ThickS4 element.

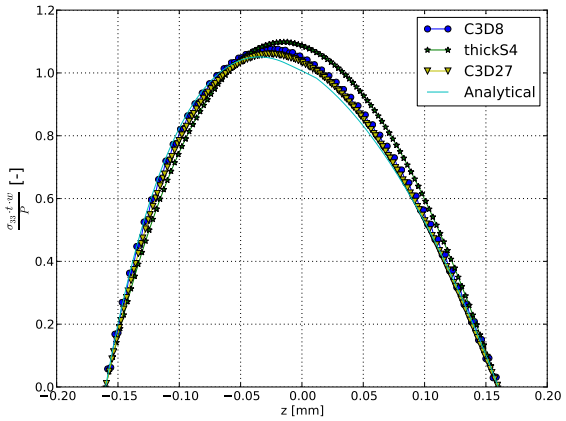

Figure 3.60: Distribution comparison of σ_{33} at the middle of the beam.

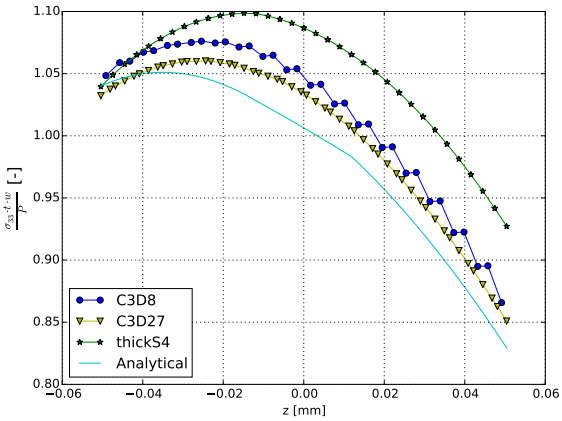

Figure 3.61: Close-up distribution comparison of σ_{33} at the middle of the beam.

In case of the interlaminar normal stress σ_{33} the Abaqus 3D elements follow the analytical solution less good than for the interlaminar shear stress τ_{13}, especially in the region of the ± 15 plies for which a close-up can be seen in Figure 3.61. It can also be seen that the maximum location of the σ_{33} stress is off by 0.0112 inch and as one ply is 0.00593 inch, this is equivalent to 2 plies. For the ThickS4 element this discrepancy is even bigger with a difference of 4 plies. The reason why the analyses of the structure with the elements do not show the same behaviour as the analytical solution could be because the number of plies in the ± 15 direction is only 4 out of a total number of 54. Therefore there are only 3.7% of all plies in these directions (being a small angle of $15°$ and thus not changing too much to the total stiffness of the structure).

Distribution Comparison for End Moment

For the case of the curved beam subjected to an end moment the distribution of the σ_{11} and σ_{33} stresses are analysed and can be seen in Figures 3.62 and 3.63 respectively. The interlaminar shear stress τ_{13} is not shown as in the case of pure bending, the τ_{13} should be zero.

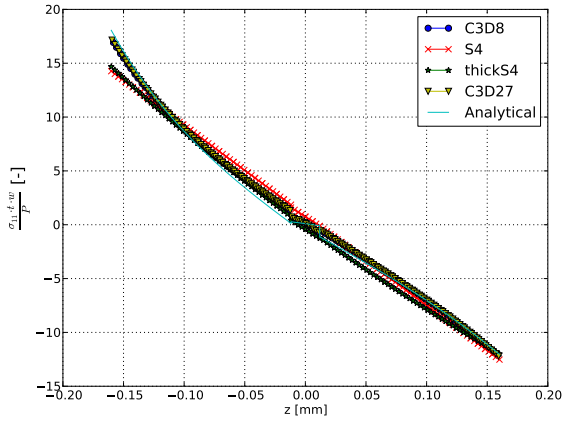

Figure 3.62: Distribution comparison of σ_{11} at the middle of the beam.

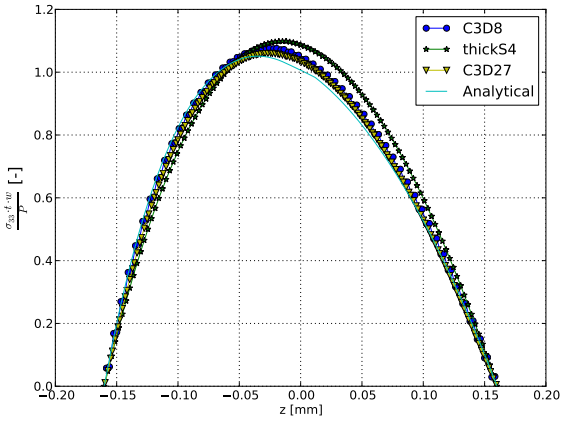

Figure 3.63: Distribution comparison of σ_{33} at the middle of the beam.

The discrepancies in the distribution over the thickness is very similar to the case of the end loads. This is why these discrepancies will not be discussed again. The errors with respect to the analytical solution for the elements turned out to be $e = 0.0148$, $e = 0.0152$, $e = -0.0770$ and $e = -0.1075$ for the σ_{11} stress for the C3D8, C3D27, ThickS4 and S4 element respectively. For the σ_{33} the errors were found to be $e = 0.0355$, $e = 0.0303$ and $e = 0.0335$ for the elements C3D8, C3D27 and ThickS4 element respectively.

3.2.4.2. Other Layups

In this section the same multilayer theory is applied to the same structure, however with different stacking sequences than discussed in the article by Ko and Jackson. Investigations are done for the mesh convergence, radius convergence and distribution comparison for the stacking sequence of $[[-45,45,0,90]_3]_s$. This is followed by an investigation of the interesting stresses σ_{33}, τ_{13} and τ_{23} for a couple of different layups, the material used is the same as used for the cantilever beam as given in subsection 3.1.1.

Mesh Convergence

The mesh convergence for the multilayer theory for a different stacking sequence is shown for only the case of an end load, due to the fact that the results for an end moment are very similar and thus not of interest. The mesh convergence has been done for the case the stresses σ_{11}, σ_{22}, τ_{13} and σ_{33} and are shown in Figures 3.64 to 3.67 respectively. The stresses for the convergence are the stresses taken at the middle of the beam and are the global element stresses. The mesh convergence has been done for a structure with an average radius of $R = 15.24$ resulting in a radius over thickness ratio of $R/t = 2.5$. As was the case for the other regular multilayer theory benchmark, the starting point for the mesh convergence is a three by one mesh.

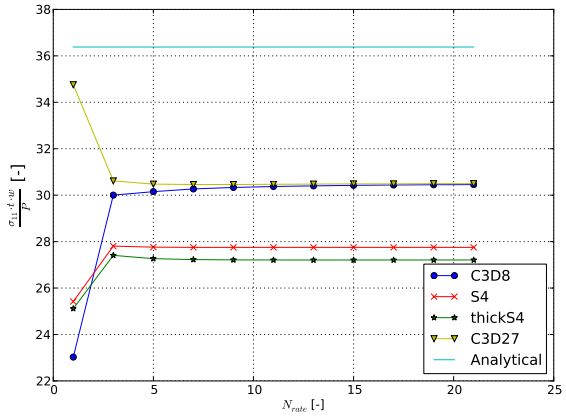

Figure 3.64: Mesh convergence of σ_{11} at the middle of the beam.

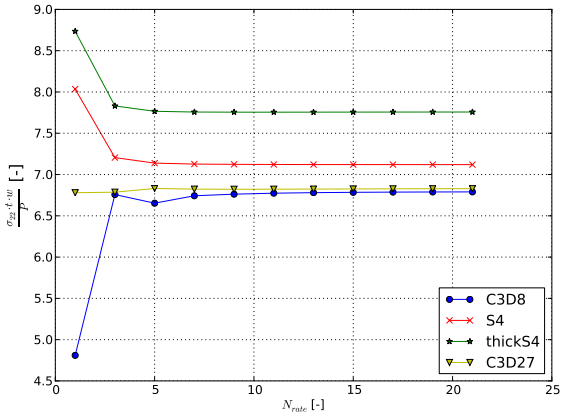

Figure 3.65: Mesh convergence of σ_{22} at the middle of the beam.

The solutions of all elements are already converged at three elements through the width for σ_{11} as for the next refinement the change in stress is less than 1% for all elements. This is however not the case for σ_{22} where all but the Abaqus C3D8 element are converged at three elements through the width whereas the Abaqus C3D8 element requires seven elements. When considering the accuracy, it is the question whether the analytical solution is that accurate, as the solution for all the elements is far off from this analytical solution. When the solutions would be compared to the analytical solution, it would lead to errors of $e = -0.1629$, $e = -0.1618$, $e = -0.2521$ and $e = -0.2372$ for the C3D8, C3D27, ThickS4 and S4 element respectively. From this it can however be seen that the ThickS4 is the furthest off of all. Though there is no analytical solution for the σ_{22} stress, it can be seen that from the four solutions of the elements, the ThickS4 is clearly the outlier.

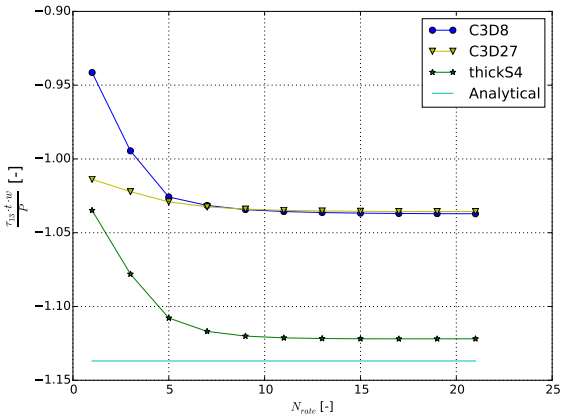

Figure 3.66: Mesh convergence of τ_{13} at the middle of the beam.

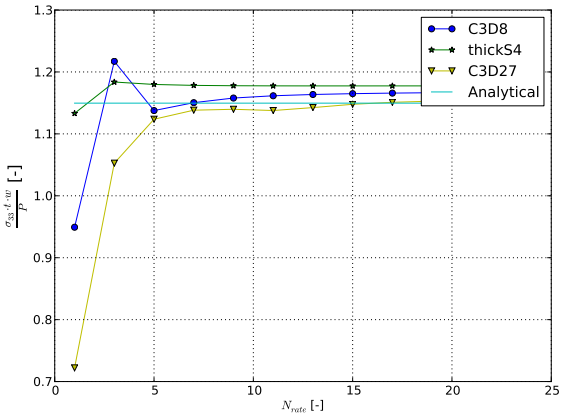

Figure 3.67: Mesh convergence of σ_{33} at the middle of the beam.

Though that in almost all other cases the ThickS4 element was the element to converge the fastest for the out-of-plane stresses, for the interlaminar shear stress τ_{13} of this configuration the ThickS4 element is the slowest. The ThickS4 element needs seven elements through the width as does the C3D8 Abaqus element. The C3D27 Abaqus element is already converged with three elements through the width. However when considering the case of the interlaminar normal stress σ_{33}, the ThickS4 element is the fastest to converge. The ThickS4 element needs five elements through the width, where the three dimensional Abaqus element both need nine elements through the width.

If the analytical solution is taken as the reference solution, the ThickS4 element is the most accurate for the τ_{13} stress with an error of only $e = -0.0132$, where the Abaqus C3D8 and C3D27 elements have errors of $e = -0.0878$ and $e = -0.0891$ respectively. For the σ_{33} stress the Abaqus C3D27 is the most accurate with an error of $e = 0.0037$ and the ThickS4 element is the least accurate, though not far off, with an error of $e = 0.0243$.

Radius Convergence for End Load

As was the case for the Lekhnitskii benchmark, also for the benchmark of the multilayer theory with a different layup a radius convergence is done. The difference though is that in this case in order to keep the in-plane properties the same, no radius convergence could be done where the radius was kept constant and the thickness was changed. The radius convergence for the case of an end load is shown for the four most interesting variables being the maximum values of the stresses σ_{11}, τ_{13} and σ_{33}, and the location of the maximum stress of σ_{33} and are shown in Figures 3.68 to 3.71 respectively.

From Figure 3.68 it can be seen that for the configuration used, the analytical solution is far off from the solution of the four elements. However, though not clearly visible in this graph, the solutions of the Abaqus elements are less than a half percent off from one another, whereas the ThickS4 element is off by more than 22% from the Abaqus solutions at a radius over thickness ratio of $R/t = 1$. When increasing the radius over thickness ratio, the solution of the ThickS4 element converges towards the solution of the Abaqus S4 element and is within 1% at a radius over thickness ratio of $R/t = 3.25$.

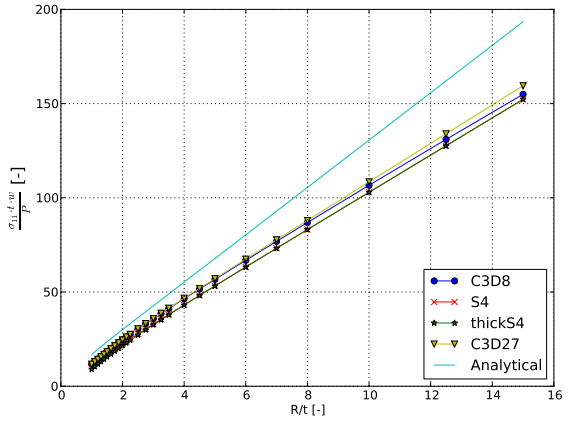

Figure 3.68: Radius convergence of the maximum σ_{11} at the middle of the beam.

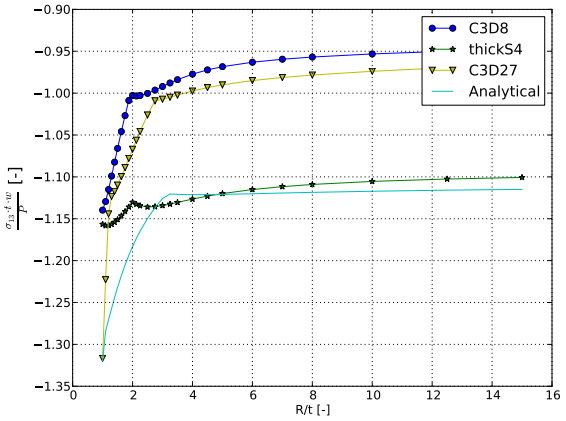

Figure 3.69: Radius convergence of the maximum τ_{13} at the middle of the beam.

Considering the more interesting out-of-plane shear stress τ_{13} it can be seen in Figure 3.69 that for almost all radius over thickness ratios, the ThickS4 element is the closest to the analytical solution. However it must be noted that this analytical solution has only been tested for the stacking sequence as described in the article of Ko & Jackson and therefore taking the analytical solution as a reference is not entirely valid. It can however be seen that the two Abaqus element show a similar convergence behaviour as the ThickS4 element after a radius over thickness ratio of about $R/t = 3.5$.

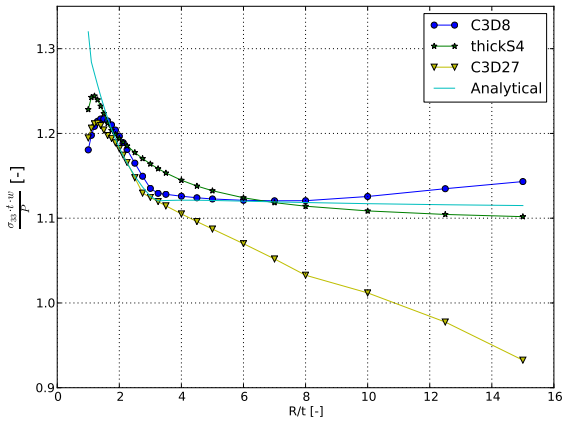

Figure 3.70: Radius convergence of the maximum σ_{33} at the middle of the beam.

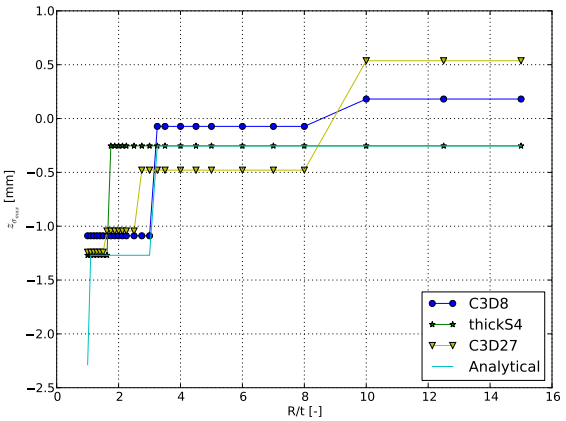

Figure 3.71: Radius convergence of the location of the maximum σ_{33} at the middle of the beam.

The next interesting stress result is the one of the maximum interlaminar normal stress σ_{33} and its location. From the graph in Figure 3.70 it can be seen that when taking the analytical solution as a reference the Abaqus C3D8 element is the closest until a radius over thickness ratio of $R/t = 8$. Furthermore it can be seen that the C3D8 elements' location of this maximum σ_{33} stress has the same behaviour of the one of the analytical solution. The difference seen in Figure 3.71 is due to the fact that the C3D8 Abaqus element has linear distribution between the two interpolation points. If the average would be taken, the C3D8 and the analytical solution would be spot on.

From the radius convergence graphs of the interlaminar normal stress σ_{33} it can also be noted that though not entirely following the trend of the analytical solution, the ThickS4 element is also within 7% of the analytical solution and even outperforming the C3D8 element after a radius over thickness ratio bigger than $R/t = 10$. This however is probably due to the fact that the ThickS4 element has a better convergence for larger elements. Furthermore it can be seen that for a R/t ratio smaller than or equal to 1.625 and bigger than or equal to 3.25 the ThickS4 element is able to predict the maximum location as well. However it must be noted that the analytical solution has not been verified for different layups and it may be wiser to take the

solution of the Abaqus element as being correct, as these elements are verified and validated.

Radius Convergence for End Moment

The radius convergence of the same structure subjected to an end moment showed nothing interesting for the in-plane stress σ_{11}, which is why these results are left out. Furthermore in a case of pure bending, no interlaminar shear stress should appear. Though not living in a perfect world, the interlaminar shear stresses are more than one magnitude lower than the interlaminar normal stresses and thus not interesting either. Therefore for the case of an end moment the radius convergence for the maximum σ_{33} stress and its location are shown in Figures 3.72 and 3.73 respectively.

The multilayer theory for a curved beam solution subjected to an end moment did not work for other stacking sequences than for the one provided in the article of Ko & Jackson, therefore there is no analytical solution present in this radius convergence. In this radius convergence, the solution of the ThickS4 element is compared to the solution of the two three-dimensional Abaqus elements.

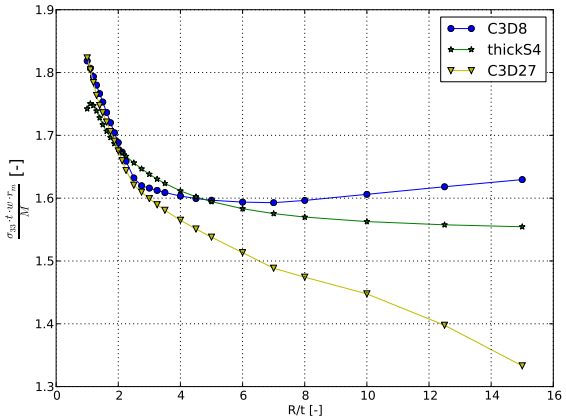

Figure 3.72: Radius convergence of the maximum σ_{33} at the middle of the beam.

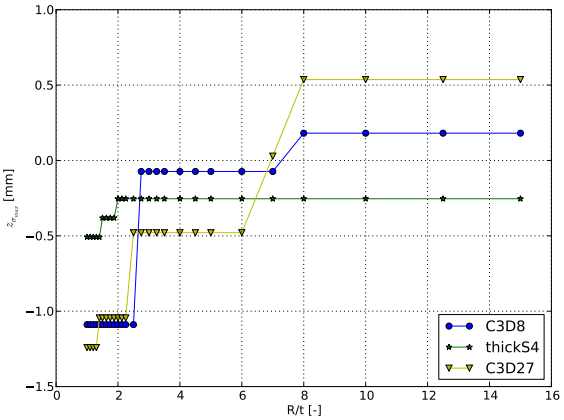

Figure 3.73: Radius convergence of the location of the maximum σ_{33} at the middle of the beam.

A similar behaviour can be seen for the solution for σ_{33} of the three elements when comparing to the case of an end load, though there are minor differences for the radius convergences of the curved beam subjected to an end moment. First of all in Figure 3.72 it can be seen that for the lowest radius over thickness ratios, the two 3D Abaqus elements do not have the same kink downward as was the case for the radius convergence for the curved beam subjected to an end load (Figure 3.70). In the end load case it could also be seen that the analytical solution did not have this kink either and therefore if the analytical solution for the end moment case would have worked, the solutions of the two Abaqus elements would probably have been closer to it than before. The second major difference visible is in the graph for the location of the maximum σ_{33} in Figure 3.73. In the plot it can be seen that the ThickS4 element does not show the same behaviour as in the end load case, where the element showed a correct maximum location for a range of low radius over thickness ratios. This behaviour will be further shown in the distribution comparison in the next section.

Distribution Comparison

In this section the distribution of the stresses over the thickness will be compared of the different elements. This is done for several interesting cases as were identified in the radius convergence for the end load and the end moment. These interesting cases include the difference in the in-plane stress σ_{11} with the analytical solution for a small and larger radius over thickness ratio as can be seen in Figures 3.74 and 3.75. Furthermore it shows the difference between the distributions of the out-of-plane stresses for the case of an end moment for a radius over thickness ratio of $R/t = 1$ and $R/t = 4$ in Figures 3.76 and 3.77 respectively. The distribution of the interlaminar normal stress σ_{33} for an end moment at the smallest radius over thickness ratio can then be compared to the σ_{33} for the case of an end load in Figure 3.79. Finally the change in distribution due to different radius over thickness ratios can be seen in Figures 3.78 to 3.85.

In both the graphs for the in-plane stress σ_{11}, Figures 3.74 and 3.75, the big difference between the solution of the elements and the analytical solution can be seen. For the smallest radius over thickness ratio, the analytical solution shows an unexpected distribution. Though a higher peak is expected, the solutions is

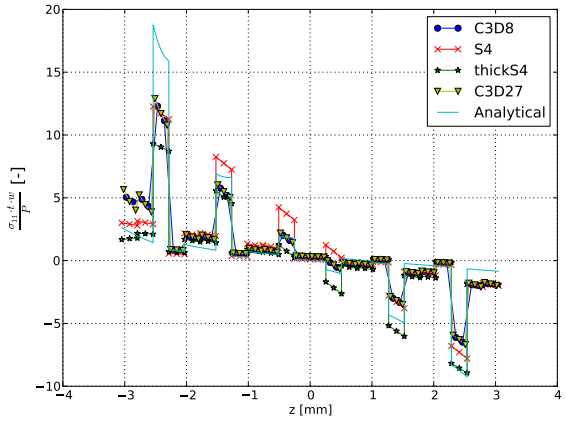

Figure 3.74: Distribution comparison of σ_{11} over the thickness of the laminate at the middle of the beam for $R/t = 1$ in case of an end load.

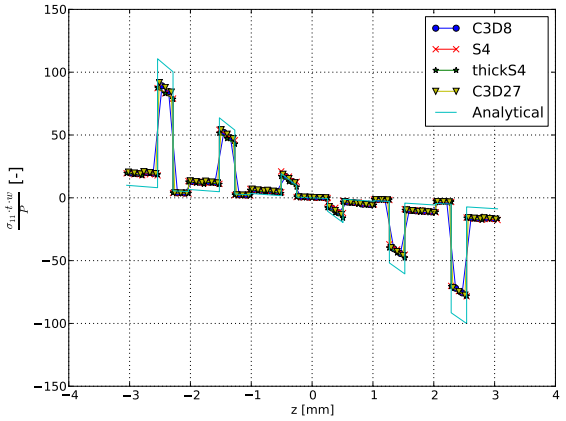

Figure 3.75: Distribution comparison of σ_{11} over the thickness of the laminate at the middle of the beam for $R/t = 8$ in case of an end load.

also expected to have a fluent distribution throughout the thickness (for plies in the same direction), which it does have for the bigger radius over thickness ratio. Furthermore for the solution of the ThickS4 element the same behaviour can be seen as was already the case in the Lekhnitskii benchmark. Instead of showing a peak, as the two three dimensional Abaqus elements show, the solution does the opposite. In this case the regular Abaqus S4 is better able to predict the highest stress and is on average for the maximum ply is within 1% from the three dimensional Abaqus solutions. The Abaqus S4 element however does overestimate the stresses for the more outer plies, when comparing to the 3D Abaqus elements. In the case of the case of the largest radius over thickness ratio, the solution of the four elements for the most important peaks differs less than 5%.

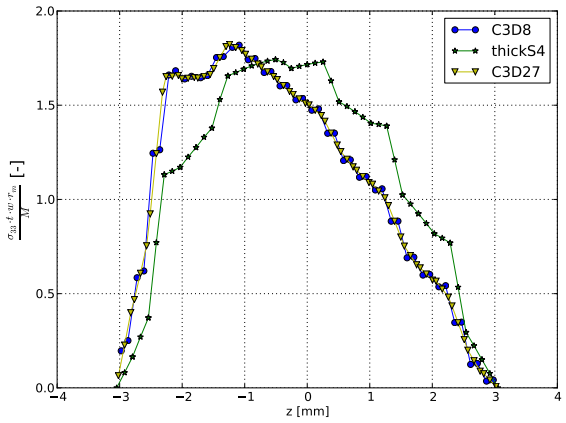

Figure 3.76: Distribution comparison of σ_{33} over the thickness of the laminate at the middle of the beam for $R/t = 1$ in case of an end moment.

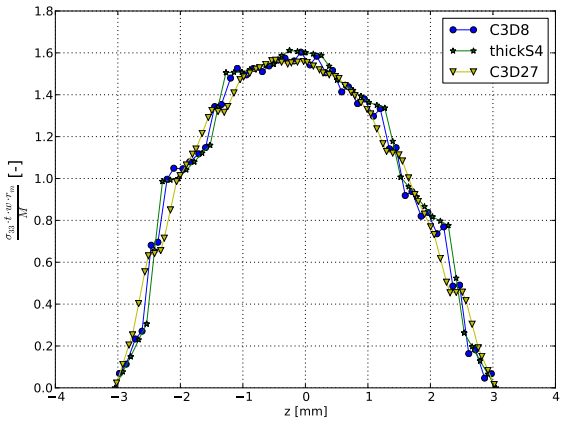

Figure 3.77: Distribution comparison of σ_{33} over the thickness of the laminate at the middle of the beam for $R/t = 4$ in case of an end moment.

In Figure 3.76 it can indeed be seen that for the small radius over thickness ratio the distribution of the ThickS4 element is quite off from the solution of the Abaqus elements, with only showing a few similarities. The peak of the σ_{33} is off by three plies and the higher part in front of the peak in the solution for the Abaqus elements is not even there. However when looking at the thickness distribution for a radius over thickness ratio of $R/t = 4$, it can be seen in Figure 3.77 that the distributions of the three elements are very similar to one another. It must also be noted that especially for the interesting region with the higher stresses the average stress of the ThickS4 over the ply remains within 2% of the solution of the C3D8 Abaqus element and within 7% of the solution of the C3D27 Abaqus element.

In Figure 3.78 can be seen that neither of the solutions follows the analytical solution perfectly, though the two Abaqus elements are best at predicting the peak of the shear stress τ_{13}. Though not able to follow the solution the ThickS4 does show a better agreement with the analytical solution towards the outer radius.

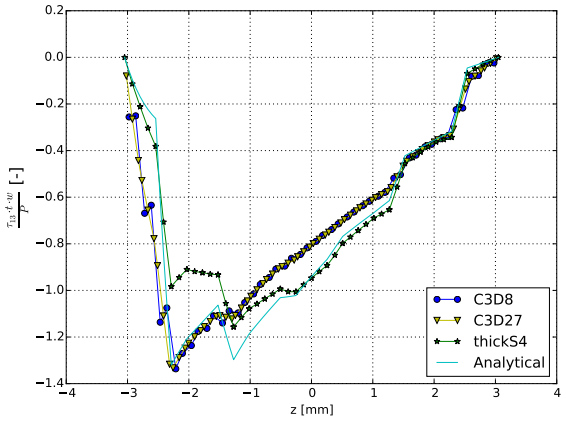

Figure 3.78: Distribution comparison of τ_{13} over the thickness of the laminate at the middle of the beam for $R/t = 1$ in case of an end load.

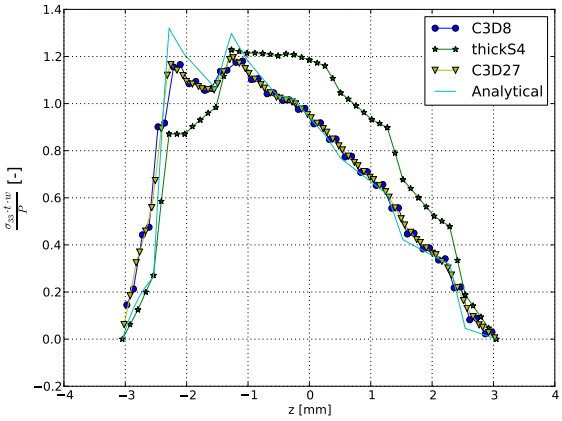

Figure 3.79: Distribution comparison of σ_{33} over the thickness of the laminate at the middle of the beam for $R/t = 1$ in case of an end load.

As was the case for the in-plane stress σ_{11}, it seems that the ThickS4 element is again not able to show the behaviour which is expected at the inner-radius for the case of such a low radius over thickness ratio. This can also be seen in Figure 3.79, where the solution of the ThickS4 is even more off. In this case the three dimensional Abaqus elements are able to follow the analytical solution, though not showing the extreme sharp peaks. The ThickS4 element shows the maximum more centred around the mid-surface of the laminate.

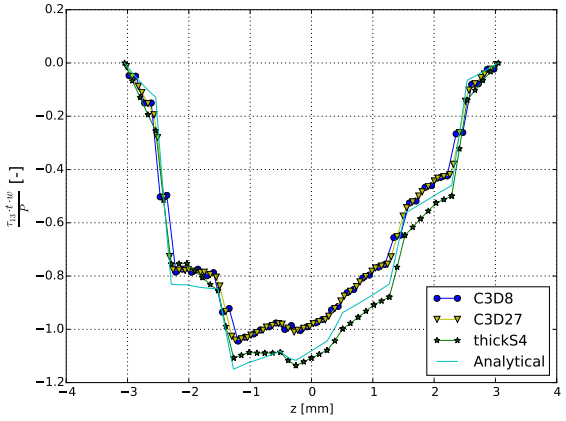

Figure 3.80: Distribution comparison of τ_{13} over the thickness of the laminate at the middle of the beam for $R/t = 2.5$ in case of an end load.

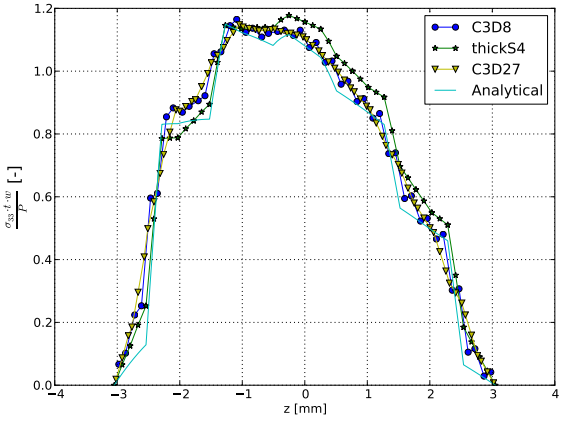

Figure 3.81: Distribution comparison of σ_{13} over the thickness of the laminate at the middle of the beam for $R/t = 2.5$ in case of an end load.

That the solution of the ThickS4 gets more accurate, or at least that the distribution gets more similar when the radius over thickness ratio is increased, can be seen in Figures 3.80 and 3.81. However the ThickS4 element is for a radius over thickness ratio of $R/t = 2.5$ still not able to predict the location of the maximum out-of-plane stress correctly. The maximum location is off by 4 plies.

From the radius convergence it is known, that from a radius over thickness ratio of $R/t = 3.25$, the ThickS4 element is able to predict the maximum location of both the out-of-plane stress σ_{33}. For that reason the distribution of the out-of-plane stresses for the case of $R/t = 4$ is shown in Figures 3.82 and 3.83. When the distribution of this radius over thickness ratio is compared to the previous two radius over thickness ratios, it can be seen that for each step in R/t, the distribution tilts less backwards. Furthermore it must be noticed that though the solution for the interlaminar normal stress σ_{33} is rather similar, the magnitude of the solution for the interlaminar shear stress τ_{13} is quite off, though having a similar distribution when comparing the ThickS4 element with the Abaqus elements.

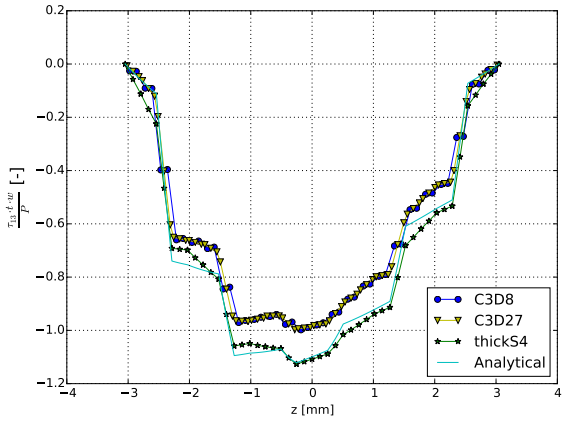

Figure 3.82: Distribution comparison of τ_{13} over the thickness of the laminate at the middle of the beam for $R/t = 4$ in case of an end load.

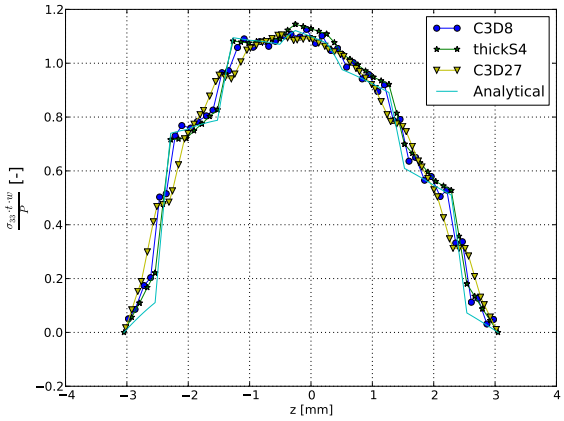

Figure 3.83: Distribution comparison of σ_{33} over the thickness of the laminate at the middle of the beam for $R/t = 4$ in case of an end load.

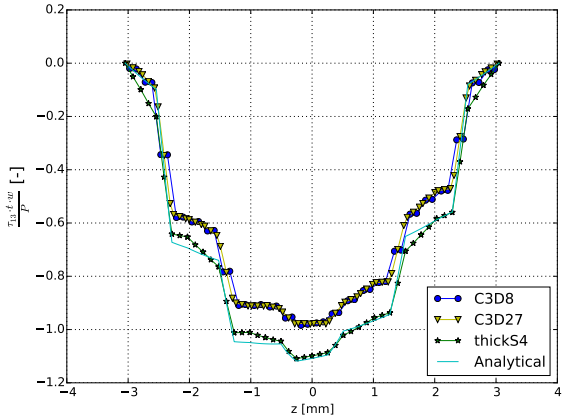

Figure 3.84: Distribution comparison of τ_{13} over the thickness of the laminate at the middle of the beam for $R/t = 8$ in case of an end load.

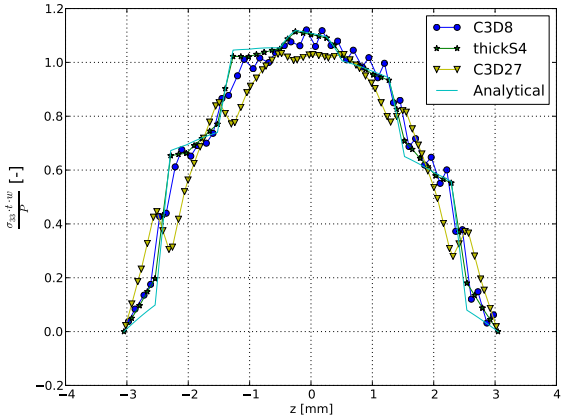

Figure 3.85: Distribution comparison of σ_{33} over the thickness of the laminate at the middle of the beam for $R/t = 8$ in case of an end load.

In the last distribution comparison for this stacking sequence in Figures 3.84 and 3.85 it can be seen that the solution of the ThickS4 element converges more to the analytical solution. In this comparison however it must be noted that the distributions for τ_{13} are still rather similar. However, when comparing the interlaminar normal stress σ_{33} it must be noted that the distribution of the two Abaqus elements get rather strange. This is however due to the fact, as was suggested in the radius convergence section, that the solution of the σ_{33} is not fully converged for this mesh density due to the increasing size of the elements when a larger radius is taken, as the number of elements is kept the same.

Stacking Sequence Investigation

This paragraph show the result for the stacking sequence investigation as was described in the benchmark description in subsection 3.1.2. The comparisons for the interlaminar normal stress σ_{33} for the four layups for a radius over thickness ratio of $R/t = 1$ can be seen in Figures 3.86 to 3.89. The comparisons for the interlaminar shear stress τ_{13} for the four layups for a radius over thickness ratio of $R/t = 1$ can be seen in Figures 3.90 to 3.93. The comparisons for σ_{33} for $R/t = 4$ can be seen in Figures 3.94 to 3.97. The comparisons for τ_{13} for $R/t = 4$ can be seen in Figures 3.98 to 3.101.

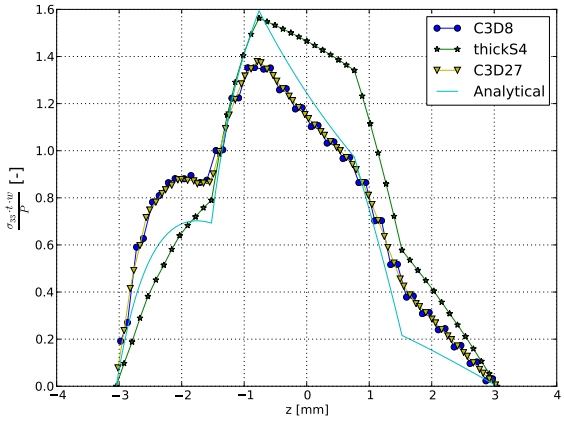

Figure 3.86: Distribution comparison of σ_{33} over the thickness of the laminate at the middle of the beam for $R/t = 1$ for layup 1.

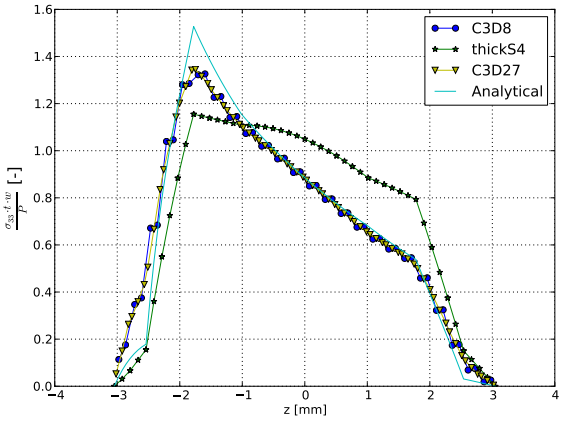

Figure 3.87: Distribution comparison of σ_{33} over the thickness of the laminate at the middle of the beam for $R/t = 1$ for layup 2.

In general from the previous tests it is known that the ThickS4 element is not able to predict the stresses for the most extreme case of a radius over thickness ratio of $R/t = 1$, however as can be seen in Figures 3.86 and 3.87 for some cases it is able to predict the maximum location of these stresses. Despite the fact that the ThickS4 element is able to predict the maximum location of the σ_{33} correctly, the distribution itself is off from both the Abaqus solutions and the analytical solution (though following some parts) as well as the magnitude of this peak.

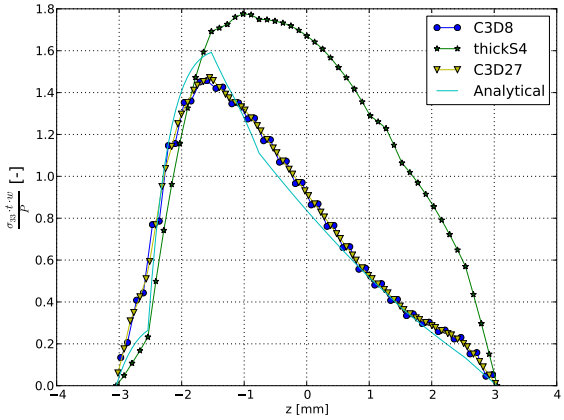

Figure 3.88: Distribution comparison of σ_{33} over the thickness of the laminate at the middle of the beam for $R/t = 1$ for layup 3.

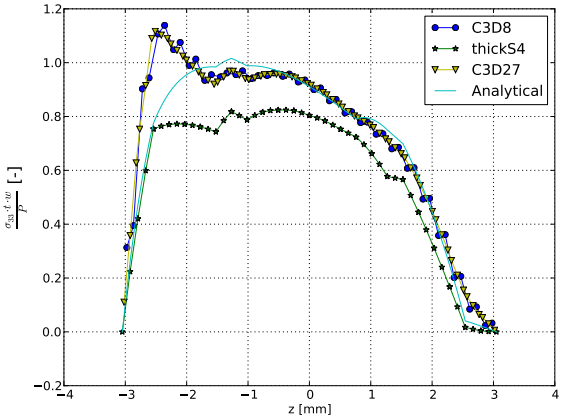

Figure 3.89: Distribution comparison of σ_{33} over the thickness of the laminate at the middle of the beam for $R/t = 1$ for layup 4.

In contrary to the symmetrical stacking sequences, for the two asymmetrical stacking sequences the ThickS4 element is not even able to predict the maximum location of the ILNS σ_{33} as can be seen in Figures 3.88 and 3.89. Furthermore it can be seen that the distributions of the ThickS4 only follow the other solutions in a small range of the thickness. For layup four it can be seen that the ThickS4 element does show similarities with the analytical solution, however it must be remembered that the analytical solution has not been validated for different stacking sequences and the Abaqus elements are validated three dimensional elements.

As can be seen in Figures 3.90 and 3.91, contradicting the previous seen behaviour regarding the similarities to the analytical solution, the ThickS4 element is able to follow the distribution behaviour of the analytical solution. Be that as it may, for layup 1, the solution of the two Abaqus elements is completely off and as said before should be taken as a reference. However when looking at the solution for layup 2, it can be seen that the distributions of all solutions is quite similar. The main difference here is that the analytical solution and the solution of the ThickS4 element show a sharp behaviour where the Abaqus element show a smoother peak.

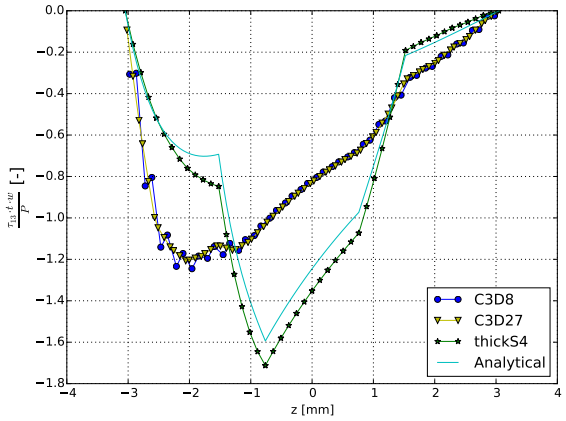

Figure 3.90: Distribution comparison of τ_{13} over the thickness of the laminate at the middle of the beam for $R/t = 1$ for layup 1.

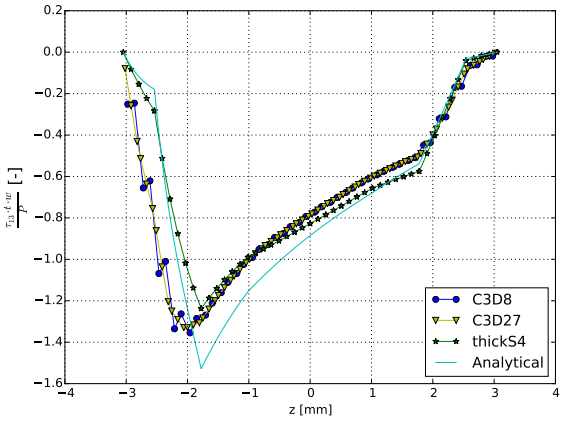

Figure 3.91: Distribution comparison of τ_{13} over the thickness of the laminate at the middle of the beam for $R/t = 1$ for layup 2.

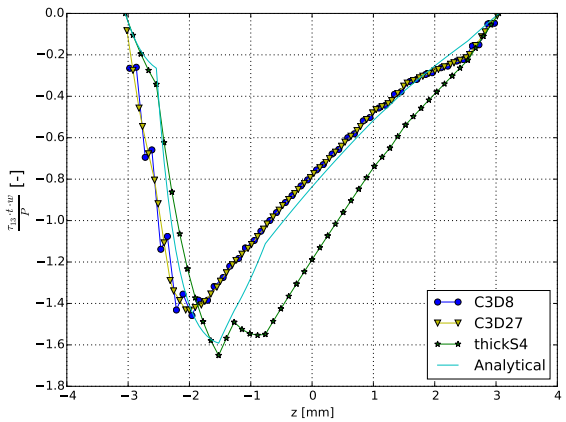

Figure 3.92: Distribution comparison of τ_{13} over the thickness of the laminate at the middle of the beam for $R/t = 1$ for layup 3.

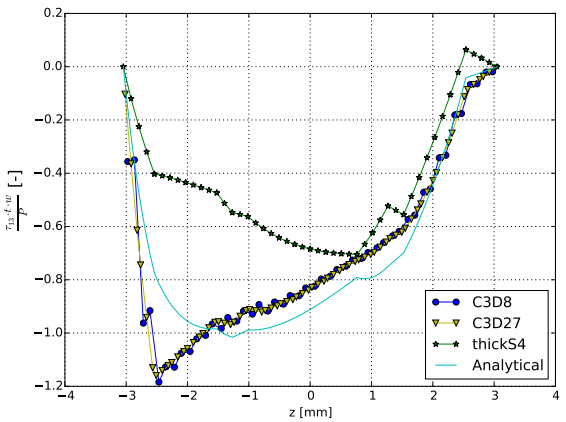

Figure 3.93: Distribution comparison of τ_{13} over the thickness of the laminate at the middle of the beam for $R/t = 1$ for layup 4.

Interesting to notice in the comparisons for layup 3 and 4 in Figures 3.92 and 3.93 respectively, is that though the ThickS4 element was able to follow the analytical solution for layup 1 and 2, it is not for the asymmetrical layups 3 and 4. The analytical solution seems to be close to the two Abaqus elements, however showing a higher peak in a different location, thus predicting the wrong location for the maximum interlaminar shear stress τ_{13}. For layup 4 it can be seen that though the analytical solution is quite capable of following the Abaqus elements towards the outer radius, it is not able to show the same peak which the two Abaqus solutions have. Furthermore the ThickS4 solution for this stacking sequence and radius over thickness ratio is completely off.

From the radius convergence and distribution comparison with the initial stacking sequence it is known that for a radius over thickness ratio of $R/t = 4$, the distribution of the ThickS4 element is similar to the analytical solution and the solution of the two Abaqus elements. This behaviour was also found in the results for the first two layups, as can be seen in Figures 3.94 and 3.95. Despite the fact that there are differences in the values for the σ_{33} (in the case of layup 1), the shape of the distribution is very similar for the solution for all four elements.

In contrary to the previously stated similarity, the distribution for the layup 3 and 4 show a different behaviour for the ThickS4 element. From Figures 3.96 and 3.97 it can be seen that despite the fact that the ThickS4 element is able to follow the shape of the three-dimensional elements at the beginning, it is unable to follow the distribution above from $z = -1$ mm approximately. It can also be seen that the analytical solution is able to follow the solution of the three-dimensional elements for layup 3, however not able to completely follow the shape for the solution of layup 4 and thus predicting the wrong maximum location for the interlaminar normal stress.

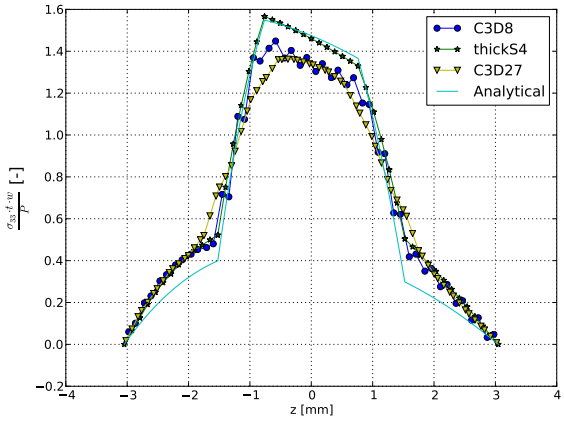

Figure 3.94: Distribution comparison of σ_{33} over the thickness of the laminate at the middle of the beam for $R/t = 4$ for layup 1.

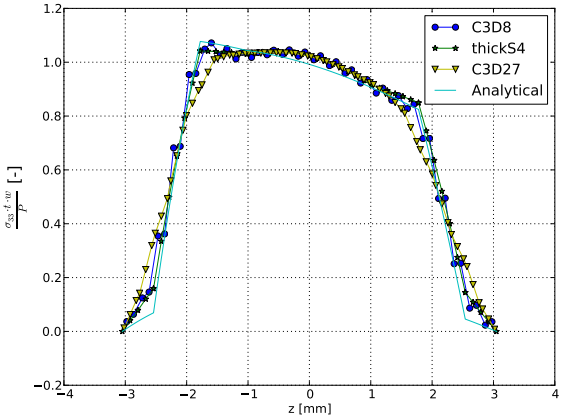

Figure 3.95: Distribution comparison of σ_{33} over the thickness of the laminate at the middle of the beam for $R/t = 4$ for layup 2.

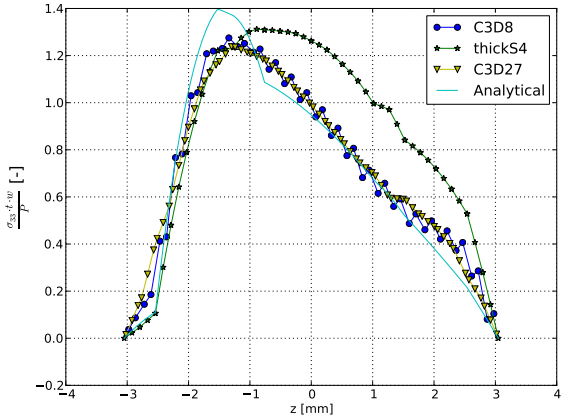

Figure 3.96: Distribution comparison of σ_{33} over the thickness of the laminate at the middle of the beam for $R/t = 4$ for layup 3.

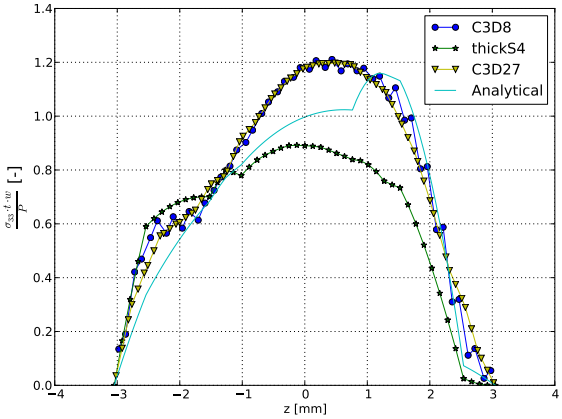

Figure 3.97: Distribution comparison of σ_{33} over the thickness of the laminate at the middle of the beam for $R/t = 4$ for layup 4.

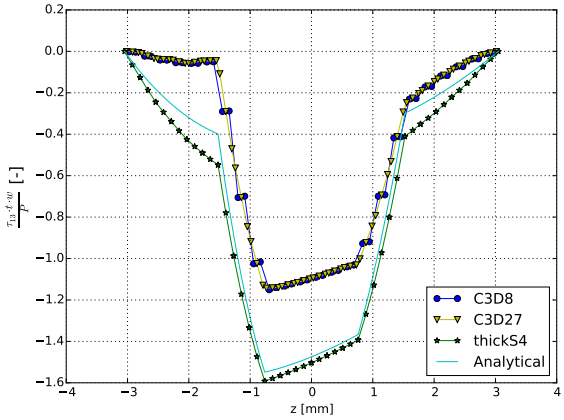

Figure 3.98: Distribution comparison of τ_{13} over the thickness of the laminate at the middle of the beam for $R/t = 4$ for layup 1.

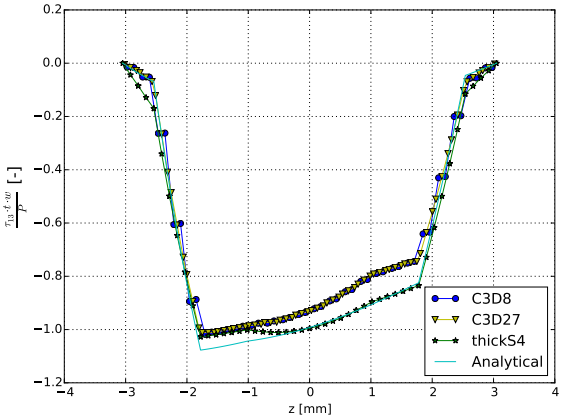

Figure 3.99: Distribution comparison of τ_{13} over the thickness of the laminate at the middle of the beam for $R/t = 4$ for layup 2.

In Figures 3.98 and 3.99 a few interesting things can be seen. First of all it can be seen that the shape of the distribution for the solution of all the four elements is very similar. However the main thing to notice is that, though the shape of the distribution is similar, the absolute maximum value of τ_{13} for layup 1 is off by $e = 0.354$ and $e = 0.386$ respectively when comparing the solutions of the ThickS4 element and of the

analytical solution to the solution of the Abaqus C3D8 element. This behaviour is not present in the graph for layup 2. The results for τ_{13} for layup 2 show that up until the absolute maximum value, the ThickS4 element follows the three-dimensional solutions with respect to magnitude after which it slowly converges to the analytical solution.

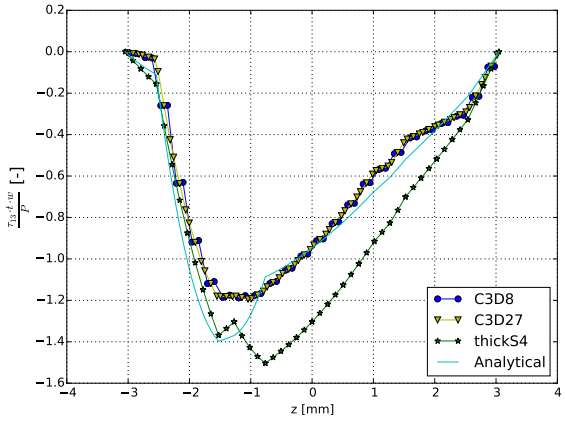

Figure 3.100: Distribution comparison of τ_{13} over the thickness of the laminate at the middle of the beam for $R/t = 4$ for layup 3.

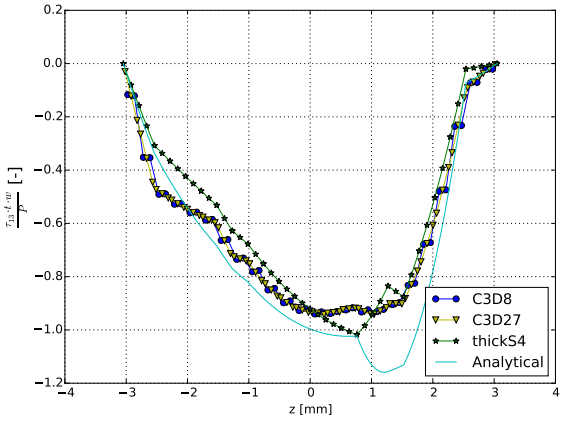

Figure 3.101: Distribution comparison of τ_{13} over the thickness of the laminate at the middle of the beam for $R/t = 4$ for layup 4.

A similar behaviour as can be seen in the previous comparisons can be seen in Figures 3.100 and 3.101 for layup 3 and 4. The analytical solution and the solution of the ThickS4 are off with respect to the shape. However it must be noticed that for the current radius over thickness ratio of four, the differences have become smaller. For layup 4 it can be seen that the solution for the ThickS4 element (in the maximum region of $z = -1$ mm until $z = 2$ mm) is within an error of about $e = 0.15$ when compared to the three-dimensional abaqus elements.

3.3. Conclusions on Performance and Working Range of ThickS4 UEL

This section will give conclusions regarding the performance and working range of the ThickS4 UEL. This will be done by first giving separate conclusions regarding the individual benchmark results. Following the separate conclusions is a final conclusion with remark about element selection for the rest of the project.

3.3.1. Seperate Conclusions

Considering the "Regular" case, which is the a non curved structure as the cantilever beam. For the regular case the S4 Abaqus element (or a comparable shell element from a comparable software) is the standard element used in calculations in the industry, which is why the concluding remarks regarding the regular case will be mostly with respect to the S4 element. It can be concluded that with respect to mesh convergence for the in-plane stress σ_{11} and the displacement, the ThickS4 has a good convergence and is comparable to the S4 Abaqus element.

Furthermore it can be concluded that the general convergence of the element is quite good. In all the benchmark results the ThickS4 element was at least as good as the other elements and in most cases better than the Abaqus 3D elements. Furthermore it must be noted, as already said in the introduction of the thesis itself, that the Abaqus 3D elements require a lot more computing time, which is not only due to the fact that the 3D Abaqus elements have more nodes, but also because they need an element for every layer of plies.

From the curved beam subjected to an end load or end moment analysed using the Lekhnitskii solution a few things can be concluded. First of all when considering the in-plane stress σ_{11}, the radius over thickness ratio from which the UEL can be used would be $R/t > 2.5$. However this is not the only criterion which the element should fulfill. When considering the out-of-plane stresses, the range would be a lot higher, namely a ratio of $R/t > 6.0$ due to the fact that the maximum location of the σ_{33} it predicts, is close to the location predicted by the 3D Abaqus elements.

Furthermore when comparing the two different radius convergence results (constant thickness and constant radius), it can be concluded that the ThickS4 element does not perform very well when thick laminates are considered (for the curved beam subjected to an end load). This can be seen when the the errors for the

σ_{11} are compared. For the case of a constant thickness there was difference of 83% where for the case of a constant thickness there was a difference of 92%.

However it must be noted that the Lekhnitskii solution and therefore also these conclusions only hold for the case where the laminate consists of only 0° orientated plies. As this is not the case in most applications of curved structures, it is best to make conclusions regarding the multilayer theory instead.

From the multilayer there are quite a few conclusions to make. First of all regarding the comparison with the structure as described by Ko and Jackson. When comparing the solution of ThickS4 element to the analytical solution, it could be seen that the ThickS4 element was not able to show the same results, though being similar. The solution was off in location of maximum out-of-plane stresses and in the magnitude of the σ_{33}, though not being far off with an error of $e = 0.0455$. However again the stacking sequence used for this benchmark test does not represent one used commonly in aerospace structures and is it wiser to make conclusions regarding different stacking sequences.

The layup used in the test with an other layup, the $[[-45,45,0,90]_3]_s$, is a stacking sequence which could be used in aerospace applications. The conclusions made regarding the results of this test are the most important of the benchmark. From the radius convergence it can be concluded that with respect to the in-plane stress σ_{11} that a radius over thickness ratio of $R/t > 3.25$ should be enough to be as good predicting as the Abaqus S4 element.

When regarding the more interesting out-of-plane stresses it can be concluded that the ThickS4 element is usable from above a radius over thickness ratio of $R/t \geq 3.5$ as for these ratio, the ThickS4 element shows the same radius convergence behaviour for the τ_{13} as the three dimensional Abaqus elements. Furthermore it can be concluded that from a radius over thickness ratio of $R/t = 3.25$ the ThickS4 element is able to predict the right location of the interlaminar normal stress.

In the stacking sequence investigation in subsection 3.2.4 the results were shown for four different layups. From the results for these different kind of layups it can be concluded that the ThickS4 element is not able to predict the right out-of-plane stresses when the stacking sequence is not symmetric. It has difficulty predicting the right distribution as well as the magnitude of these stresses.

Furthermore from the stacking sequence investigation it was seen that in general for radius over thickness ratios of $R/t = 4.0$ and higher the ThickS4 element is able to follow the right distribution of the out-of-plane stresses. The problem for the user element is however that in a lot of these cases, though able to predict the right distribution, the user element is not always able to predict the right magnitude of the stress.

3.3.2. Final conclusion

From the comparisons used it can be concluded that the analytical solution is not valid for all different layups. It was seen that especially for asymmetrical layups, the analytical solution differs a lot from the verified three dimensional Abaqus elements. Furthermore the solution tends to differ too in magnitude of the stresses both in the in-plane stresses as in the out-of-plane stresses when considering small radius over thickness ratios. The element is however better able to predict the expected behaviour of the stress distribution at the inner radius than the ThickS4 element and the Abaqus S4 element.

For the optimisation done in the next phase of the master thesis, certain failure criteria need to be evaluated. As the magnitude of the stress of the ThickS4 element is not always close (especially for the interlaminar shear stress) to the solution of the three dimensional Abaqus elements, it can be concluded that it is no use to use the ThickS4 element for a total optimisation. Therefore in order to get a clear view in the drivers for the out-of-plane stresses and failure criteria, for the next phase of the project, the Abaqus C3D8 element will be used. The Abaqus C3D8 is chosen over the C3D27 element as the C3D8 element outperforms the C3D27 element with respect to convergence. Furthermore the C3D8 Abaqus element is a lot faster considering computing time.

This does not say that the element is completely useless. From the individual conclusions it can be concluded that when used for a radius over thickness ratio of $R/t \geq 4.0$ the ThickS4 element is able to give a correct distribution of the out-of-plane stresses. Therefore the element can be used in the preliminary design phase in order to pick an initial design.

4

Genetic Algorithms

For the optimisation problem at hand a optimiser selection was done, from which the genetic algorithm (GA) seemed to be most suitable kind of optimiser. In this optimiser investigation other optimisers like the ant colony optimization as described by Koide et al. [7], as well as the simulated annealing as described by Rau and Arvind [12], were discussed. Two different kinds of genetic algorithms were selected, a permutation algorithm, where only plies are interchanged and the in-plane properties are kept the same and the standard genetic algorithm. The permutation algorithms and the selection of one is described in section 4.1. The standard genetic algorithm and its components is described in section 4.2.

4.1. Permutation Algorithms

Two permutation algorithms are described in this section. The first permutation algorithm is a permutation algorithm found in the article by Goldberg and Lingle [3], which will be described in subsection 4.1.1. The second is a newly designed permutation algorithm and is described in subsection 4.1.2. The fitness function used by both the permutation algorithms, is given in subsection 4.1.3. The section is concluded by putting the algorithms to the test in order to make a selection of a permutation algorithm for the optimisation at hand. The algorithm comparison is described and shown in subsection 4.1.4.

4.1.1. Permutation Algorithm Literature

The genetic Algorithm described in this section is the permutation algorithm found in literature. The flow chart of the entire algorithm can be seen in Figure 4.1.

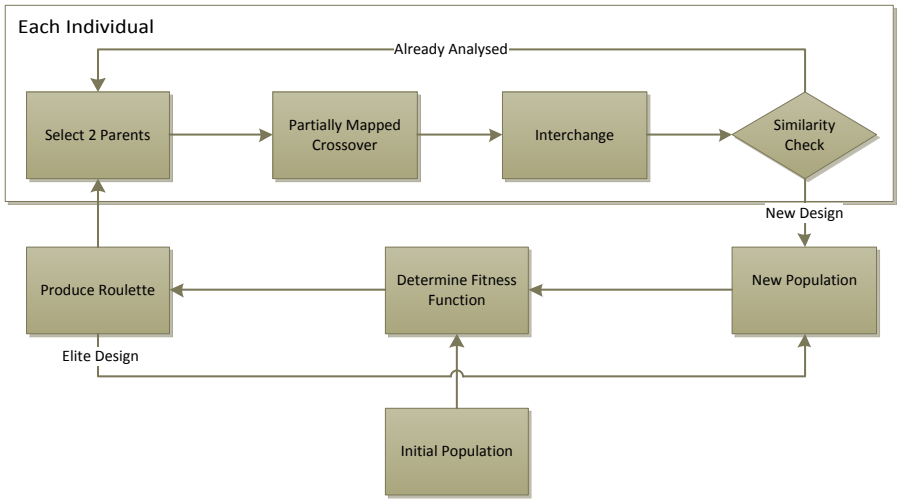

Figure 4.1: Flow chart of the permutation algorithm found in literature.

The start of the algorithm is the creation of an initial population which is done by creating n random shuffled copies of the laminate given into an excel input sheet. Where n is the number of individuals in a generation of the genetic algorithm. The FEM analyses are run for the initial population from which also the fitness function is determined (described in subsection 4.1.3). For the selection of the parents to be used in the partially mapped crossover (described in subsubsection 4.1.1.1), a roulette is produced and is described in subsubsection 4.1.1.2. Finally there is a chance for interchange to happen, this sub-process is described in subsubsection 4.1.1.3.

A new thing added to the algorithm found in literature is a check whether the design created has already been used before. If the design has already been analysed, a new design is made, this is done to increase the efficiency of the permutation algorithm. Lastly the best design found in the generation is copied directly to the new population without undergoing any changes in order to always keep the best design. As one can imagine this design does not need to be analysed again as the results from last run can be taken.

4.1.1.1. Partially Mapped Crossover

The partially mapped cross over is a crossover mechanism where the the genes of two parents are interchanged. However as for every permutation algorithm, the plies used in every generation are exactly the same. Goldberg and Lingle [3] developed a partially mapped crossover which engages the following four steps:

- Define two random breaking points.
- Copy the string between the two breaking points of the second parent to the offspring.
- Copy the genes from the first parent to the offspring which causes no conflict with the genes already present in the offspring.
- For the conflicting genes, define a mapping relationship. Fill in the conflicting gene locations using this relationship.

These four steps will now be explained using an example using a laminate with 8 plies. The basis laminate used is $[45,-45,0,90,90,0,-45,45]$ with a corresponding integer gene code $[1,2,3,4,5,6,7,8]$. The generation of an offspring is shown below:

Parent 1:	$[1,8,5,4,6,2,3,7]$
Stacking sequence:	$[45,45,90,90,0,-45,0,-45]$
Parent 2:	$[6,7,5,8,2,4,3,1]$
Stacking sequence:	$[0,-45,90,45,-45,90,0,45]$

The parent will be cut at the second and the fifth ply, therefore this segment is copied from parent 2 to the offspring.

Offspring:	$[*,7,5,8,2,*,*,*]$

In the offspring the asterisks represent currently unknown genes. The genes from parent 1 which cause no conflict with the offspring are then copied.

Offspring:	$[1,7,5,8,2,*,3,*]$

The last step will fill in the last two genes which are still unknown. This is done as said earlier by making a mapping relationship. The first conflicting gene from parent 1 is the 4, as the location in the offspring is already filled by the 8. In this case, one should look at which position the 8 fills in parent 1 which is the second position. However as can be seen, this position is filled too, in this case by the 7. Again looking at which place the 7 takes in parent 1, it can be seen that it fills the eighth position. As the eighth position is still a free spot in the offspring, this spot is filled by the 4. This results in the following offspring:

Offspring:	$[1,7,5,8,2,*,3,4]$

When this last step is repeated for the last conflicting gene, one can see that the gene 6 will fill the sixth slot in the offspring, by mapping with gene 2. The final offspring with the corresponding stacking sequence then becomes:

Offspring:	$[1,7,5,8,2,6,3,4]$
Stacking sequence:	$[45,-45,90,45,-45,0,0,90]$

4.1.1.2. Roulette

In order to make a selection for the parents of the next offspring, it is desirable that the change that the fitter individuals are more likely to be chosen. This is the reason why a roulette is chosen for the selection. A pool of a 100 designs is made according to the fitness of the individuals in the population. The number of times each individual is represented in this pool is determined in the following manner.

The sign of the weights of all the individuals is reversed after which the maximum of all the weights is added, such that the worst individual has a weight of zero and the best individual the highest number as can be seen in Equation (4.1).

$$w_i = -1 \cdot f_i + f_{max} \tag{4.1}$$

The number of times each individual occurs in the pool is then determined by dividing each of the new retrieved weights by the sum of these new retrieved weights and multiplying by 100 as can be seen in Equation (4.2).

$$n_i = \frac{w_i}{\sum_{i=1}^{N_{tot}} \omega_i} \cdot 100 \tag{4.2}$$

It is possible that the total number is not a 100, this problem is fixed by adding the remaining individuals randomly from the last generation. A visualisation of the result of such a pool can be seen in Figure 4.2.

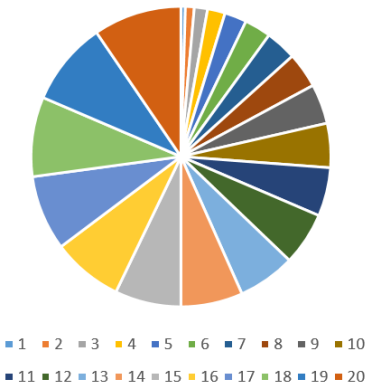

Figure 4.2: Representation of the number of times a design occurs in the roulette pool.

4.1.1.3. Interchange

In the case where a permutation algorithm is used where only the partially-mapped crossover is applied, it could be possible that the optimum found is not a global optimum but a local optimum in which it gets stuck. For that reason interchange is applied. Interchange is the sub-process where two random genes in the individual are selected and swapped as can be seen in Figure 4.3.

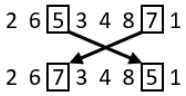

Figure 4.3: Representation of the interchange sub-process.

4.1.2. New Permutation Algorithm

Next to the partially mapped algorithm a different permutation algorithm was constructed based on several principles of a genetic algorithm. The main difference though with the standard genetic Algorithm as the one described in section 4.2 and the permutation algorithm found in literature described in subsection 4.1.1, is that this algorithm does not have a crossover with other individual. In another way this method could be seen as a cloning-mutating GA. The flow chart of this newly defined genetic algorithm can be seen in Figure 4.4.

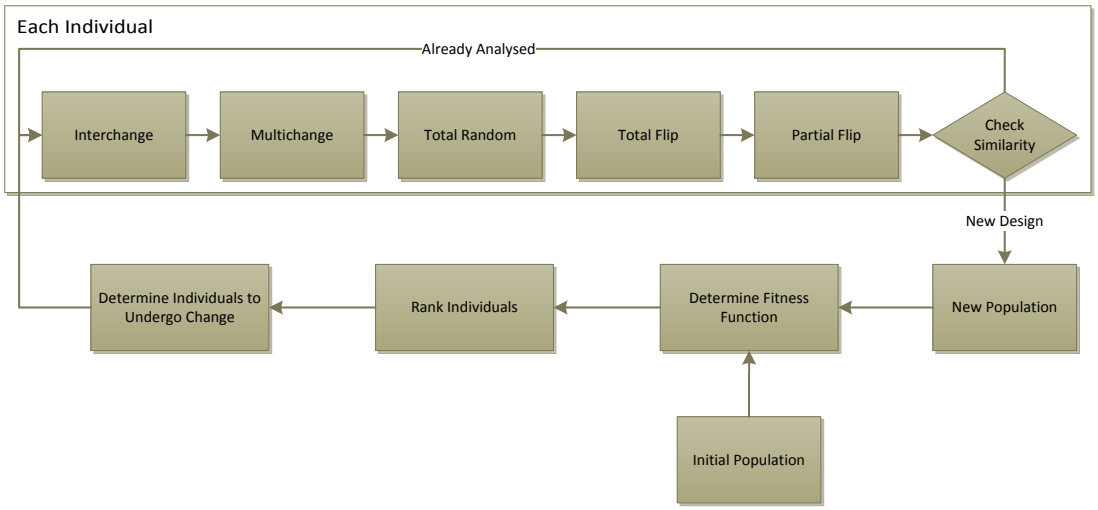

Figure 4.4: Flow chart of the new permutation algorithm.

The algorithm as shown in Figure 4.4 has some genetic operators which have not been described yet. The first one is called the multichange, this operator is based on the principle of the interchange. As for this genetic algorithm no crossover is applied and the interchange only interchanges two genes, another operator is needed to be able to make bigger changes. For this reason, the multichange operator was constructed. The multioperator first defines randomly how many times it should make an interchange and afterwards does the interchanges.

The second different operator is the total random operator. This operator is defined in order not to get stuck at a local minimum. The total random operator allows each individual to have a small chance to have its genes shuffled in a complete random manner.

The third different operator is the total flip. The purpose of the operator is to improve the convergence rate. Every individual has a small chance to flip the total stacking sequence to make sure that the reversed stacking sequence is not better in the out-of-plane performance.

The final different operator is the partial flip. The operator is based on the same principle as the total flip, however in this case two breaking points are randomly selected. The list of plies between these two breaking points is than flipped.

4.1.2.1. Next Generation

The way individuals are selected for the next generation is also different with respect to the partially mapped crossover and the standard genetic algorithm. Instead of first producing a roulette, from which the designs are randomly selected, the fitness of each individual determines directly how many times it is copied to the next generation. This process is not done in the same way as the roulette is generated, though in a similar way. Instead of subtracting the minimum, the average fitness is subtracted. After this the sign of the resulting weights are reversed as can be seen in Equation (4.3).

$$w_i = -1 \cdot \left(f_i - f_{avg}\right) \tag{4.3}$$

From these resulting weights, only the individuals with a weight above zero are taken along. After which the same is done as in Equation (4.2), though multiplying by the amount of designs taken to the next generation, this can be seen in Equations (4.4) and (4.5). As always, the elite design is taken to the next generation automatically.

$$w_i = \begin{cases} w_i & \text{if } w_i > 0 \\ 0 & \text{else} \end{cases} \tag{4.4}$$

$$n_i = \frac{w_i}{\sum_{i=1}^{N_{tot}} w_i} \cdot N_{tot} \tag{4.5}$$

4.1.3. Fitness Function

In order to asses the fitness of each design individual of the population a fitness function is used. For the two different permutation algorithms it was chosen to have the same fitness function in order to be able to compare them with each other. This fitness function is chosen to be the Kim & Soni failure criterion as described in subsubsection 2.3.2.1 and can again be seen in Equation (4.6).

$$f_{kimson} = \begin{cases} \frac{\sigma_{33}^2}{F_{33t}^2} + \frac{\tau_{13}^2}{F_{13}^2} + \frac{\tau_{23}^2}{F_{23}^2} & \text{if } \sigma_{33} > 0 \\ \frac{\sigma_{33}^2}{F_{33c}^2} + \frac{\tau_{13}^2}{F_{13}^2} + \frac{\tau_{23}^2}{F_{23}^2} & \text{else} \end{cases} \tag{4.6}$$

However the it was chosen to take the square root of the Kim & Soni criterion instead such that the fitness function is the reverse of reserve factor and is thus given by Equation (4.7). This was done such that in order to know the failure loads, the load only has to be divided by the fitness function. If the Kim & Soni failure criterion is mentioned later in the project, this reverse of the reserve factor will be meant.

$$f_i = \frac{1}{RF} = \sqrt{f_{kimson}} \tag{4.7}$$

4.1.4. Comparison and Selection

In this section a comparison is done between the new permutation algorithm and the permutation algorithm from literature. For both the algorithms the chance for the operations to happen is varied, in order to find the best algorithm as well as the best settings to the algorithm. The settings used for the comparison can be seen in Table 4.1. The optimisation is done for the case of an in-plane load with the smallest radius over thickness ratio of $R/t = 1$. For the optimisation the possibility for a asymmetric layup was kept. The result of the comparison can be seen in Figure 4.5 where the Kim & Soni failure criterion is plotted against the number of generations for all of the eight optimiser configurations. The model to which the optimisations are applied is later described in section 5.1. The starting stacking sequence is a $[(45/-45)_3/0_3/90_3]_s$ laminate.

Table 4.1: The analysed algorithm settings for the selection of a proper functioning permutation algorithm.

ID	Algorithm	Interchange	Multichange	Total Random	Total Flip	Partial Flip
1	Partially Mapped	0	-	-	-	-
2	Partially Mapped	0.1	-	-	-	-
3	Partially Mapped	0.25	-	-	-	-
4	Partially Mapped	0.9	-	-	-	-
5	New	0.9	0.1	0.1	0.1	0.5
6	New	0.7	0.5	0.1	0.1	0.1
7	New	0.9	0.3	0.1	0.1	0.3
8	New	0.9	0.3	0.1	0	0.5

From Figure 4.5 it can be seen that the end result of almost all the optimiser configurations is similar. There is only one outlier, being the permutation algorithm without any interchange. This underlines the fact that interchange is needed as one might otherwise get stuck in a local minimum as was the case for the permutation algorithm. Furthermore it can be seen that from all the optimiser configurations, the fifth configuration converges the fastest.

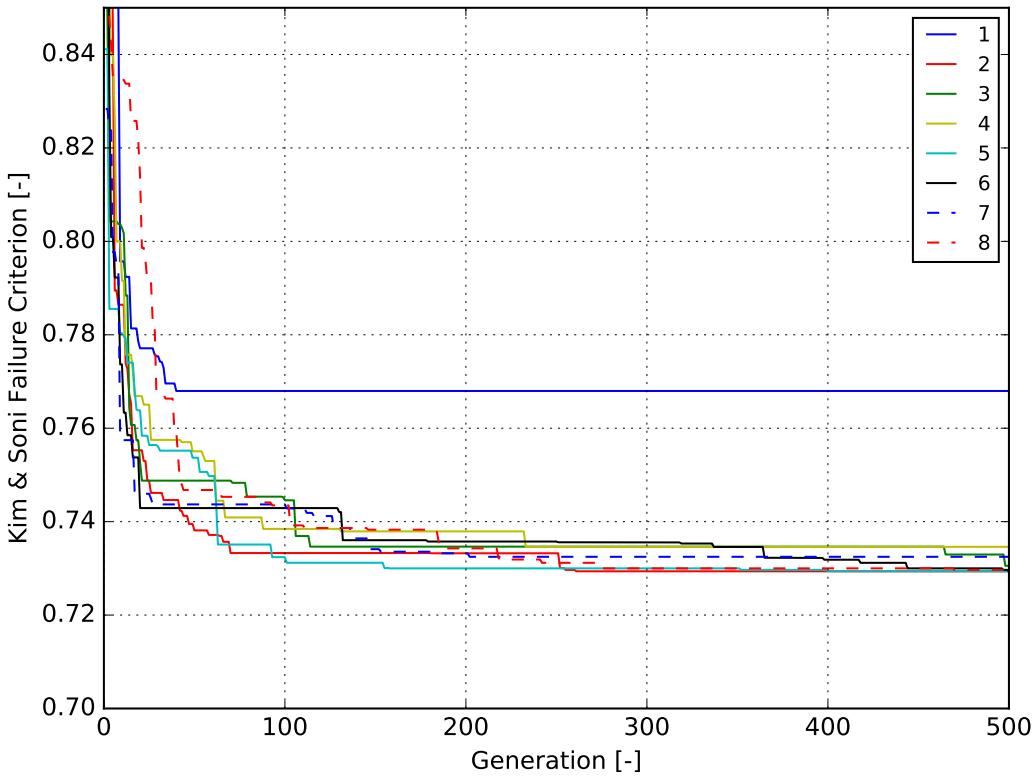

Figure 4.5: Result of the permutation algorithm comparison.

From the entire plot it can be concluded that in overall performance the newly designed permutation algorithm is as good as the permutation algorithm found in the literature. The newly designed permutation algorithm is maybe even a bit better as it is the first optimisation to converge close to the optimum value. Therefore it was chosen to use the fifth configuration for the stacking sequence optimisation. Furthermore it can be seen that the solution at a generation of 250 is already pretty close to the optimum, which is why it was chosen to set the maximum generations to 250. As the optimisation for the symmetric layups is less complex due to the smaller changeable range of plies, the maximum generations for the symmetric layups was set to a 100 generations.

4.2. Standard Genetic Algorithm

In this section the standard genetic algorithm is described. The standard GA will be used to see the influence of what changing the percentage in the ply direction changes does to the out-of-plane properties. Starting from the best designs found in the permutation algorithm, it will be looked at what stacking sequence is even better for the three different loading cases. Next to the standard loading cases, the standard genetic algorithm will also be used for a study of a few combinations of the standard loading cases. The flow chart of the standard genetic algorithm can be seen in Figure 4.6.

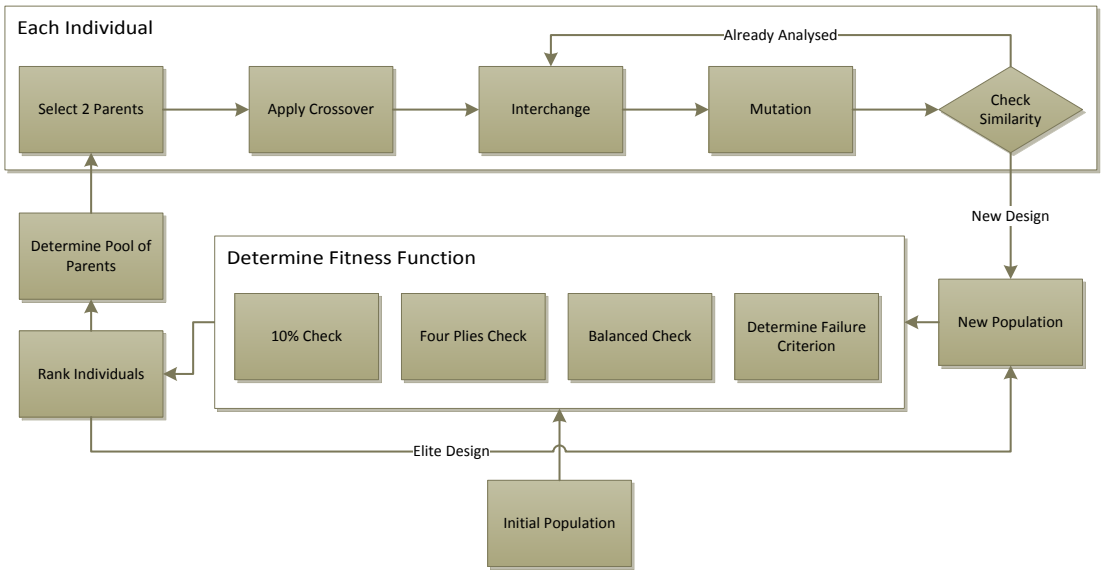

Figure 4.6: Flow chart of the standard Genetic Algorithm.

From the processes given in the flow chart, a few of the shown processes are already explained for the permutation genetic algorithms, the interchange is explained in subsubsection 4.1.1.3 and the failure criterion of Kim & Soni is already explained in subsection 4.1.3. The similarity check is the same as for the permutation algorithms and is used in order to overcome redundancy. The selection of the new pool of parents is done in the same way as was done for the new permutation algorithm and is explained in subsubsection 4.1.2.1. The first different process, which can be described as the main process of the genetic algorithm is the crossover and is described in subsection 4.2.1. The next different process is the subprocess of mutation and is described in subsection 4.2.2. The final difference is the fitness function. The fitness function does not solely consist of the failure criterion but also of a few design rules, these design rules along with the total function are described in subsection 4.2.3.

Normally in a standard genetic algorithm used for stacking sequence optimisation, two more operators are present, being ply deletion and ply addition. Which is normally done as the optimisation is used for real life problems which are going to be build and need to be optimised with respect to weight however still being able to withstand the loads applied. For the current project however this is not needed. For this project it is interesting to see what the out-of-plane failure criterion does when changing the ply percentages as well, though keeping a constant number of plies.

In order to determine the fitness function and use some of the operators, integers are used instead of the layup angles in degrees. The 0° direction is assigned the integer 1, the 45° direction is assigned the integer 2, the 90° direction is assigned the integer 3 and the -45° direction is assigned the integer 4.

4.2.1. Crossover

The crossover described is in this section is the standard crossover most common in genetic algorithms. The process of crossover will be explained by an example with two random generated stacking sequences as parents. The stacking sequences shown are only half of the total laminate as symmetry is applied. In the standard GA, these two parents are randomly selected from the pool of possible parents.

Parent 1:	$[45,-45,45,0,0,90,-45,45,90,90,0,-45]_s$
Parent 2:	$[45,-45,45,-45,45,-45,0,90,90,90,0,0]_s$

When the two parents are known, a breaking point is randomly selected, which in the case of the example is 4. The breaking point is seen from the third ply, as for design reasons, the outer two plies are kept a pair of $\pm 45°$, thus the breaking point being after the sixth ply. Both parents will be cut at the breaking point at which point the genes are switched between the two and will result in two offspring.

Parent 1:	$[45,-45,$ 45, 0, 0, 90, -45, 45, 90, 90, 0, -45$]_s$
Parent 2:	$[45,-45,$ 45, -45, 45, -45, 0 ,90 ,90, 90, 0, 0$]_s$
Offspring 1:	$[45,-45,$ 45, -45, 45, -45, -45, 45, 90, 90, 0, -45$]_s$
Offspring 2:	$[45,-45,$ 45, 0, 0, 90, 0 ,90 ,90, 90, 0, 0$]_s$

4.2.2. Mutation

The mutation is the genetic algorithm process where the fact that a gene can mutate is mimicked. For the genetic algorithm this means that the orientation of one of the plies is changed to another. The new orientation is determined by multiplying a random generated number between 0 and 1 by the maximum integer of 4 and rounding up to the nearest integer. In this way the outcome will always be one of the four possible integer directions.

4.2.3. Fitness Function

The fitness function for the standard genetic algorithm is a bit more complicated. Next to the out-of-plane failure criterion, three design rules are important. The first of the three design rules is the ten percent rule , the second design rule is that no more than four plies of the same orientation are allowed next to each other and the third design rule is that the stacking sequence should be balanced. The entire fitness function can be seen in Equation (4.8).

$$F_i = p_{10\%} + p_{4-plies} + p_{bal} + f_{kimson} \tag{4.8}$$

In this function $p_{10\%}$ is the penalty if the ten percent rule is broken, which is explained in subsubsection 4.2.3.1. $p_{4-plies}$ is the penalty if the more than four plies in a row is broken and is explained in subsubsection 4.2.3.2. Furthermore p_{bal} is the penalty if the laminate is not balanced, the way this penalty is determined is given in subsubsection 4.2.3.3

4.2.3.1. Ten Percent Rule

The first design rule is about the fact that at least each direction used in a laminate should have at least 10 percent of all plies in that direction in order to contribute to the stiffness [4]. For this reason the fitness

function will get a penalty if the statements in Equation (4.9) are not met.

$$n_0 = \frac{-\sum_{i=1}^{N}(x_i-4)(x_i-3)(x_i-2)x_i}{-6\sum_{i=1}^{N}\text{sign}(x_i)} + 0.1 < 0 \tag{4.9a}$$

$$n_{45} = \frac{-\sum_{i=1}^{N}(x_i-4)(x_i-3)(x_i-1)x_i}{4\sum_{i=1}^{N}\text{sign}(x_i)} + 0.1 < 0 \tag{4.9b}$$

$$n_{90} = \frac{-\sum_{i=1}^{N}(x_i-4)(x_i-2)(x_i-1)x_i}{-6\sum_{i=1}^{N}\text{sign}(x_i)} + 0.1 < 0 \tag{4.9c}$$

$$n_{-45} = \frac{-\sum_{i=1}^{N}(x_i-3)(x_i-2)(x_i-2)x_i}{24\sum_{i=1}^{N}\text{sign}(x_i)} + 0.1 < 0 \tag{4.9d}$$

4.2.3.2. Four Plies in a Row

One of the design rules states that no more than four plies should be placed next to each other in order to minimize delamination. This is checked by Equation (4.10) for the asymmetrical case and for Equations (4.10) and (4.11) for the symmetrical case. For each 5 adjacent plies, it is checked if the sum of these five plies divided by the minimum of these five plies should therefore be larger than 5. The condition is written down in equation form in Equation (4.10).

$$\frac{-\sum_{i=k}^{k+4}x_i}{\min(x_k,\ldots,x_{k+4})} + 5.01 < 0 \text{for} k = 1,\ldots,N-4 \tag{4.10}$$

In this equation N is the total number of plies. For the symmetrical case, the plies far most right in the list used for programming only represent half of the ones actually there. Therefore if the far most three plies are the same, there are actually six adjacent plies in the same direction. The additional equation for the symmetrical case can be seen in Equation (4.11).

$$\frac{-\sum_{i=N-2}^{N}x_i}{\min(x_{N-2},\ldots,x_N)} + 3.01 < 0 \tag{4.11}$$

4.2.3.3. Balance Check

The check for the balance is relatively easy, it is the check whether there is a $+\theta$ for every $-\theta$ ply. As for the optimisations done in the project only the four main ply directions are used, the equation for the balance check becomes as in Equation (4.12). If this equation is not met, a penalty is given to the fitness function.

$$\sum_{i=1}^{N}\cos\left(x_i\cdot\frac{1}{2}\pi\right) > 0 \tag{4.12}$$

4.2.4. Parameter Selection

In order to select the right parameters for the standard GA, a few different configurations setups are tested and compared. The comparison is again done for the in-plane loading where the stacking sequence is kept constant. This time however the stacking sequence is kept symmetric, as this is the case for the optimisation done with this optimiser. The different configurations tested can be seen in Table 4.2 and the results can be seen in Figure 4.7. The starting stacking sequence is the same one as for the permutation algorithm comparison in subsection 4.1.4.

Table 4.2: The analysed algorithm settings for the selection of a proper functioning standard genetic algorithm.

ID	Crossover	Interchange	Mutation	$p_{10\%}$	$p_{4-plies}$	p_{bal}
1	0.9	0.2	0.3	5.0	5.0	3.0
2	0.9	0.2	0.5	0.3	0.3	0.2
3	0.9	0.8	0.2	0.3	0.3	0.2
4	0.8	0.5	0.9	0.3	0.3	0.2
5	0.9	0.6	0.3	0.3	0.3	0.2

In Figure 4.7 it can be seen that for each setting, two optimisations have been plotted. For some of the settings, it can be seen that there is both a case which is quite good and a case which is slower to converge. An example of such a setting is the first setting where it can be seen that the first try converges very fast, though the second try converges the latest. From the tested settings, the one with the most constant convergence is the fourth, where both the first and second try are relatively close to one another and converge both relatively fast. Furthermore it can be seen that (except for the first try of the first and third setting) the results can be called converged after about 100 generations, which is why a maximum generations of 125 was chosen for the problem at hand.

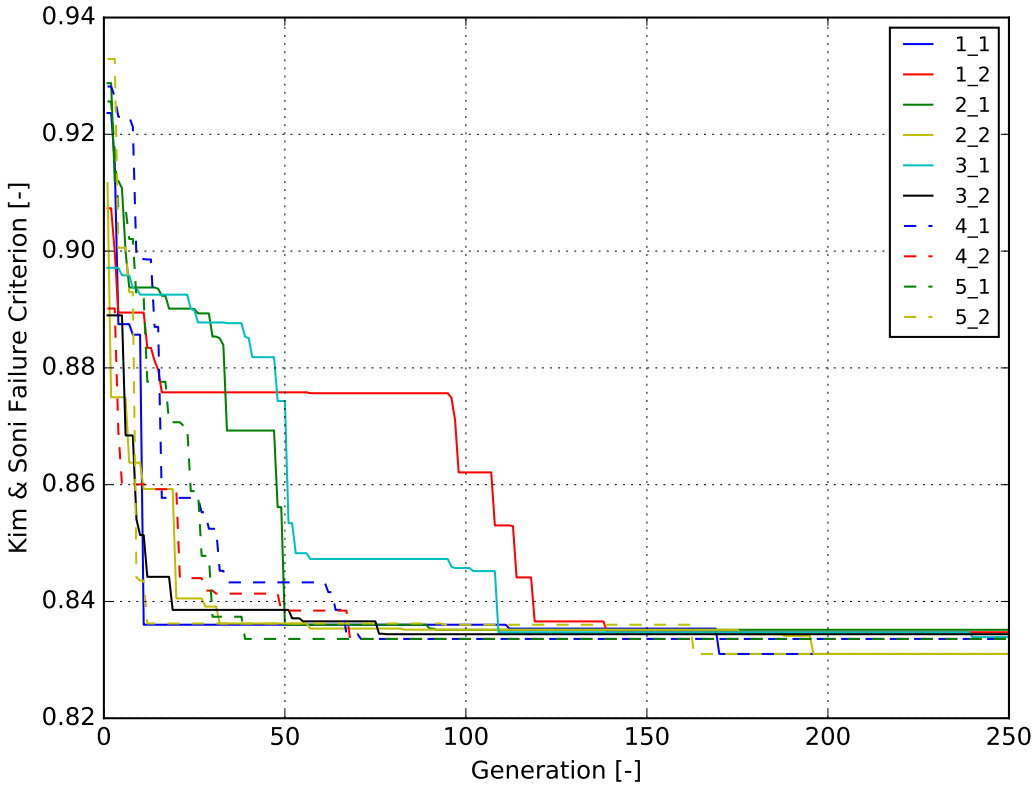

Figure 4.7: Result of the standard GA comparison.

5

Design Space Exploration

The process of designing and sizing composite structures is a complicated process. These process mostly require lots of iterations in order to converge to a final solution. An example of such a composite structure design process is the sizing of the wingtip and winglet of the Airbus A350-1000 by the cooperation of the companies FACC and Intales Engineering Solutions GmbH. In this design process the main curved structure present is the curvature found in the composite C-spars. In order to speed up the design process, a study is made of how the stacking sequence can be influenced such that the radius bending properties are most favourable, i.e. the lowest value for the out-of-plane failure criterion.

These C-spars in the wingtip and winglet are subjected to shear loading, in-plane loading and opening and closing moments. Each of these cases can have a different optimal stacking sequence, hence all of them are studied separately at first and in combination later on.

From the bench-mark tests it was concluded that the ThickS4 user element was not able to predict the stresses very accurately when compared to the three dimensional Abaqus elements. Therefore the decision was made to use one of the three dimensional elements instead to be able to give a good insight in the influence of the stacking sequence to the distribution of the out-of-plane stresses and the out-of-plane failure criteria. Furthermore it could be seen from the bench-mark tests that for the curved structures, in most cases the C3D8 element was faster to converge than the C3D27 element. Given that and the fact that the C3D27 element needs a lot more computing time, the decision was made to use the Abaqus C3D8 element for the design space exploration.

The FEM-model and material used in the optimisation is discussed in section 5.1. The mesh convergence of the structure and therefore also the mesh selection is discussed in section 5.2. The manner and location of the extraction of the results are explained in section 5.3. Furhermore the optimisation setup is described in section 5.4. The results are described in section 5.5. Finally the chapter is concluded in section 5.6.

5.1. FEM-Model

The structure as used in the bench mark test subsection 3.1.1 does not comply with all the loading conditions as the in-plane loading loading condition is not possible with the current boundary condition for that structure. For this reason a new structure was thought of which is able to handle all the three different loading types. The new structure can be seen in Figure 5.1.

The main difference with the FEM-model used in the benchmark test is that for the new FEM-model, straight parts have been added. This is done as in order to be able to apply the in-plane loading to the structure as well, a clamped configuration is needed at the other end of the beam. The boundary conditions would however influence the results too much when they would be placed directly to the curved structure. This results in an L-shaped structure. In order to have an equal mesh size for the straight and curved part (at the middle surface), the length of the straight parts is made dependent on the radius by the relation shown in Equation (5.1).

$$l = \frac{1}{2} \cdot \pi \cdot R \cdot \frac{4}{7} \tag{5.1}$$

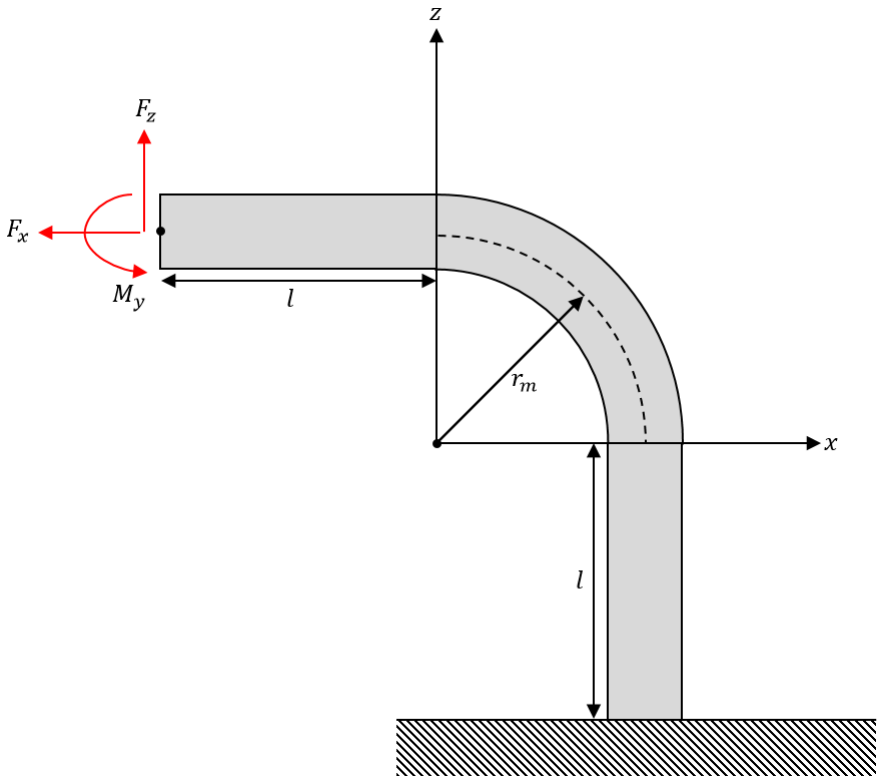

Figure 5.1: Representation of the interchange sub-process.

The load introduction is done as is described for the benchmarks described in subsection 3.1.1, i.e. with the use of rigid body elements. In this way the three different loading cases can all be applied at the same location. In case of the shear loading, the straight part in front of the curved part, will cause an extra opening moment in the structure. This additional opening moment is counteracted by applying a counteracting moment at the load introduction of $M_z = F_z \cdot l$. The visual representation of the moment compensation can be seen in Figure 5.2. In the figure, the dashed line represents the case without moment compensation and the normal line represents the compensated case.

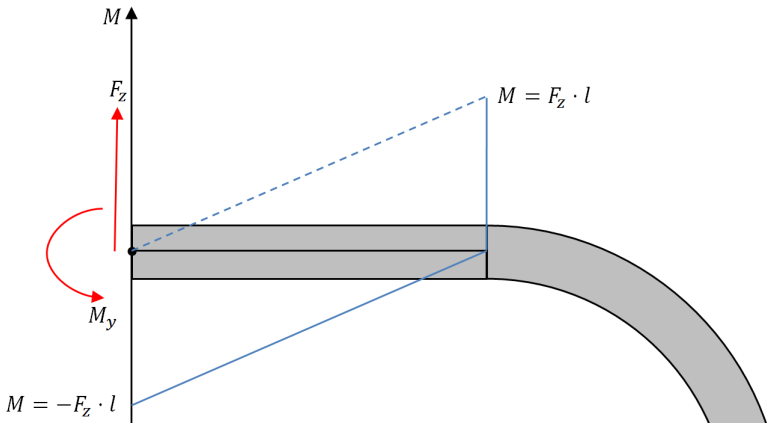

Figure 5.2: Representation of the moment compensation.

5.2. Mesh Used

In order to determine the mesh to be used, a mesh convergence was done for the 21 cases. These 21 cases consist of the three load cases each having seven different radius over thickness ratios. For each of the 21 cases, the mesh convergence was considered with respect to the interesting stresses σ_{11}, σ_{33} and τ_{13}, from which the out-of-plane stresses are the most important as these are taken up in the fitness function. The summary of the mesh convergence is given in Table 5.1.

Table 5.1: Summary for the mesh convergence

	R/t	σ_{11}		σ_{33}		τ_{13}	
Mesh		3 × 15	9 × 45	3 × 15	9 × 45	3 × 15	9 × 45
In-Plane Force	1	-0.015	-0.00134	-0.02496	-0.00212	-0.29518	-0.02864
	2	8.99E-05	0	-0.03957	-0.00365	-0.44672	-0.06349
	3	0.023975	0.002069	-0.03017	-0.00288	-0.55388	-0.10273
	4	0.053758	0.004506	-0.01495	-0.00199	-0.63617	-0.14665
	6	0.135915	0.011233	0.021175	0.002422	-0.71221	-0.23549
	8	0.24762	0.020324	0.087857	0.007355	-0.74578	-0.31179
Out-of-Plane Force	1	0.012132	0.001053	0.030822	0.002592	-0.30425	-0.02825
	2	0.024065	0.00199	0.030299	0.002489	-0.43388	-0.06313
	3	0.044307	0.00354	0.037009	0.003268	-0.53824	-0.10237
	4	0.072041	0.005755	0.04708	0.004082	-0.62214	-0.14622
	6	0.149842	0.011974	0.076307	0.006869	-0.71763	-0.23394
	8	0.256067	0.020631	0.116056	0.011113	-0.75409	-0.31193
Opening Moment	1	0.007094	0.000568	0.004452	0.000339	-	-
	2	0.018535	0.001449	0.003591	0.000447	-	-
	3	0.038818	0.003018	0.011155	0.001018	-	-
	4	0.066608	0.005194	0.021972	0.002251	-	-
	6	0.144986	0.011664	0.05389	0.004933	-	-
	8	0.25251	0.020559	0.097135	0.008917	-	-

The values given in the table are the changes due to a next step in mesh refinement. This means that the value in the column for the mesh 3 × 15 is the change in the stress if a mesh of 9 × 45 is taken instead and the value in the column for the mesh 9 × 45 is the change in the stress if a mesh of 15 × 75 is taken instead. From Table 5.1 it can be seen that in a lot of cases a mesh of 3 × 15 is not enough as the values for the stress still change by three to eleven percent for the stresses σ_{11} and σ_{33}. A next step in mesh refinement seems to be enough for these stresses as the percentage a next refinement changes the stresses is at most 2%. However it must be noticed that the τ_{13} is not fully converged and still changes 31 percent for the most extreme the biggest radius over thickness ratio of $R/t = 8$. However due to the exponential additional computing time a next step in mesh refinement would take, it was chosen to take a mesh of 9 × 45.

5.3. Results Extraction

In order to make the process of the result extraction as fast as possible, it was chosen to only retrieve the results of one row of elements (width wise) of the structure. To get the most general result for the optimisation, the results of the middle row are taken as being the general results. However, to speed up the process of the analyses and since it is known that the curved part of the structure is the most interesting, only a part of this slice of elements is used in the results processing. The representation of these elements is visualised in Figures 5.3 and 5.4.

In Figure 5.4 it can be seen that not only the curved area is highlighted yellow, but also a small part of both straight parts. It was chosen to include this part due to the fact that for the non pure bending cases the structure showed a peak in interlaminar stresses at the boundary of the curved part with the straight part. To make sure that the peak was included, as it sometimes fell in the element outside of the curved part, a fourth of the elements on the straight parts was also taken into account with the processing of the results.

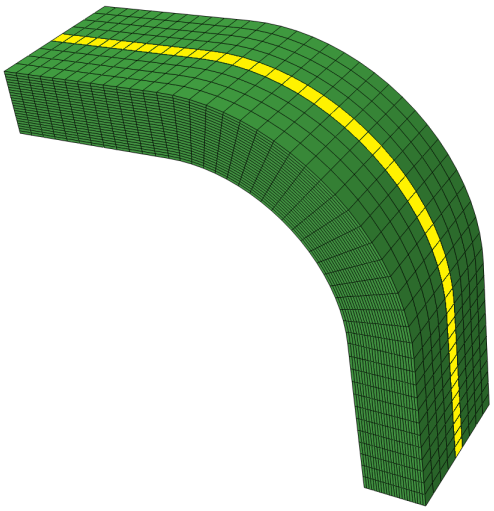

Figure 5.3: Total structure with yellow highlighted middle row.

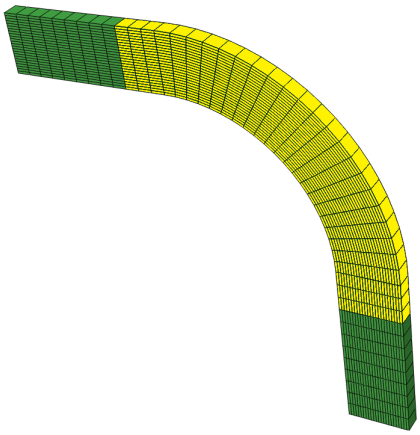

Figure 5.4: Middle row of structure with yellow highlighted area of result extractions.

5.4. Optimisation Setup

To be able to see a trend in the stacking sequence to the out-of-plane behaviour of the curved laminate, the in-plane properties of the laminate are kept constant. This was chosen to be a quasi-isotropic stacking sequence with 24 plies in the four main ply directions 0°, 45°, 90° and −45°. Therefore the starting point of the optimisation will be a $\left[(45°,-45°)_3, 0°_3, 90°_3\right]_s$ stacking sequence.

The loads applied to the structure will both be applied in their positive form and negative form. The positive loading being the loads which cause the structure to open the curve. This means that a positive F_x load in Figure 5.1 is actually the other way around, as well as a positive M_y also called an opening moment is also the other way around than shown in the figure. The F_z in Figure 5.1 is shown correctly. The negative loading is thus the loading which create a closing of the structure, i.e. the interlaminar normal stress becomes compressive, and are thus the opposite of the positive loading.

The different kind of loadings are not the only interesting changeable variables of this thesis. Next to changing the loads, these optimisation runs are also done for different values for the radius over thickness ratio. The loading types and testing these for different radii of curvature should give an initial understanding of the drivers in the radius bending problem. The most extreme cases, $R/t = 1$ and $R/t = 8$ are shown in Figures 5.5 and 5.6 respectively. The entire range of radius over thickness ratios is $R/t = 1, 1.5, 2, 3, 4, 6, 8$.

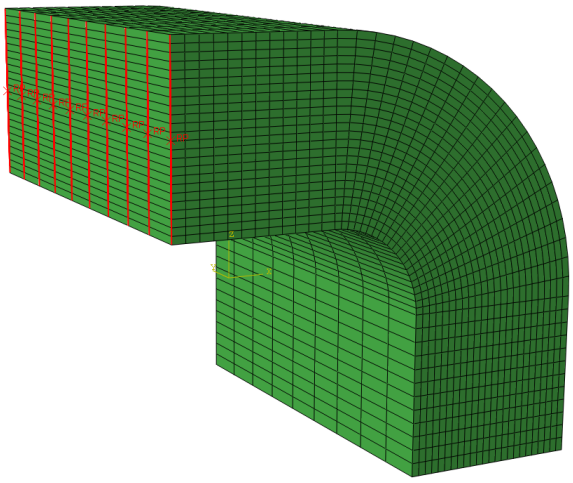

Figure 5.5: FEM-model for optimisation, $R = 6.096$ mm, $R/t = 1$.

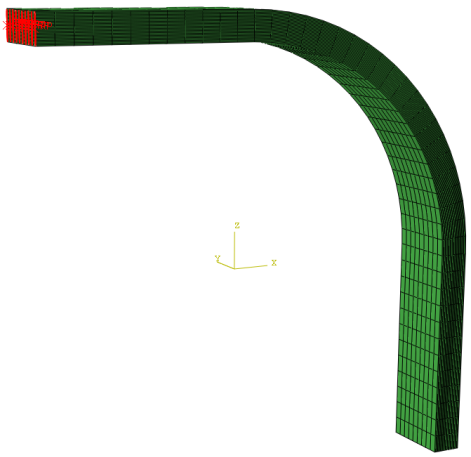

Figure 5.6: FEM-model for optimisation, $R = 48.768$ mm, $R/t = 8$.

The materials used for the optimisation are the materials as used for the C-Spar designed for the A350-1000 given in Table 5.2. The material used is a uni-directional tape.

Table 5.2: Materials used as specified by the company intales, the thickness is given in [mm], the moduli in [GPa] and the Poison's ratios are dimensionless.

t	0.254
E_1	1.54e+05
E_2	8.50e+03
E_3	8.50e+03
G_{12}	4.20e+03
G_{13}	4.20e+03
G_{23}	3.36e+03
ν_{12}	0.33
ν_{13}	0.33
ν_{23}	0.33

This first optimisation is done by using a permutation genetic algorithm. The permutation algorithm is the one selected from the comparison and parameter selection in section 4.1, being a self designed permutation GA. The result of the optimisation is how the stacking sequence influences the out-of-plane properties.

As for impact properties it is desirable to have a ± 45 layer on the outside of the structure [5], this is another constraint set to the optimisation problem. This constraint means that on both sides of the stacking sequence this ± 45 layer is placed and the plies in between are left to be intertwined. In other words this means that this constraint limits some of the possibilities.

The permutation optimisation will be done for both symmetric layups and asymmetric layups. This is done because of manufacturing reasons it is desirable to have a symmetric layup, as this will preclude warping if the laminate is released from the mould [4]. However in order to see the full effect of the stacking sequence on the distribution of the out-of-plane stresses, the case of allowing asymmetric stacking sequences to exists is also analysed. It may also be possible that the coupling due to an asymmetric layup is favourable towards the out-of-plane failure criterion. As one can imagine, for the symmetrical case, the number of plies which can be changed is half compared to the case where the entire laminate is allowed to change. This results in a changeable range of 20 plies for the asymmetrical case and a changeable range of 10 plies for the symmetrical case.

After this first optimisation is finished, a second optimisation is done. This optimisation uses the standard GA, as described in section 4.2, to see how the stacking sequence changes if the in-plane properties are also allowed to change. The load input for this optimisation will be a scaled load in order to set failure in the optimum stacking sequence to one. As was already stated in description of the standard GA, in this stage of the investigation further design rules are also applied, these being the ten percent rule and the four plies in a row rule. In contrary to the previous permutation, this optimisation is only done for the symmetrical case, as for now, all stacking sequences used in the design of the Airbus A350-1000 Winglet C-spars are symmetrical.

The final stage of the optimisation is changing the loading of the structures to combinations of the three loading cases. For these load combinations the S_{33}/S_{13} ratio will be investigated due to the optimum stacking sequences. The load combinations are created with respect to the failure for each individual loading configuration, i.e. if for in-plane loading the failure is at 3000 N, the failure for shear loading is at 4000 N and the failure for a opening moment is at 10000 Nm, a one to one to one ratio will be a 1000 N in-plane, 1333 N shear and 3333 Nm opening moment combinational loading.

5.5. Optimisation Results

This section discusses the results of the various stages of the optimisation. First the results of the permutation algorithm results will be discussed in subsection 5.5.1. This is followed by the results of the standard genetic algorithm results in subsection 5.5.2.

5.5.1. Permutation Algorithm Results

As discussed previously, the permutation algorithm was applied to the optimisation of the case where the stacking sequence is symmetrical and for the case where the stacking sequence is allowed to be asymmetric. The results for the symmetrical case are given in subsubsection 5.5.1.2 and the results for the asymmetrical case are given in subsubsection 5.5.1.1. These two result cases are both for the positive loading, the results for both the symmetrical and asymmetrical case for the negative loading can be found in subsubsection 5.5.1.3.

5.5.1.1. Asymmetric

The best stacking sequences for each of the separate cases for which the asymmetric optimisation has been done can be seen in Table 5.3. In this table also the maximum values of the Kim & Soni failure criterion are given for each case. For every seperate loading case, for the most extreme radius over thickness ratio of $R/t = 1$, plots have been made in order to see a difference in the distribution of the Kim & Soni failure criterion. These plots can be seen in Appendix C.

The first three figures given in Figures C.1 to C.3 are for the in-plane loading case and are for the best individual of the first generation. The next three figures given in Figures C.4 to C.6 are for the same loading case but for the best stacking sequence. These are followed by the three first figures of the out-of-plane loading case for the best individual of the first generation in Figures C.7 to C.9. The next three figures are again for the same loading case, but for the best stacking sequence and are given in Figures C.10 to C.12. The last figures are for the opening moment case and are given for the best individual of the first generation in Figures C.13 to C.15 and for the best stacking sequence in Figures C.13 to C.15. In the figures the S_{33} as shown in the figures is determined as in Equation (5.2), the S_{x3} is determined as in Equation (5.3)

$$S_{33} = \begin{cases} \frac{\sigma_{33}}{F_{33t}} & \text{if } \sigma_{33} > 0 \\ \frac{\sigma_{33}}{F_{33c}} & \text{else} \end{cases} \tag{5.2}$$

$$S_{x3} = \sqrt{\frac{\tau_{13}^2}{F_{13}^2} + \frac{\tau_{23}^2}{F_{23}^2}} \tag{5.3}$$

From these plots it can be seen that for all cases the the best stacking sequence has a flatter distribution of the out-of-plane failure criterion than the first best individual. Another thing that can be seen from the plots is the location of the maximum failure criterion, which can be interesting for when the different loading cases are combined.

From the results for the best sequences a lot of things can be noticed. To be able to see the behaviour clearly the directions of the plies were seperated into three categories, the $\pm 45°$, the $0°$ and the $90°$. Each were given a color as with visualisation it is easier to see patterns. From the result it was noticed that for all three different loading cases the $0°$ plies were located towards the outer radius, i.e. on the right side of the table. Furthermore the $90°$ plies can be found to be placed at the center for all the three different loading cases. This leaves us with the $\pm 45°$ plies which should then be located towards the inner radius of the laminate and it can be seen that this is indeed the case.

It must be noted that for the results of the asymmetric cases more than four plies in a row can be found. The decision was made not to take the four plies in a row rule into account in order to see what the stacking sequence would become without any restrictions (apart from the $\pm 45°$ on the outsides).

Another interesting behaviour, though not so clearly visible as the previous stated behaviours, is the fact that when the radius over thickness ratio is increased, the $0°$ plies appear to move a bit away from the outer radius. Furthermore it can be seen that $90°$ plies start to appear at the outer radius. This is probably due to the fact that when the radius over thickness ratio gets bigger, the peak stress (if a uniform laminate would be chosen with only $0°$ plies) would move from the inner radius towards the middle. Therefore in order to get a flatter distribution, the stiff $0°$ plies should be located less towards the outside as the outside should attract less load.

It seems that no real big differences can be seen between the out-of-plane loading case and the opening moment loading case. For the in-plane loading case a difference can be seen though. Especially for the

middle range of radius over thickness ratios, it can be seen that the 0° plies are spread out a little more and not as much in blocks as for the other two loading cases.

Furthermore a check was done if a trend could be seen for the different stacking sequences analysed. Among other parameters, the B and D matrix of the stacking sequences were analysed. However no clear correlation could be found between the out-of-plane failure criterion and the B and D matrix could be found.

Table 5.3: Best stacking sequences for the asymmetric cases

Case	R/t	Stacking Sequence	Kim & Soni
In-Plane Force	1	45 -45 -45 45 45 45 90 45 -45 -45 90 -45 90 90 00 00 90 00 90 00 00 00 -45 45	0.738275641
	1.5	45 -45 45 45 -45 -45 90 -45 90 -45 90 90 90 90 00 00 00 45 00 45 00 00 -45 45	0.7521918
	2	45 -45 00 45 -45 -45 -45 45 -45 45 90 90 00 90 00 90 45 90 90 00 00 00 -45 45	0.800220025
	3	45 -45 00 -45 -45 -45 90 90 90 90 90 00 00 00 45 -45 45 45 45 90 00 00 -45 45	0.795310885
	4	45 -45 00 -45 45 45 45 45 90 90 90 90 00 00 00 90 -45 -45 -45 90 00 00 -45 45	0.790590175
	6	45 -45 45 45 -45 -45 -45 90 90 90 90 90 90 00 00 00 00 00 45 -45 45 00 -45 45	0.712928887
	8	45 -45 45 -45 45 -45 -45 -45 90 90 90 90 90 00 00 00 00 00 00 45 45 90 -45 45	0.682231047
Out-of-Plane Force	1	45 -45 45 45 45 -45 -45 -45 -45 45 00 90 00 00 90 90 90 00 90 90 00 00 -45 45	0.73662093
	1.5	45 -45 45 90 45 90 90 -45 90 90 45 90 00 45 00 -45 -45 00 -45 00 00 00 -45 45	0.760900305
	2	45 -45 -45 -45 45 -45 90 45 90 -45 90 45 45 90 00 00 00 00 90 90 00 00 -45 45	0.732121179
	3	45 -45 -45 45 45 45 -45 90 -45 90 90 90 90 45 -45 00 00 00 00 00 00 90 -45 45	0.666103874
	4	45 -45 45 -45 -45 45 45 -45 -45 90 90 90 90 90 00 00 00 00 00 45 00 90 -45 45	0.612443695
	6	45 -45 45 -45 45 45 -45 -45 -45 90 90 90 90 90 00 00 00 00 00 00 90 45 -45 45	0.582837425
	8	45 -45 00 45 -45 45 90 -45 90 90 90 00 00 00 90 45 45 -45 -45 00 00 90 -45 45	0.666712804
Opening Moment	1	45 -45 90 90 90 90 45 90 -45 90 -45 -45 00 00 45 45 -45 45 00 00 00 00 -45 45	0.414205892
	1.5	45 -45 -45 45 45 -45 -45 -45 90 45 90 90 00 90 00 90 90 45 00 00 00 00 -45 45	0.264914884
	2	45 -45 45 -45 -45 -45 -45 90 45 90 90 90 90 90 00 00 45 45 00 00 00 00 -45 45	0.180440469
	3	45 -45 -45 45 -45 45 -45 45 90 45 90 90 90 90 90 -45 00 00 00 00 00 00 -45 45	0.111174275
	4	45 -45 45 -45 45 45 -45 -45 -45 90 90 90 90 90 00 00 00 00 00 45 00 90 -45 45	0.078911405
	6	45 -45 -45 45 45 -45 45 -45 45 90 -45 90 90 90 90 00 00 00 00 00 00 90 -45 45	0.052742088
	8	45 -45 45 -45 45 -45 -45 -45 90 90 90 90 00 00 00 00 00 00 45 45 90 90 -45 45	0.030133071

5.5.1.2. Symmetric

The results for the symmetric case are given in the same format as was done for the asymmetric case. The list with the best stacking sequences for all the cases is given in Table 5.4. Again for the smallest radius over thickness ratio the best individual of the first generation and the overall best stacking sequence are compared for each of the three different loading cases and are given in Appendix C in Figures C.19 to C.36.

Though it is less obvious than for the asymmetric case, it can again be seen that the distribution of the Kim & Soni failure criterion becomes flatter for the best stacking sequence compared to the best individual of the first generation. The reason it is less obvious is because the best individual of the first generation is already closer to the best result because a lot less combinations are possible if the stacking sequence is kept symmetric. This can also be seen from the maximum values for the failure criterion given in the figures.

As was the case for the asymmetrical results a general pattern can be seen for all results, though a lot different as the stacking sequences must remain symmetric. The pattern which can be seen is that the 0° plies are located towards the centre and towards the outsides of the laminate. Furthermore for most best stacking sequences it can be seen that the 90° plies are located towards the centre of the laminate, except for the small radius over thickness ratios for the out-of-plane loading case and opening moment case. The smallest radius over thickness ratio for the in-plane loading case and opening moment case do not show more zero plies in the centre of the laminate. However it does have more ±45° plies located here, which also attract more load than the 90° plies.

Another trend can be seen when increasing the radius over thickness ratio. It can be seen that for larger radius over thickness ratios, one of the 0° plies from the middle switches towards the outside of the laminate. The 0° ply on the outside of the laminate is probably there to increase the bending resistance of the laminate.

As was the case for the asymmetric layups, also for the symmetric layups an investigation was done for the ABD-matrix. In this case only the D-matrix needed to be checked as for symmetrical stacking sequences, the B-matrix is zero. Unfortunately as for the asymmetrical case, no correlation could be found between the out-of-plane failure criterion and the D-matrix.

Table 5.4: Best stacking sequences for the symmetric cases

Case	R/t	Stacking Sequence	Kim & Soni
In-Plane Force	1	[45/-45/00/90/-45/45/90/00/90/00/45/-45/-45/45/00/90/00/90/45/-45/90/00/-45/45]$_s$	0.875663505
	1.5	[45/-45/00/45/-45/45/-45/90/90/00/90/00/00/90/00/90/90/-45/45/-45/45/00/-45/45]$_s$	0.86362075
	2	[45/-45/00/45/-45/45/-45/90/90/90/00/00/00/00/90/90/90/-45/45/-45/45/00/-45/45]$_s$	0.851064832
	3	[45/-45/00/-45/45/-45/45/90/90/90/00/00/00/00/90/90/90/45/-45/45/-45/00/-45/45]$_s$	0.865634818
	4	[45/-45/00/00/-45/45/90/-45/90/90/45/00/00/45/90/90/-45/90/45/-45/00/00/-45/45]$_s$	0.878968178
	6	[45/-45/00/00/-45/45/-45/45/90/90/90/00/00/90/90/90/45/-45/45/-45/00/00/-45/45]$_s$	0.889612523
	8	[45/-45/00/00/-45/45/-45/45/90/90/90/00/00/90/90/90/45/-45/45/-45/00/00/-45/45]$_s$	0.905582535
Out-of-Plane Force	1	[45/-45/90/45/90/-45/45/90/-45/00/00/00/00/00/00/-45/90/45/-45/90/45/90/-45/45]$_s$	0.851348789
	1.5	[45/-45/00/90/-45/45/-45/90/00/90/00/45/45/00/90/00/90/-45/45/-45/90/00/-45/45]$_s$	0.884601744
	2	[45/-45/00/90/45/90/-45/45/-45/90/00/00/00/00/90/-45/45/-45/90/45/90/00/-45/45]$_s$	0.848036964
	3	[45/-45/00/-45/45/-45/45/90/90/90/00/00/00/00/90/90/90/45/-45/45/-45/00/-45/45]$_s$	0.846344558
	4	[45/-45/00/00/45/90/-45/90/45/90/-45/00/00/-45/90/45/90/-45/90/45/00/00/-45/45]$_s$	0.825414958
	6	[45/-45/00/00/-45/45/-45/45/90/90/90/00/00/90/90/90/45/-45/45/-45/00/00/-45/45]$_s$	0.816376444
	8	[45/-45/00/00/-45/45/-45/45/90/90/90/00/00/90/90/90/45/-45/45/-45/00/00/-45/45]$_s$	0.817948709
Opening Moment	1	[45/-45/00/90/90/90/00/45/00/-45/45/-45/-45/45/-45/00/45/00/90/90/90/00/-45/45]$_s$	0.515099127
	1.5	[45/-45/00/90/45/90/-45/45/90/00/-45/00/00/-45/00/90/45/-45/90/45/90/00/-45/45]$_s$	0.319455472
	2	[45/-45/00/90/-45/45/90/-45/90/45/00/00/00/00/45/90/-45/90/45/-45/90/00/-45/45]$_s$	0.227456737
	3	[45/-45/00/00/45/90/45/90/-45/90/-45/00/00/-45/90/-45/90/45/90/45/00/00/-45/45]$_s$	0.143128986
	4	[45/-45/00/00/-45/45/90/-45/45/90/90/00/00/90/90/45/-45/90/45/-45/00/00/-45/45]$_s$	0.104384981
	6	[45/-45/00/00/-45/45/45/-45/90/90/90/00/00/90/90/90/-45/45/45/-45/00/00/-45/45]$_s$	0.06881113
	8	[45/-45/00/00/-45/45/-45/45/90/90/90/00/00/90/90/90/45/-45/45/-45/00/00/-45/45]$_s$	0.051682001

5.5.1.3. Negative Loading

In this section the results for the cases where the loads are reversed are shown. The results for the asymmetric case are shown in Table 5.5 and the results for the symmetric case are shown in Table 5.6. The biggest difference with the positive loading, is that these negative loads create a closing moment instead of an opening moment in the curved beam. This means that instead of tensional interlaminar normal stresses, there are compressive interlaminar normal stresses. This can also be seen in the results, as the best layups are now different than before. The differences will be discussed for both the asymmetric and symmetric case.

Asymmetric

First of all one can notice that in all cases, the value for the out-of-plane failure criterion of Kim & Soni is lower. This is due to the fact that instead of creating an opening moment, these load cases create a closing moment. This means that the stress in magnitude is probably similar, though the out-of-plane failure stress where the stresses are compressive is around five times higher. In other words the Kim & Soni is in this case mainly driven by the shear stresses τ_{x3}.

For the closing moment this means that the result is still driven by the ILNS however in this case the ILNS is compressive, which in its case cannot lead to delaminations. Therefore it can be concluded that the results for the closing moment are not useful for the current project. This is the reason why they are not taken into account in the next phase of the stacking sequence investigation.

When looking at the best layups for the in-plane force a few things can be noticed. First of all when comparing the best layups for the negative loading with the positive loading it can be seen that again the 90° and 0° plies are close to one another again. However, in this case the total block has shifted towards the inner radius.

The results for the out-of-plane force show most similarities with the positive loading case. Though being very similar it can be seen that in the best layups for the negative loading case, the block of the 90° and 0° plies are, as in the in-plane loading case, a bit more shifted toward the radius. as can be seen from the ±45° plies appearing at the outer radius and the 0° plies appearing at the inner radius.

Table 5.5: Best stacking sequences for the asymmetric cases due to negative loading

Case	R/t	Stacking Sequence	Kim & Soni
In-Plane Force	1	[45/-45/0]$_{2}$/-45/45/45/0/90/0/45/0/90/0/90/-45/90/-45/90/90/45/-45/0/-45/45	0.679563833
	1.5	[45/-45/0]$_{2}$/-45/45/90/90/90/90/90/0/0/0/0/-45/45/90/45/-45/45/-45/0/-45/45	0.648182772
	2	[45/-45/0]$_{2}$/45/-45/45/90/-45/90/90/90/90/90/0/0/0/-45/45/0/45/-45/0/-45/45	0.607191375
	3	[45/-45/0]$_{2}$/45/90/90/90/90/90/0/0/0/0/-45/90/45/-45/45/-45/45/-45/0/-45/45	0.569329462
	4	[45/-45/0]$_{2}$/45/45/90/90/90/90/90/90/0/0/0/0/-45/-45/-45/45/-45/45/0/-45/45	0.53370564
	6	[45/-45/0]$_{2}$/0/45/-45/-45/90/-45/90/90/0/0/90/90/90/45/45/45/-45/0/0/-45/45	0.569602303
	8	[45/-45/0]$_{2}$/-45/-45/90/90/90/90/90/90/0/0/0/45/45/0/45/-45/-45/45/0/-45/45	0.547527912
Out-of-Plane Force	1	45/-45/45/-45/-45/45/-45/45/-45/90/90/0/90/0/45/90/90/90/0/0/0/0/-45/45	0.604834781
	1.5	45/-45/-45/45/-45/-45/45/45/90/45/90/90/90/90/90/0/0/0/0/-45/0/0/-45/45	0.580841355
	2	45/-45/0/45/-45/45/-45/-45/45/90/45/0/0/0/90/90/90/90/-45/90/0/0/-45/45	0.575915492
	3	45/-45/-45/45/45/45/-45/-45/-45/90/90/90/90/90/90/0/0/0/0/45/0/0/-45/45	0.546699915
	4	45/-45/0/-45/45/45/45/90/90/90/90/90/90/0/0/0/-45/-45/-45/45/0/0/-45/45	0.542839624
	6	45/-45/0/-45/45/45/90/90/90/90/90/90/0/0/0/0/45/-45/-45/-45/45/0/-45/45	0.543460865
	8	45/-45/0/45/-45/-45/45/45/90/90/90/90/90/90/0/0/0/-45/45/-45/0/0/-45/45	0.543501612
Closing Moment	1	45/-45/90/90/90/90/0/0/0/-45/45/45/-45/45/-45/-45/45/90/90/0/0/0/-45/45	0.146224751
	1.5	45/-45/90/90/0/90/0/0/90/45/45/-45/45/-45/45/-45/90/-45/90/0/0/0/-45/45	0.077811577
	2	45/-45/90/90/0/90/0/90/90/-45/-45/45/-45/45/-45/45/45/90/0/0/0/0/-45/45	0.051291927
	3	45/-45/45/0/90/90/90/-45/90/-45/90/90/-45/45/-45/0/45/45/0/0/0/0/-45/45	0.030326575
	4	45/-45/45/-45/-45/0/-45/-45/90/90/90/45/90/90/0/45/0/90/45/0/0/0/-45/45	0.021341117
	6	45/-45/0/45/-45/-45/-45/45/90/45/90/90/90/90/90/0/45/0/-45/0/0/0/-45/45	0.013236542
	8	45/-45/0/0/-45/45/45/90/45/90/90/0/0/45/-45/-45/-45/90/90/90/0/0/-45/45	0.010138392

Symmetric

The same reasoning applies for the overall failure criterion being lower than for the positive loading case as was the case for the asymmetric layups. Which is again the reason why the results for the closing moment are not very similar to the positive loading case (except for $R/t = 4$ and $R/t = 6$). When comparing the other negative loading cases, similarities can be seen with the best layups for the positive loading cases. The main difference is that the zero plies for the negative loading are more centered around the middle of the laminate. The next interesting thing to notice is that the best layups for the in-plane and out-of-plane force all look very similar.

Table 5.6: Best stacking sequences for the symmetric cases due to negative loading

Case	R/t	Stacking Sequence	Kim & Soni
In-Plane Force	1	[45/-45/00/45/-45/-45/45/00/90/90/00/90/90/00/90/90/00/45/-45/-45/45/00/-45/45]$_s$	0.690465421
	1.5	[45/-45/00/-45/45/-45/45/90/90/90/00/00/00/00/90/90/90/45/-45/45/-45/00/-45/45]$_s$	0.657504383
	2	[45/-45/00/-45/45/-45/45/90/90/90/00/00/00/00/90/90/90/45/-45/45/-45/00/-45/45]$_s$	0.626053696
	3	[45/-45/00/45/-45/-45/45/90/90/90/00/00/00/00/90/90/90/45/-45/-45/45/00/-45/45]$_s$	0.582078269
	4	[45/-45/00/-45/45/-45/45/90/90/90/00/00/00/00/90/90/90/45/-45/45/-45/00/-45/45]$_s$	0.555456763
	6	[45/-45/00/-45/45/-45/45/90/90/90/00/00/00/00/90/90/90/45/-45/45/-45/00/-45/45]$_s$	0.551378749
	8	[45/-45/00/-45/45/-45/45/90/90/90/00/00/00/00/90/90/90/45/-45/45/-45/00/-45/45]$_s$	0.555354091
Out-of-Plane Force	1	[45/-45/-45/45/-45/45/90/90/00/90/00/00/00/00/90/00/90/90/45/-45/45/-45/-45/45]$_s$	0.669447294
	1.5	[45/-45/00/-45/45/-45/45/90/00/90/00/90/90/00/90/00/90/45/-45/45/-45/00/-45/45]$_s$	0.637914168
	2	[45/-45/00/-45/-45/45/45/90/90/90/00/00/00/00/90/90/90/45/45/-45/-45/00/-45/45]$_s$	0.587102949
	3	[45/-45/00/-45/45/-45/45/90/90/90/00/00/00/00/90/90/90/45/-45/45/-45/00/-45/45]$_s$	0.568639537
	4	[45/-45/00/-45/45/-45/45/90/90/90/00/00/00/00/90/90/90/45/-45/45/-45/00/-45/45]$_s$	0.558445699
	6	[45/-45/00/-45/45/-45/45/90/90/90/00/00/00/00/90/90/90/45/-45/45/-45/00/-45/45]$_s$	0.550729394
	8	[45/-45/00/-45/45/-45/45/90/90/90/00/00/00/00/90/90/90/45/-45/45/-45/00/-45/45]$_s$	0.547325486
Closing Moment	1	[45/-45/90/00/00/00/90/90/45/-45/45/-45/-45/45/-45/45/90/90/00/00/00/90/-45/45]$_s$	0.157011398
	1.5	[45/-45/90/00/00/00/90/90/45/45/-45/-45/-45/-45/45/45/90/90/00/00/00/90/-45/45]$_s$	0.083985943
	2	[45/-45/90/00/00/90/00/90/-45/-45/45/45/45/45/-45/-45/90/00/90/00/00/90/-45/45]$_s$	0.055535839
	3	[45/-45/00/00/00/90/90/-45/45/90/-45/45/45/-45/90/45/-45/90/90/00/00/00/-45/45]$_s$	0.032411096
	4	[45/-45/00/00/45/90/90/-45/45/90/-45/00/00/-45/90/45/-45/90/90/45/00/00/-45/45]$_s$	0.02333181
	6	[45/-45/00/00/-45/45/-45/45/90/90/90/00/00/90/90/90/45/-45/45/-45/00/00/-45/45]$_s$	0.015264863
	8	[45/-45/00/00/00/-45/45/45/-45/90/90/90/90/90/90/-45/45/45/-45/00/00/00/-45/45]$_s$	0.011393028

5.5.2. Standard Genetic Algorithm Results

This section will discuss the results for the standard genetic algorithm. As was described in section 4.2, the ply-percentage is allowed to change in order to be able to see best how the layup is changed if this restriction is left out. Furthermore no ply-deletion is applied such that the outcome of the standard genetic algorithm can be compared with the results of the permutation algorithm. Only symmetric layups will be used for the standard genetic algorithm as this is also the case in current industrial projects of the company. The cases analysed with the standard genetic algorithm are the regular load cases with both positive and negative loads in subsubsection 5.5.2.1 and the combined cases in subsubsection 5.5.2.2. The results found in the optimisations are layups which could be used in real life applications as the design rules are taken into account. It must however be noted that all the results given in this section are optimised for the Kim & Soni failure criterion and might thus have a larger value for any other failure criterion.

5.5.2.1. Regular Load Cases

The regular load cases are split into the positive loading cases and the negative loading cases.

Positive Loading

The best stacking sequences as result of the standard genetic algorithm due to the curved beam subjected to the standard positive loading cases are given in Table 5.7. Differences and similarities can be noticed when comparing the results of the standard genetic algorithm with the results for the permutation algorithm. Interesting is the fact that the percentage of 0° direction plies is in almost all cases the minimum of four. The minimum is four because there are 24 plies in total and due to symmetry it can be either two or four plies, where two plies would be to few. Furthermore when the in-plane force is considered it can also be seen, apart from the smallest radius over thickness ratio, that the number of plies in 90° direction are also minimum. Finally for the in-plane force it can be seen that the way the plies are spread is similar to the permutation algorithm, where the zero plies are located on the outsides and the inside of the laminate.

For the out-of-plane force, in almost all cases, except for $R/t = 2$ and $R/t = 6$, the number of plies in 90° direction is increased with respect to the permutation algorithm results. When further comparing to the permutation algorithm results it must be noticed that the way the 0° directed plies are similarly distributed over the laminate. It must be noted that the 0° plies in case of the biggest radius over thickness ratio have disappeared from the middle of the laminate.

The final comparison for the case of positive loading is the opening moment loading case. Again similarities in the distribution of the plies over the laminate can be seen, though there are also some very clear differences. First of all for the smallest three radius over thickness ratios, 90° plies appear between the 0° plies

in the middle of the laminate. Furthermore it can be seen that for the largest radius over thickness ratios, the 0° plies disappear again from the middle of the laminate and are moved towards the outside of the laminate (which was already the case for the results of the permutation algorithm).

Table 5.7: Best stacking sequences of the standard GA optimisation for the symmetric cases due to standard loading

Case	R/t	Stacking Sequence	Kim & Soni
In-Plane Force	1	45 -45 -45 90 45 90 -45 90 45 90 00 00 00 00 90 45 90 -45 90 45 90 -45 -45 45	0.839419543
	1.5	45 -45 00 90 45 -45 45 -45 -45 45 00 90 90 00 45 -45 -45 45 -45 45 90 00 -45 45	0.857598906
	2	45 -45 00 45 -45 45 -45 45 -45 90 00 90 90 00 90 -45 45 -45 45 -45 45 00 -45 45	0.834606543
	3	45 -45 00 -45 -45 45 -45 90 45 45 90 00 00 90 45 45 90 -45 45 -45 -45 00 -45 45	0.813585321
	4	45 -45 00 -45 45 -45 45 -45 45 90 90 00 00 90 90 45 -45 45 -45 45 -45 00 -45 45	0.806009975
	6	45 -45 00 -45 45 -45 45 45 -45 90 90 00 00 90 90 -45 45 45 -45 45 -45 00 -45 45	0.823851732
	8	45 -45 00 -45 45 -45 45 -45 45 90 90 00 00 90 90 45 -45 45 -45 45 -45 00 -45 45	0.839874893
Out-of-Plane Force	1	45 -45 90 45 90 -45 90 90 00 45 00 -45 -45 00 45 00 90 90 -45 90 45 90 -45 45	0.847214265
	1.5	45 -45 00 90 -45 45 -45 90 00 45 00 00 00 00 45 00 90 -45 45 -45 90 00 -45 45	0.875513302
	2	45 -45 00 90 45 90 -45 45 -45 90 00 00 00 00 90 -45 45 -45 90 45 90 00 -45 45	0.848036964
	3	45 -45 00 90 90 90 -45 90 45 90 90 00 00 90 90 45 90 -45 90 90 90 00 -45 45	0.808535009
	4	45 -45 00 90 45 90 90 -45 90 90 90 00 00 90 90 90 -45 90 90 45 90 00 -45 45	0.79990853
	6	45 -45 00 -45 45 -45 45 -45 45 90 90 00 00 90 90 45 -45 45 -45 45 -45 00 -45 45	0.796758888
	8	45 -45 00 00 45 -45 45 -45 90 45 -45 90 90 -45 45 90 -45 45 -45 45 00 00 -45 45	0.793230185
Opening Moment	1	45 -45 00 90 90 90 00 45 00 -45 90 90 90 90 -45 00 45 00 90 90 90 00 -45 45	0.510556799
	1.5	45 -45 00 90 45 90 -45 90 45 00 -45 90 90 -45 00 45 90 -45 90 45 90 00 -45 45	0.314184515
	2	45 -45 00 90 90 90 -45 90 45 90 00 90 90 00 90 45 90 -45 90 90 90 00 -45 45	0.221636676
	3	45 -45 00 90 45 90 -45 90 90 90 90 00 00 90 90 90 90 -45 90 45 90 00 -45 45	0.138783084
	4	45 -45 00 00 90 90 90 90 45 90 90 -45 -45 90 90 45 90 90 90 90 00 00 -45 45	0.101985965
	6	45 -45 00 00 -45 45 -45 -45 90 45 90 45 45 90 45 90 -45 -45 45 -45 00 00 -45 45	0.067316519
	8	45 -45 00 00 -45 45 -45 -45 45 90 90 45 45 90 90 45 -45 -45 45 -45 00 00 -45 45	0.049856276

Negative Loading

In Table 5.8 the best stacking sequences of the results of the standard genetic algorithm due to the curved beam subjected to the standard negative loadings are given. It should be noticed that for the negative loading case, the closing moment has been left out due to the reasons discussed for the results of the permutation optimisation.

Many similarities can be seen between the results for the standard genetic algorithm and the results for the permutation algorithm. For the smallest radius over thickness ratio for the in-plane force, the standard genetic algorithm was not able to find a better stacking sequence than the one already found by the permutation algorithm. Furthermore a similar behaviour can be seen with respect to the result of the permutation algorithm. It can be seen that for the smaller radius over thickness ratios a 0° is still present at the outsides of the laminate where for the bigger radius over thickness ratios these disappear and the stacking sequence that is left has the minimum amount of 0° and 90° direction plies left.

When comparing the out-of-plane stacking sequence results, it can be seen that almost all the results are the same as the best layup for the bigger radius over thickness ratios of the in-plane force results. Furthermore when comparing to the results of the permutation algorithm it can be seen that the plies are distributed similarly, though not having the 0° at the outsides of the laminate and having the minimum number of 0° and 90° directed plies.

Table 5.8: Best stacking sequences of the standard GA optimisation for the symmetric cases due to negative loading

Case	R/t	Stacking Sequence	Kim & Soni
In-Plane Force	1	[45/-45/0_2/45/-45/-45/45/0_2/90/90/0_2/90/90/0_2/90/90/0_2/45/-45/-45/45/0_2/-45/45]$_s$	0.690465421
	1.5	[45/-45/0_2/45/-45/45/-45/45/-45/90/0_2/90/90/0_2/90/-45/45/-45/45/-45/45/0_2/-45/45]$_s$	0.633363293
	2	[45/-45/0_2/-45/45/-45/45/90/45/90/-45/0_2/0_2/-45/90/45/90/45/-45/45/-45/0_2/-45/45]$_s$	0.598326141
	3	[45/-45/0_2/45/-45/45/-45/-45/45/90/90/0_2/0_2/90/90/45/-45/-45/45/-45/45/0_2/-45/45]$_s$	0.529492486
	4	[45/-45/45/-45/-45/-45/45/45/90/90/0_2/0_2/0_2/90/90/45/45/-45/-45/-45/45/-45/45]$_s$	0.460077705
	6	[45/-45/-45/45/45/-45/-45/45/90/90/0_2/0_2/0_2/90/90/45/-45/-45/45/45/-45/-45/45]$_s$	0.432360231
	8	[45/-45/-45/45/45/-45/-45/45/90/90/0_2/0_2/0_2/90/90/45/-45/-45/45/45/-45/-45/45]$_s$	0.441207705
Out-of-Plane Force	1	[45/-45/-45/45/45/-45/-45/45/0_2/90/0_2/90/90/0_2/90/0_2/45/-45/-45/45/45/-45/-45/45]$_s$	0.636261588
	1.5	[45/-45/-45/45/45/-45/-45/45/90/90/0_2/0_2/0_2/90/90/45/-45/-45/45/45/-45/-45/45]$_s$	0.569769525
	2	[45/-45/-45/45/-45/45/-45/45/90/90/0_2/0_2/0_2/90/90/45/-45/45/-45/45/-45/-45/45]$_s$	0.531897868
	3	[45/-45/-45/45/-45/-45/45/45/90/90/0_2/0_2/0_2/90/90/45/45/-45/-45/45/-45/-45/45]$_s$	0.476144643
	4	[45/-45/-45/45/-45/45/-45/45/90/90/0_2/0_2/0_2/90/90/45/-45/45/-45/45/-45/-45/45]$_s$	0.459180026
	6	[45/-45/-45/45/-45/45/45/-45/90/90/0_2/0_2/0_2/90/90/-45/45/45/-45/45/-45/-45/45]$_s$	0.439318369
	8	[45/-45/-45/45/-45/45/45/-45/90/90/0_2/0_2/0_2/90/90/-45/45/45/-45/45/-45/-45/45]$_s$	0.431706297

5.5.2.2. Combined Loading Cases

In this section the results for the combined loading cases are given and discussed. The combinations of the different loading cases can be seen in Table 5.9. The fractions in the table represent the fractions of the failure load for that standard case. For example the Kim & Soni failure criterion for the in-plane force for $R/t = 1$ is 0.839, with an applied load of 3000 N, this leads to a failure load of 3573.9 N. Taking half this load thus means an in-plane loading of 1786.9 N.

Table 5.9: Different combined loading cases.

Analysis ID	In-Plane Force	Out-of-Plane Force	Opening Moment
1	$\frac{1}{2}$	$\frac{1}{2}$	0
2	$\frac{1}{2}$	0	$\frac{1}{2}$
3	0	$\frac{1}{2}$	$\frac{1}{2}$
4	$-\frac{1}{2}$	$\frac{1}{2}$	0
5	$\frac{1}{2}$	$-\frac{1}{2}$	0
6	$-\frac{1}{2}$	0	$\frac{1}{2}$
7	0	$-\frac{1}{2}$	$\frac{1}{2}$
8	$\frac{1}{3}$	$\frac{1}{3}$	$\frac{1}{3}$
9	$-\frac{1}{3}$	$\frac{1}{3}$	$\frac{1}{3}$
10	$-\frac{1}{3}$	$-\frac{1}{3}$	$\frac{1}{3}$
11	$\frac{1}{3}$	$-\frac{1}{3}$	$\frac{1}{3}$

The optimum stacking sequences of all the eleven cases can be seen in Tables D.1 and D.2 in Appendix D. It can be seen in the results for the combinations with only positive loading cases, the Kim & Soni failure criterion is indeed close to 1 as predicted by taking a third of each failing load. For the other combined loading cases, the different load cases work against one another. This is mainly due to the fact that the negative loading cases create a closing moment, which in its turn counteracts the opening moment of the positive loading case. What this does to the contribution of the ILSS and ILNS to the failure criterion will be further discussed for all the single load cases and combined loading cases in subsection 5.5.3. In this section the differences in optimum stacking sequences will also be discussed, thus also taking into account the ratio between ILSS and ILNS.

5.5.3. Shear Stress Versus Normal Stress

Previously only the best layups were shown and comparisons were made regarding the change in layup with respect to the change in radius over thickness ratios. Next to the best stacking sequence the next interesting information is about the ratio between shear failure and normal stress failure. Therefore in this section the S_{33} over S_{X3} ratio, or the other way around, will be discussed of all the loading cases which were discussed before. In this case the S_{33} is given in Equation (5.4) and S_{X3} is as given in Equation (5.5).

$$S_{33} = \begin{cases} \frac{\sigma_{33}^2}{F_{33t}^2} & \text{if } \sigma_{33} > 0 \\ \frac{\sigma_{33}^2}{F_{33c}^2} & \text{else} \end{cases} \tag{5.4}$$

$$S_{X3} = \frac{\tau_{13}^2}{F_{13}^2} + \frac{\tau_{23}^2}{F_{23}^2} \tag{5.5}$$

The results for all the different load cases are split over five different plots. The first two plot are for the separate loadcases, the positive loading cases and negative loading cases are shown in Figures 5.7 and 5.8 respectively. The results for the combined loading cases are split into three. The first plot in Figure 5.10 shows the ratio of S_{33}/S_{X3}, these are the cases where S_{X3} is dominant. The second plot in Figure 5.9 shows the ratio of S_{X3}/S_{33} for the loading cases where S_{33} is dominant. The final plot is for a single loading case where the dominance of S_{X3} and S_{33} differed for different radius over thickness ratios, however for most radius over thickness ratios S_{X3} is dominant so the ratio of S_{33}/S_{X3} is plotted.

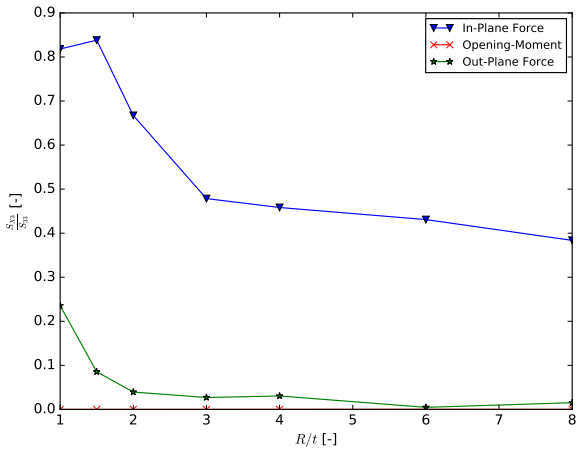

Figure 5.7: Shear stress versus normal stress of positive loading cases.

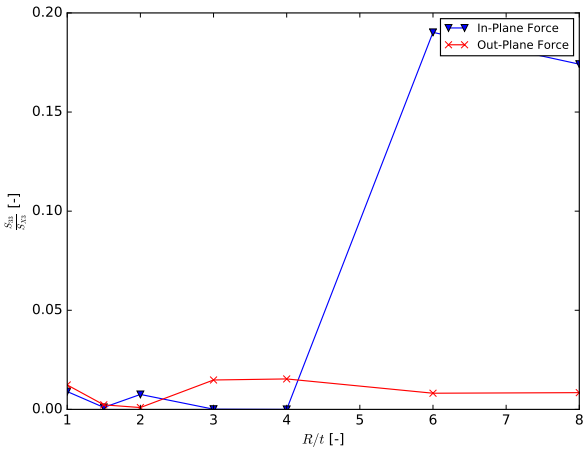

Figure 5.8: Shear stress versus normal stress of negative loading cases.

In all three positive separate loading cases the contribution of S_{33} outweighs the contribution of S_{X3} as can be seen in Figure 5.7. Furthermore it can be seen that for the in-plane loading case for the most extreme case of $R/t = 1$, the contribution of the shear stress to the failure criterion is almost equal to the normal stress. When the radius over thickness ratio gets bigger, this contribution decreases and converges to a contribution of about half compared to the contribution of the normal stress. For the out-of-plane loadcase a similar decrease in influence can be seen. However for the positive out-of-plane loading case, the entire contribution of the shear stress is less, starting at a ratio of about $S_{X3}/S_{33} = 0.25$ and converging to a value near to zero. The opening moment has no contribution at all from the shear stress, as is expected for the pure bending case.

The plots of the contributions for the negative in-plane loading case have a somewhat less obvious shape, as can be seen in Figure 5.8. One would expect the shear stress to be dominant in this case as this was the case for the positive in-plane loading and since the compressive failure stress F_{33_c} is about five times higher. However as one can see, for the two highest radius over thickness ratios there is a somewhat higher influence of the ILNS. The negative out-of-plane loading does not show any unexpected behaviour, though that in the case of positive loading the ILNS was dominating by far, as the compressive failure stress is a lot higher than the tensile failure stress, the ILSS is in this case dominating.

In Figure 5.9 it can be seen what loading combinations cause a ILNS dominated failure criterion and in Figure 5.10 it can be seen what loading combinations cause a ILSS dominated failure criterion. When one

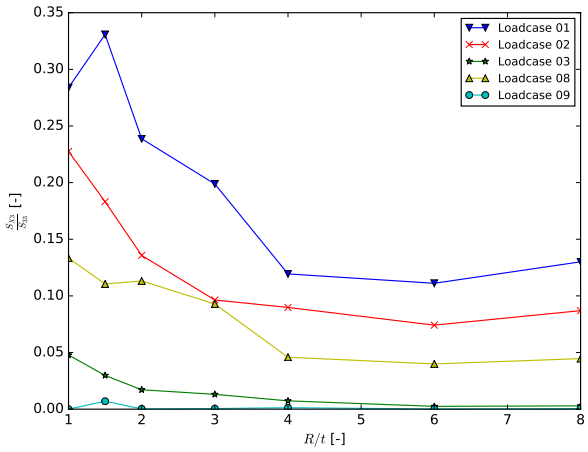

Figure 5.9: Shear stress versus normal stress of cases with higher normal stress.

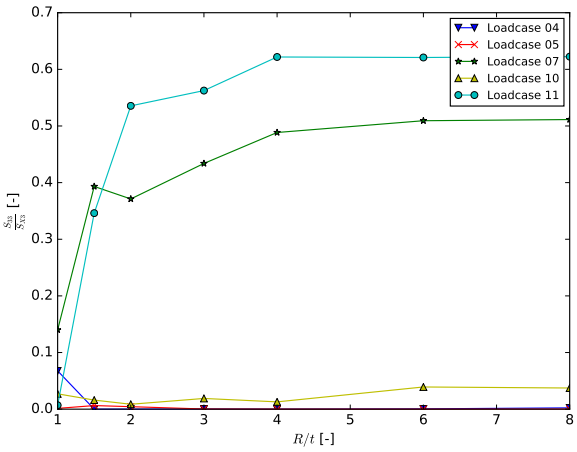

Figure 5.10: Shear stress versus normal stress of cases with higher shear stress.

would look at which loading combinations Figure 5.9 are built of which loading cases (Table 5.9), one would see that four of these five loading cases are actually combinations of only positive loading cases. This is no surprise as each of these three positive loading cases was dominated by the ILNS. The more interesting loading case for this plot is loadcase 09, which is built up from a negative in-plane loading, a positive out-of-plane loading and an opening moment. In this case the shear stresses of the in-plane and out-of-plane loading probably cancel one another, as well as their ILNS (compressive for the in-plane loading and tensile for the out-of-plane loading), leaving a tensile ILNS from the opening moment. This can also be seen from the fact that the values for the Kim & Soni failure criterion in Table D.2 is between $f_{kimson} = 0.40$ and $f_{kimson} = 0.45$.

Three of the five cases in Figure 5.10 are clearly dominated by ILSS. Two of these loading cases are combinations of the in-plane and the out-of-plane loading cases combined, each time having one of the cases in the negative configuration. For these two loading cases (04 & 05), the tensile ILNS of the positive loading case and the compressive ILNS of the negative loading case work against each other, leaving a very low absolute ILNS, thus leading to having almost no contribution to the Kim & Soni failure criterion. This can also be seen in the values for the failure criterion, as these are about half from the solely positive loading combinations. The third loading case clearly dominated by ILSS is a combination of all three different loadings, where the in-plane and out-plane loading are negative (the opening moment is always positive). In this case the two negative loading cases completely remove the contribution of the tensile ILNS from the opening-moment, which only leaves the ILSS and a small compressive ILNS.

The final two cases in Figure 5.10 are less dominated by ILSS, the contribution of ILNS can still clearly be seen. The first of the two is loadcase 07 which is a combination of a negative out-of-plane loading and an opening moment. The negative out-of-plane loading is only able to compensate a part of the tensile ILNS from the opening moment, therefore still leaving a contribution of the ILNS. The increasing influence of the ILNS towards higher radius over thickness ratios is in compliance with the decreasing influence of ILSS for the positive out-of-plane loading case in Figure 5.7. The last of these two cases is loadcase 11 which can be seen as a combination of loadcase 07 and the single positive in-plane loading case. The positive in-plane loading case causes the contribution of the ILNS to increase. It does not increases it more due to the fact that the ratio of ILNS to ILSS for the single case is also one to two, i.e. quite influenced by the ILSS.

The final loading case is the loadcase 06 in Figure 5.11. This loadcase is plotted separately as the dominant stress switches for different radius over thickness ratios and would cause the other plots to become unclear. The loadcase is a combination of a negative in-plane loading and an opening moment. In all of the cases, the compressive ILNS of the negative in-plane loading counteracts the tensile ILNS of the opening moment. It can be seen that it does not completely counteracts the ILNS in all cases and for three radius over thickness ratios, the ILNS is actually dominant.

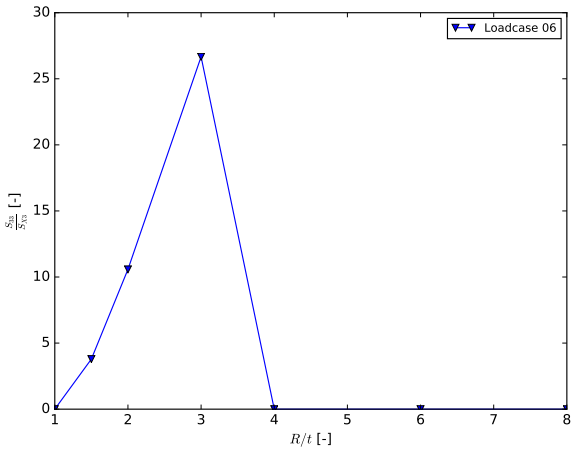

Figure 5.11: Shear stress versus normal stress of cases with changing dominant stress.

5.5.3.1. Stacking Sequence Discussion

An interesting phenomena can be seen when comparing the best stacking sequences in Tables D.1 and D.2 with the plots given in Figures 5.9 to 5.11. It can be seen that for the cases where the ILNS is dominant, that the best stacking sequence is a lot different from for the cases where the ILSS is dominant. For the cases where ILNS is dominant, more 90° directed plies are present for the smaller radius over thickness ratios. These 90° directed plies are then also more ore less scattered over the laminate, whereas for the case where ILSS is dominant the 90° directed plies are located towards the middle of the laminate, next to the 0° directed plies in the middle. Furthermore it should be noticed that in almost each configuration of the cases where ILSS is dominant (except for $R/t = 1.5$ for loadcase 04), the number of 90° plies in the optimum stacking sequence is the minimum of four as well as the minimum of four 0° directed plies, the latter also being the case for the ILNS dominated loadcases.

5.6. Concluding Remarks

The optimisation itself turned out to be a big computational effort and in its turn rather expensive with respect to time. However from the optimisations interesting conclusions can be made. First of all, in the permutation optimisation, an asymmetrical and symmetrical stacking sequence optimisation were done. From these two optimisation it can be concluded that in all cases an asymmetrical stacking sequence would lead to a lower the Kim & Soni failure criterion. The smallest difference is a difference of 6.4% for an in-plane force and a radius over thickness ratio of $R/t = 2$. The biggest difference is a difference of 71.5% for an opening moment with a radius over thickness ratio of $R/t = 8$. The average difference is about 25%, which is a serious difference as the structure could thus become a lot lighter if a asymmetric stacking sequence would be used. However one should remember that the manufacturing of a asymmetric laminates causes coupling stresses after curing which of course need to be studied before final conclusions regarding the use of asymmetric stacking sequences in singly curved structures.

Considering the optimum stacking sequences for the permutation optimisation for the asymmetric cases, it could be seen that in general the 0° directed plies were located towards the outer radius of the curved structure, the 90° directed plies were located around the mid-surface of the laminate and that the remaining ±45° directed plies were located more towards the inner-radius of the curved structure. Considering the symmetric stacking sequences it could be seen that in general the 0° directed plies were both located towards the mid-surface and the outsides of the laminates, depending on what radius over thickness ratio. Furthermore in most cases the 90° are located near the 0° directed plies at the mid-surface, however sometimes scattered over the laminate.

For the negative loading the optimum stacking sequence for the asymmetric cases changed by moving the 0° and 90° a bit towards the inner radius, leaving ±45° directed plies on the outsides. For the symmetric stacking sequences it meant that most 0° directed plies are located towards the mid-surface with in most cases one 0° directed ply on the outsides of the laminate. The 90° directed plies are located near the 0° directed plies at the mid-surface of the laminate. Furthermore from the negative loading cases it could be concluded that the closing-moment case was not interesting for the rest of the project, as the failure criterion

is influenced by ILSS though none should be present for a pure bending case, furthermore only compressive ILNS are present which do not lead to delaminations.

Allowing the in-plane properties to change (thus also changing out-of-plane properties) for the symmetric stacking sequence investigation, showed that the failure mode could be decreased for most cases. The biggest change in the failure criterion is a difference of 8.3% for the in-plane loading case for a radius over thickness ratio of $R/t = 4$. No better stacking sequence could be found for the out-of-plane loading case with a radius over thickness ratio of $R/t = 2$. The general change in ply-direction percentage is that the number of 0° directed plies is reduced in almost all cases. Furthermore it can be seen that for the in-plane loading case the number of 90° directed plies is reduced to the minimum as well. When looking at the out-of-plane loading and the opening-moment it can be noticed that in general the number of 90° is increased and are scattered over the laminate. The negative loading results in almost all cases to a minimum number of 90° and 0° directed plies. The distribution of the plies is very similar to the permutation optimisation.

The main conclusion which can be made from the optimisations done for different loading combinations is that the optimum stacking sequence is quite different when the loading leads to ILNS dominated failure or to ILSS dominated failure in the failure criterion. In general if the failure criterion is dominated by ILSS the minimum of four plies is used for both 0° and 90° directions. In these cases the 0° directed plies are either all located at the mid-plane or have one 0° at the outside. The 90° directed plies are located next to the 0° at the mid-plane of the laminate. For the ILNS dominated failure the behaviour of the distribution of the plies over the laminate is comparable to the cases of the single cases of positive out-of-plane loading or opening moment. In general the number of 90° directed plies is increased and they are scattered over the laminate. However it must be noticed that for bigger radius over thickness ratios the optimum stacking sequence tends to get the same as for the ILSS dominated cases. The number of 0° directed plies is also for the ILNS dominated case brought to the minimum of four.

Finally, one should keep in mind that all the optimisations done have been done with respect to an out-of-plane failure criterion. In many cases of the optimisations in-plane failure became critical and these results should therefore be taken as a guideline to design for out-of-plane failure.

6

Conclusions and Recommendations

The conclusions and recommendations will be split into conclusions regarding the validation of the element and conclusions regarding the stacking sequence investigation.

6.1. Element Validation

From all benchmark tests it can be concluded that in general the ThickS4 element is comparable in performance with respect to mesh convergence with the S4 Abaqus element in the in-plane stresses and in most cases superior in mesh-convergence when considering the out-of-plane stresses when compared to the two 3D Abaqus elements C3D8 and C3D27. When considering the most simple case of a cantilever beam subjected to an end load, the ThickS4 element is comparable with the Abaqus S4 element as the difference between the two solutions is less than 0.5% for all output variables.

Different comparisons were done for a singly curved configuration. From a UD-plied curved laminate it could be concluded that from a radius over thickness ratio of about $R/t = 2.5$ when considering the in-plane stresses and for a radius over thickness ratio of about $R/t = 6.0$ when considering the out-of-plane stresses. However most structures in aerospace are not UD-plied. Therefore when considering different layups the conclusion can be made that the for a radius over thickness ratio of above $R/t = 4$ the ThickS4 element is able to predict the correct location of the maximum ILSS and ILNS. Furthermore for these ratios the element is also able to outperform the Abaqus S4 element for the in-plane stresses. The element showed good correspondence with the 3D Abaqus elements when regarding the ILNS. The ThickS4 element was however not able to predict the right magnitude of the ILSS for these ratios, though showing a correct distribution.

Furthermore in these comparisons, symmetric and asymmetric layups were used to analyse the element. This results in the conclusion that the ThickS4 element is not able to predict the element stresses correctly if an asymmetric layup is used. In the comparisons different radius over thickness convergences were done. From these comparisons it can be concluded that the solution of the ThickS4 element gets worse when the laminate assigned to the element gets thicker.

The final conclusion regarding the validation of the element is that the element is usable in problems where the radius over thickness ratio is bigger than four. However as there are still discrepancies in the magnitude of the ILSS and as long as these discrepancies are not solved, the element should be used in the process of picking an initial design of a stacking sequence only.

However if the element should be further developed and tested. First of all the performance of the element should be tested with respect to doubly-curved structures if it is to be used in all configurations. As said before the magnitude difference of the ILSS should be researched further as well. The final recommendation regarding improvement is that the specific distribution of the stresses at the smaller radius over thickness ratios ($R/t < 4$) should be researched and improved.

6.2. Stacking Sequence Investigation

The conclusions of the element validation lead to the use of the Abaqus C3D8 element for the stacking sequence investigation. In the stacking sequence investigation, permutation optimisations were done where the in-plane properties were kept constant as well as a more regular optimisation where the in-plane properties were also allowed to change though keeping the same number of plies.

The first conclusion which can be drawn is that if an asymmetric stacking sequence is used, the failure criterion can be reduced by at least 6%, where the average reduction in failure criterion is 25%. However if one chooses to use asymmetric layups, the manufacturing of them should be considered as they lead to shearing and bending coupling after curing as well as behaviour in springback. Furthermore it should be researched whether the use of asymmetric layups implies the use of knock-down factors and what these knock-down factors are with respect to the gain/reduction in the failure criterion.

Furthermore from the permutation it could be seen that for the asymmetric case the 0° plies are located towards the outer radius, the 90° are located around the mid-plane and the ±45° are located towards the inner-radius. For the symmetric case it could be seen that in general the 0° directed plies are located at the mid-plane and towards the outside of the laminate, having one or two plies on the outside depending on the radius over thickness ratio. For the loading cases where the ILSS has a big influence on the failure criterion (positive and negative in-plane loading and negative out-of-plane loading) the 90° are located next to the 0° directed plies at the mid-plane of the laminate. For the other cases, they are somewhat scattered over the laminate, though changing to the same stacking sequence of the ILSS influenced layups towards the higher radius over thickness ratios.

The "regular" optimisation was done for the separate loading cases as well as these single cases combined in multiple ways in both negative and positive configuration with respect to loading (not taking into account the closing moment loadcase). With respect of the distribution of the plies the same behaviour could be seen as in the permutation optimisation. A clear difference in the stacking sequences for the loadcases where the ILSS has a big influence in the failure criterion and where the ILNS is the dominant contributor. This difference also resulted into differences with respect to the percentage of plies in each direction. Despite a few exceptions the number of 0° directed plies decreased to the minimum of four. The number of 90° directed plies increased for the cases where ILNS is dominant in the failure criterion and decreased to the minimum of four for the cases where ILSS has a big influence. Again the layups of the ILNS dominated laminates change towards the optimum ILSS laminates for higher radius over thickness ratios.

A quite thorough investigation has been done for the most critical radius over thickness ratios which could be used as a guideline to the design against out-of-plane failure for composite C-spars or stringers. However more investigation should be done what the influence in the design is when the in-plane failure is also taken into account. Finally in order to finish the knowledge about the influence of the stacking sequence to the distribution of the out-of-plane failure, the optimum stacking sequences found in this project should be checked by the Airbus ISAMI CORIN radius bending calculation method.

A

Excel Input Sheet

AnalysisID	Model	nx	ny	R	L1	L2	phi	T-ply	nu21	nu31	nu32	E1	E2	E3	G12	G13	G23	Load	Loaddir	f11t	f11c	f22t	f22c	f33t	f33c	f12	f13	f23	locatie [B,M,L]	sigL or sigT	Convergence	To Plot
1	LehknitskyForce	3	1	15	-	6	0,0,0,0,0,0,0,0,0,0,0,0,0,0,0,0,0,0,0,0,0,0,0,0,0,0,0,0,0,0,0,0	0.254	0.33	0.33	0.33	1.54E+005	8.50E+003	8.50E+003	4.20E+003	4.20E+003	3.36E+003	1	3	2610	-1450	55	-285	55	-250	105	68	68	L	sigL	Mesh	thickS4,C3D27,S4,anal,C3D8
1	LehknitskyForce	9	3	15	-	6	0,0,0,0,0,0,0,0,0,0,0,0,0,0,0,0,0,0,0,0,0,0,0,0,0,0,0,0,0,0,0,0	0.254	0.33	0.33	0.33	1.54E+005	8.50E+003	8.50E+003	4.20E+003	4.20E+003	3.36E+003	1	3	2610	-1450	55	-285	55	-250	105	68	68	L	sigL	Mesh	thickS4,C3D27,S4,anal,C3D8
1	LehknitskyForce	15	5	15	-	6	0,0,0,0,0,0,0,0,0,0,0,0,0,0,0,0,0,0,0,0,0,0,0,0,0,0,0,0,0,0,0,0	0.254	0.33	0.33	0.33	1.54E+005	8.50E+003	8.50E+003	4.20E+003	4.20E+003	3.36E+003	1	3	2610	-1450	55	-285	55	-250	105	68	68	L	sigL	Mesh	thickS4,C3D27,S4,anal,C3D8
1	LehknitskyForce	21	7	15	-	6	0,0,0,0,0,0,0,0,0,0,0,0,0,0,0,0,0,0,0,0,0,0,0,0,0,0,0,0,0,0,0,0	0.254	0.33	0.33	0.33	1.54E+005	8.50E+003	8.50E+003	4.20E+003	4.20E+003	3.36E+003	1	3	2610	-1450	55	-285	55	-250	105	68	68	L	sigL	Mesh	thickS4,C3D27,S4,anal,C3D8
1	LehknitskyForce	27	9	15	-	6	0,0,0,0,0,0,0,0,0,0,0,0,0,0,0,0,0,0,0,0,0,0,0,0,0,0,0,0,0,0,0,0	0.254	0.33	0.33	0.33	1.54E+005	8.50E+003	8.50E+003	4.20E+003	4.20E+003	3.36E+003	1	3	2610	-1450	55	-285	55	-250	105	68	68	L	sigL	Mesh	thickS4,C3D27,S4,anal,C3D8
1	LehknitskyForce	33	11	15	-	6	0,0,0,0,0,0,0,0,0,0,0,0,0,0,0,0,0,0,0,0,0,0,0,0,0,0,0,0,0,0,0,0	0.254	0.33	0.33	0.33	1.54E+005	8.50E+003	8.50E+003	4.20E+003	4.20E+003	3.36E+003	1	3	2610	-1450	55	-285	55	-250	105	68	68	L	sigL	Mesh	thickS4,C3D27,S4,anal,C3D8
1	LehknitskyForce	39	13	15	-	6	0,0,0,0,0,0,0,0,0,0,0,0,0,0,0,0,0,0,0,0,0,0,0,0,0,0,0,0,0,0,0,0	0.254	0.33	0.33	0.33	1.54E+005	8.50E+003	8.50E+003	4.20E+003	4.20E+003	3.36E+003	1	3	2610	-1450	55	-285	55	-250	105	68	68	L	sigL	Mesh	thickS4,C3D27,S4,anal,C3D8
1	LehknitskyForce	45	15	15	-	6	0,0,0,0,0,0,0,0,0,0,0,0,0,0,0,0,0,0,0,0,0,0,0,0,0,0,0,0,0,0,0,0	0.254	0.33	0.33	0.33	1.54E+005	8.50E+003	8.50E+003	4.20E+003	4.20E+003	3.36E+003	1	3	2610	-1450	55	-285	55	-250	105	68	68	L	sigL	Mesh	thickS4,C3D27,S4,anal,C3D8
1	LehknitskyForce	51	17	15	-	6	0,0,0,0,0,0,0,0,0,0,0,0,0,0,0,0,0,0,0,0,0,0,0,0,0,0,0,0,0,0,0,0	0.254	0.33	0.33	0.33	1.54E+005	8.50E+003	8.50E+003	4.20E+003	4.20E+003	3.36E+003	1	3	2610	-1450	55	-285	55	-250	105	68	68	L	sigL	Mesh	thickS4,C3D27,S4,anal,C3D8
1	LehknitskyForce	57	19	15	-	6	0,0,0,0,0,0,0,0,0,0,0,0,0,0,0,0,0,0,0,0,0,0,0,0,0,0,0,0,0,0,0,0	0.254	0.33	0.33	0.33	1.54E+005	8.50E+003	8.50E+003	4.20E+003	4.20E+003	3.36E+003	1	3	2610	-1450	55	-285	55	-250	105	68	68	L	sigL	Mesh	thickS4,C3D27,S4,anal,C3D8
1	LehknitskyForce	63	21	15	-	6	0,0,0,0,0,0,0,0,0,0,0,0,0,0,0,0,0,0,0,0,0,0,0,0,0,0,0,0,0,0,0,0	0.254	0.33	0.33	0.33	1.54E+005	8.50E+003	8.50E+003	4.20E+003	4.20E+003	3.36E+003	1	3	2610	-1450	55	-285	55	-250	105	68	68	L	sigL	Mesh	thickS4,C3D27,S4,anal,C3D8
2	LehknitskyMoment	3	1	15	-	6	0,0,0,0,0,0,0,0,0,0,0,0,0,0,0,0,0,0,0,0,0,0,0,0,0,0,0,0,0,0,0,0	0.254	0.33	0.33	0.33	1.54E+005	8.50E+003	8.50E+003	4.20E+003	4.20E+003	3.36E+003	1	5	2610	-1450	55	-285	55	-250	105	68	68	L	sigL	Mesh	thickS4,C3D27,S4,anal,C3D8
2	LehknitskyMoment	9	3	15	-	6	0,0,0,0,0,0,0,0,0,0,0,0,0,0,0,0,0,0,0,0,0,0,0,0,0,0,0,0,0,0,0,0	0.254	0.33	0.33	0.33	1.54E+005	8.50E+003	8.50E+003	4.20E+003	4.20E+003	3.36E+003	1	5	2610	-1450	55	-285	55	-250	105	68	68	L	sigL	Mesh	thickS4,C3D27,S4,anal,C3D8
2	LehknitskyMoment	15	5	15	-	6	0,0,0,0,0,0,0,0,0,0,0,0,0,0,0,0,0,0,0,0,0,0,0,0,0,0,0,0,0,0,0,0	0.254	0.33	0.33	0.33	1.54E+005	8.50E+003	8.50E+003	4.20E+003	4.20E+003	3.36E+003	1	5	2610	-1450	55	-285	55	-250	105	68	68	L	sigL	Mesh	thickS4,C3D27,S4,anal,C3D8
2	LehknitskyMoment	21	7	15	-	6	0,0,0,0,0,0,0,0,0,0,0,0,0,0,0,0,0,0,0,0,0,0,0,0,0,0,0,0,0,0,0,0	0.254	0.33	0.33	0.33	1.54E+005	8.50E+003	8.50E+003	4.20E+003	4.20E+003	3.36E+003	1	5	2610	-1450	55	-285	55	-250	105	68	68	L	sigL	Mesh	thickS4,C3D27,S4,anal,C3D8
2	LehknitskyMoment	27	9	15	-	6	0,0,0,0,0,0,0,0,0,0,0,0,0,0,0,0,0,0,0,0,0,0,0,0,0,0,0,0,0,0,0,0	0.254	0.33	0.33	0.33	1.54E+005	8.50E+003	8.50E+003	4.20E+003	4.20E+003	3.36E+003	1	5	2610	-1450	55	-285	55	-250	105	68	68	L	sigL	Mesh	thickS4,C3D27,S4,anal,C3D8
2	LehknitskyMoment	33	11	15	-	6	0,0,0,0,0,0,0,0,0,0,0,0,0,0,0,0,0,0,0,0,0,0,0,0,0,0,0,0,0,0,0,0	0.254	0.33	0.33	0.33	1.54E+005	8.50E+003	8.50E+003	4.20E+003	4.20E+003	3.36E+003	1	5	2610	-1450	55	-285	55	-250	105	68	68	L	sigL	Mesh	thickS4,C3D27,S4,anal,C3D8
2	LehknitskyMoment	39	13	15	-	6	0,0,0,0,0,0,0,0,0,0,0,0,0,0,0,0,0,0,0,0,0,0,0,0,0,0,0,0,0,0,0,0	0.254	0.33	0.33	0.33	1.54E+005	8.50E+003	8.50E+003	4.20E+003	4.20E+003	3.36E+003	1	5	2610	-1450	55	-285	55	-250	105	68	68	L	sigL	Mesh	thickS4,C3D27,S4,anal,C3D8
2	LehknitskyMoment	45	15	15	-	6	0,0,0,0,0,0,0,0,0,0,0,0,0,0,0,0,0,0,0,0,0,0,0,0,0,0,0,0,0,0,0,0	0.254	0.33	0.33	0.33	1.54E+005	8.50E+003	8.50E+003	4.20E+003	4.20E+003	3.36E+003	1	5	2610	-1450	55	-285	55	-250	105	68	68	L	sigL	Mesh	thickS4,C3D27,S4,anal,C3D8
2	LehknitskyMoment	51	17	15	-	6	0,0,0,0,0,0,0,0,0,0,0,0,0,0,0,0,0,0,0,0,0,0,0,0,0,0,0,0,0,0,0,0	0.254	0.33	0.33	0.33	1.54E+005	8.50E+003	8.50E+003	4.20E+003	4.20E+003	3.36E+003	1	5	2610	-1450	55	-285	55	-250	105	68	68	L	sigL	Mesh	thickS4,C3D27,S4,anal,C3D8
2	LehknitskyMoment	57	19	15	-	6	0,0,0,0,0,0,0,0,0,0,0,0,0,0,0,0,0,0,0,0,0,0,0,0,0,0,0,0,0,0,0,0	0.254	0.33	0.33	0.33	1.54E+005	8.50E+003	8.50E+003	4.20E+003	4.20E+003	3.36E+003	1	5	2610	-1450	55	-285	55	-250	105	68	68	L	sigL	Mesh	thickS4,C3D27,S4,anal,C3D8
2	LehknitskyMoment	63	21	15	-	6	0,0,0,0,0,0,0,0,0,0,0,0,0,0,0,0,0,0,0,0,0,0,0,0,0,0,0,0,0,0,0,0	0.254	0.33	0.33	0.33	1.54E+005	8.50E+003	8.50E+003	4.20E+003	4.20E+003	3.36E+003	1	5	2610	-1450	55	-285	55	-250	105	68	68	L	sigL	Mesh	thickS4,C3D27,S4,anal,C3D8

Figure A.1: Screenshot of the excel input sheet used to start the benchmark tests.

B

Matrix Equations for Boundary Conditions for Multilayer Theory

$$
\begin{bmatrix}
\beta_1 a_0^{\beta_1} & -\beta_1 a_0^{-\beta_1} & 1 & 0 & 0 & 0 & 0 & 0 & 0 \\
\beta_1 a_1^{\beta_1} & -\beta_1 a_1^{-\beta_1} & 1 & -\beta_2 a_1^{\beta_2} & \beta_2 a_1^{-\beta_2} & -1 & 0 & 0 & 0 \\
0 & 0 & 0 & \beta_2 a_2^{\beta_2} & -\beta_2 a_2^{-\beta_2} & 1 & -\beta_3 a_2^{\beta_3} & \beta_3 a_2^{-\beta_3} & -1 \\
0 & 0 & 0 & 0 & 0 & 0 & \beta_3 a_3^{\beta_3} & -\beta_3 a_3^{-\beta_3} & 1 \\
a_1^{\beta_1}\left[\frac{1}{E^{(1)}}-(1+\beta_1)\frac{\nu_{\theta r}^{(1)}}{E_\theta^{(1)}}\right] & a_1^{-\beta_1}\left[\frac{1}{E^{(1)}}-(1-\beta_1)\frac{\nu_{\theta r}^{(1)}}{E_\theta^{(1)}}\right] & (\ln a_1)\left(\frac{1}{E^{(1)}}-\frac{\nu_{\theta r}^{(1)}}{E_\theta^{(1)}}\right) & -a_1^{\beta_2}\left[\frac{1}{E^{(2)}}-(1+\beta_2)\frac{\nu_{\theta r}^{(2)}}{E_\theta^{(2)}}\right] & -a_1^{-\beta_2}\left[\frac{1}{E^{(2)}}-(1-\beta_2)\frac{\nu_{\theta r}^{(2)}}{E_\theta^{(2)}}\right] & -(\ln a_1)\left(\frac{1}{E^{(2)}}-\frac{\nu_{\theta r}^{(2)}}{E_\theta^{(2)}}\right) & 0 & 0 & 0 \\
0 & 0 & 0 & a_2^{\beta_2}\left[\frac{1}{E^{(2)}}-(1+\beta_2)\frac{\nu_{\theta r}^{(2)}}{E_\theta^{(2)}}\right] & a_2^{-\beta_2}\left[\frac{1}{E^{(2)}}-(1-\beta_2)\frac{\nu_{\theta r}^{(2)}}{E_\theta^{(2)}}\right] & (\ln a_2)\left(\frac{1}{E^{(2)}}-\frac{\nu_{\theta r}^{(2)}}{E_\theta^{(2)}}\right) & -a_2^{\beta_3}\left[\frac{1}{E^{(3)}}-(1+\beta_3)\frac{\nu_{\theta r}^{(3)}}{E_\theta^{(3)}}\right] & -a_2^{-\beta_3}\left[\frac{1}{E^{(3)}}-(1-\beta_3)\frac{\nu_{\theta r}^{(3)}}{E_\theta^{(3)}}\right] & -(\ln a_2)\left(\frac{1}{E^{(3)}}-\frac{\nu_{\theta r}^{(3)}}{E_\theta^{(3)}}\right) \\
\frac{a_1^{\beta_1}\beta_1}{E_\theta^{(1)}}\left[(1+\beta_1)-\nu_{\theta r}^{(1)}\right] & -\frac{a_1^{-\beta_1}\beta_1}{E_\theta^{(1)}}\left[(1-\beta_1)-\nu_{\theta r}^{(1)}\right] & \frac{1-\nu_{\theta r}^{(1)}}{E_\theta^{(1)}} & -\frac{a_1^{\beta_2}\beta_2}{E_\theta^{(2)}}\left[(1+\beta_2)-\nu_{\theta r}^{(2)}\right] & \frac{a_1^{-\beta_2}\beta_2}{E_\theta^{(2)}}\left[(1-\beta_2)-\nu_{\theta r}^{(2)}\right] & \frac{1-\nu_{\theta r}^{(2)}}{E_\theta^{(2)}} & 0 & 0 & 0 \\
0 & 0 & 0 & \frac{a_2^{\beta_2}\beta_2}{E_\theta^{(2)}}\left[(1+\beta_2)-\nu_{\theta r}^{(2)}\right] & -\frac{a_2^{-\beta_2}\beta_2}{E_\theta^{(2)}}\left[(1-\beta_2)-\nu_{\theta r}^{(2)}\right] & \frac{1-\nu_{\theta r}^{(2)}}{E_\theta^{(2)}} & -\frac{a_2^{\beta_3}\beta_3}{E_\theta^{(3)}}\left[(1+\beta_3)-\nu_{\theta r}^{(3)}\right] & \frac{a_2^{-\beta_3}\beta_3}{E_\theta^{(3)}}\left[(1-\beta_3)-\nu_{\theta r}^{(3)}\right] & \frac{1-\nu_{\theta r}^{(3)}}{E_\theta^{(3)}} \\
a_1^{\beta_1}-a_0^{\beta_1} & a_1^{-\beta_1}-a_0^{-\beta_1} & \ln a_1-\ln a_0 & a_2^{\beta_2}-a_1^{\beta_2} & a_2^{-\beta_2}-a_1^{-\beta_2} & \ln a_2-\ln a_1 & a_3^{\beta_3}-a_2^{\beta_3} & a_3^{-\beta_3}-a_2^{-\beta_3} & \ln a_3-\ln a_2
\end{bmatrix}
\begin{bmatrix} A_1 \\ B_1 \\ D_1 \\ A_2 \\ B_2 \\ D_2 \\ A_3 \\ B_3 \\ D_3 \end{bmatrix}
=
\begin{bmatrix} 0 \\ 0 \\ 0 \\ 0 \\ 0 \\ 0 \\ 0 \\ 0 \\ P \end{bmatrix}
\tag{B.1}
$$

$$
\begin{bmatrix}
2 & (1+k_1)a_0^{k_1-1} & (1-k_1)a_0^{-k_1-1} & 0 & 0 & 0 & 0 & 0 & 0 \\
2 & (1+k_1)a_1^{k_1-1} & (1-k_1)a_1^{-k_1-1} & -2 & -(1+k_2)a_1^{k_2-1} & -(1-k_2)a_1^{-k_2-1} & 0 & 0 & 0 \\
0 & 0 & 0 & 2 & (1+k_2)a_2^{k_2-1} & (1-k_2)a_2^{-k_2-1} & -2 & -(1+k_3)a_2^{k_3-1} & -(1-k_3)a_2^{-k_3-1} \\
0 & 0 & 0 & 0 & 0 & 0 & 2 & (1+k_3)a_3^{k_3-1} & (1-k_3)a_3^{-k_3-1} \\
2a_1\left(\frac{1}{E_r^{(1)}}-\frac{\nu_{\theta r}^{(1)}}{E_\theta^{(1)}}\right) & (1+k_1)a_1^{k_1}\left(\frac{1}{k_1E_r^{(1)}}-\frac{\nu_{\theta r}^{(1)}}{E_\theta^{(1)}}\right) & -(1-k_1)a_1^{-k_1}\left(\frac{1}{k_1E_r^{(1)}}-\frac{\nu_{\theta r}^{(1)}}{E_\theta^{(1)}}\right) & -2a_1\left(\frac{1}{E_r^{(2)}}-\frac{\nu_{\theta r}^{(2)}}{E_\theta^{(2)}}\right) & -(1+k_2)a_1^{k_2}\left(\frac{1}{k_2E_r^{(2)}}-\frac{\nu_{\theta r}^{(2)}}{E_\theta^{(2)}}\right) & (1-k_2)a_1^{-k_2}\left(\frac{1}{k_2E_r^{(2)}}-\frac{\nu_{\theta r}^{(2)}}{E_\theta^{(2)}}\right) & 0 & 0 & 0 \\
0 & 0 & 0 & 2a_2\left(\frac{1}{E_r^{(2)}}-\frac{\nu_{\theta r}^{(2)}}{E_\theta^{(2)}}\right) & (1+k_2)a_2^{k_2}\left(\frac{1}{k_2E_r^{(2)}}-\frac{\nu_{\theta r}^{(2)}}{E_\theta^{(2)}}\right) & -(1-k_2)a_2^{-k_2}\left(\frac{1}{k_2E_r^{(2)}}-\frac{\nu_{\theta r}^{(2)}}{E_\theta^{(2)}}\right) & -2a_2\left(\frac{1}{E_r^{(3)}}-\frac{\nu_{\theta r}^{(3)}}{E_\theta^{(3)}}\right) & -(1+k_3)a_2^{k_3}\left(\frac{1}{k_3E_r^{(3)}}-\frac{\nu_{\theta r}^{(3)}}{E_\theta^{(3)}}\right) & (1-k_3)a_2^{-k_3}\left(\frac{1}{k_3E_r^{(3)}}-\frac{\nu_{\theta r}^{(3)}}{E_\theta^{(3)}}\right) \\
\frac{1}{E_\theta^{(1)}}-\frac{1}{E_r^{(1)}} & 0 & 0 & \frac{1}{E_\theta^{(2)}}-\frac{1}{E_r^{(2)}} & 0 & 0 & 0 & 0 & 0 \\
0 & 0 & 0 & \frac{1}{E_\theta^{(2)}}-\frac{1}{E_r^{(2)}} & 0 & 0 & \frac{1}{E_\theta^{(3)}}-\frac{1}{E_r^{(3)}} & 0 & 0 \\
a_1^2-a_0^2 & k_1\left(a_1^{k_1+1}-a_0^{k_1+1}\right) & -k_1\left(a_1^{-k_1+1}-a_0^{-k_1+1}\right) & a_2^2-a_1^2 & k_2\left(a_2^{k_2+1}-a_1^{k_2+1}\right) & -k_2\left(a_2^{-k_2+1}-a_1^{-k_2+1}\right) & a_3^2-a_2^2 & k_3\left(a_3^{k_3+1}-a_2^{k_3+1}\right) & -k_3\left(a_3^{-k_3+1}-a_2^{-k_3+1}\right)
\end{bmatrix}
\begin{bmatrix} B_1' \\ C_1' \\ D_1' \\ B_2' \\ C_2' \\ D_2' \\ B_3' \\ C_3' \\ D_3' \end{bmatrix}
=
\begin{bmatrix} 0 \\ 0 \\ 0 \\ 0 \\ 0 \\ 0 \\ 0 \\ 0 \\ -M \end{bmatrix}
\tag{B.2}
$$

C

Optimisation Distribution

In this appendix the optimisation distributions of the asymmetric and symmetric case for the positive loads is given for the smallest radius over thickness ratio of $R/t = 1.0$.

C.1. Asymmetric

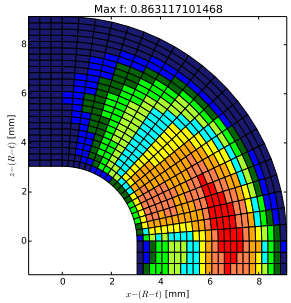

Figure C.1: Kim & Soni failure criterion distribution for best individual of the first generation due to in-plane loading, $R/t = 1$.

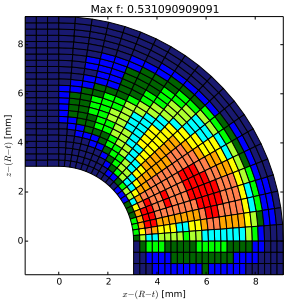

Figure C.2: S_{33} distribution for best individual of the first generation due to in-plane loading, $R/t = 1$.

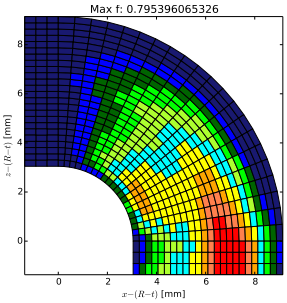

Figure C.3: S_{x3} distribution for best individual of the first generation due to in-plane loading, $R/t = 1$.

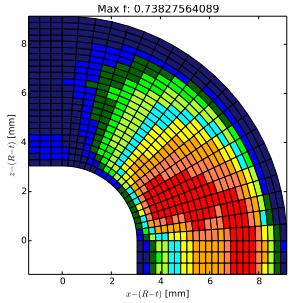

Figure C.4: Kim & Soni failure criterion distribution for the best stacking sequence due to in-plane loading, $R/t = 1$.

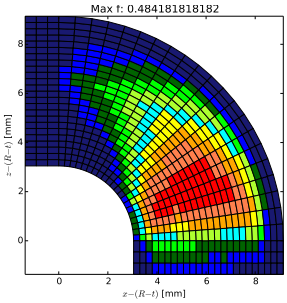

Figure C.5: S_{33} distribution for the best stacking sequence due to in-plane loading, $R/t = 1$.

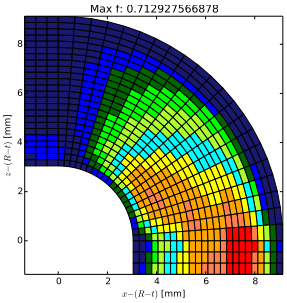

Figure C.6: S_{x3} distribution for the best stacking sequence due to in-plane loading, $R/t = 1$.

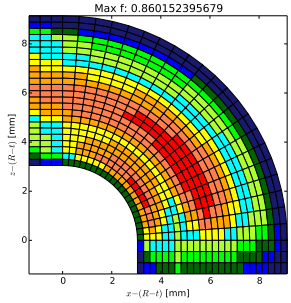

Figure C.7: Kim & Soni failure criterion distribution for best individual of the first generation due to out-of-plane loading, $R/t = 1$.

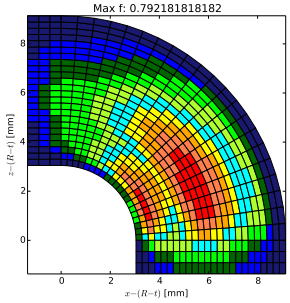

Figure C.8: S_{33} distribution for best individual of the first generation due to out-of-plane loading, $R/t = 1$.

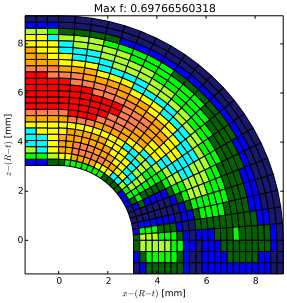

Figure C.9: S_{x3} distribution for best individual of the first generation due to out-of-plane loading, $R/t = 1$.

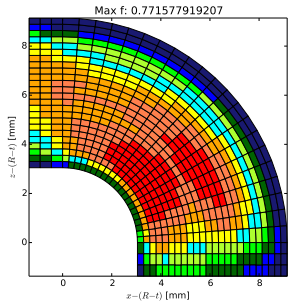

Figure C.10: Kim & Soni failure criterion distribution for the best stacking sequence due to out-of-plane loading, $R/t = 1$.

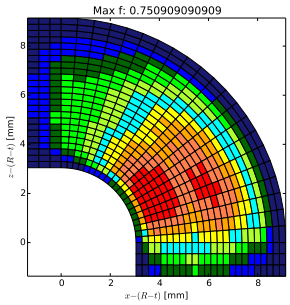

Figure C.11: S_{33} distribution for the best stacking sequence due to out-of-plane loading, $R/t = 1$.

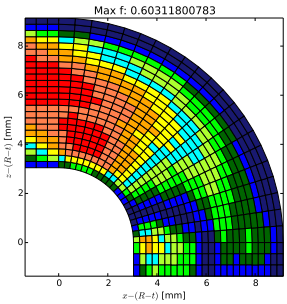

Figure C.12: S_{x3} distribution for the best stacking sequence due to out-of-plane loading, $R/t = 1$.

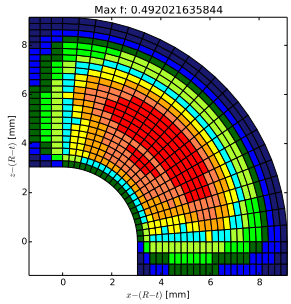

Figure C.13: Kim & Soni failure criterion distribution for best individual of the first generation due to an opening moment, $R/t = 1$.

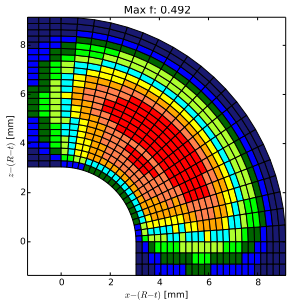

Figure C.14: S_{33} distribution for best individual of the first generation due to an opening moment, $R/t = 1$.

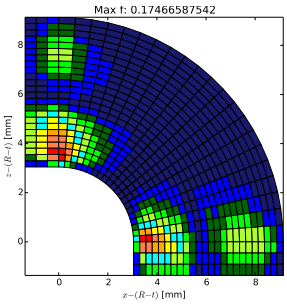

Figure C.15: S_{x3} distribution for best individual of the first generation due to an opening moment, $R/t = 1$.

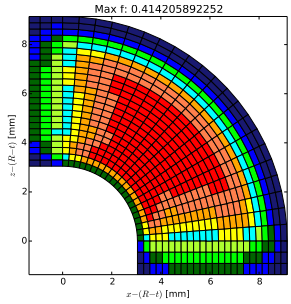

Figure C.16: Kim & Soni failure criterion distribution for the best stacking sequence due to an opening moment, $R/t = 1$.

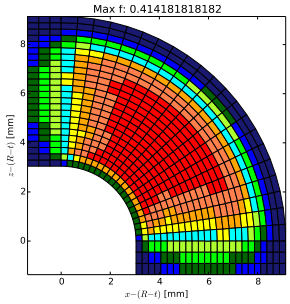

Figure C.17: S_{33} distribution for the best stacking sequence due to an opening moment, $R/t = 1$.

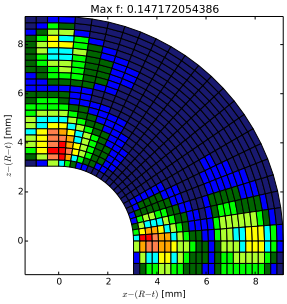

Figure C.18: S_{x3} distribution for the best stacking sequence due to an opening moment, $R/t = 1$.

C.2. Symmetric

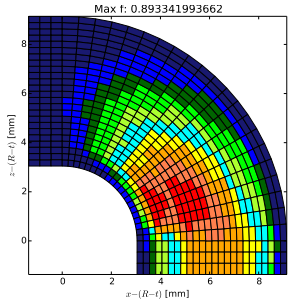

Figure C.19: Kim & Soni failure criterion distribution for best individual of the first generation due to in-plane loading, $R/t = 1$.

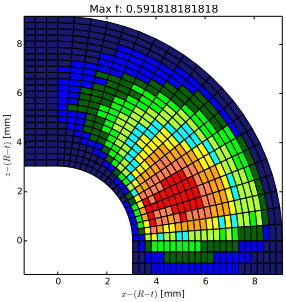

Figure C.20: S_{33} distribution for best individual of the first generation due to in-plane loading, $R/t = 1$.

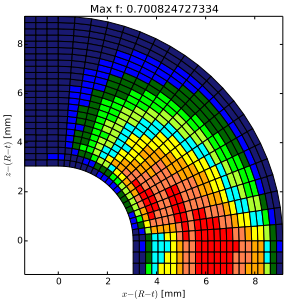

Figure C.21: S_{x3} distribution for best individual of the first generation due to in-plane loading, $R/t = 1$.

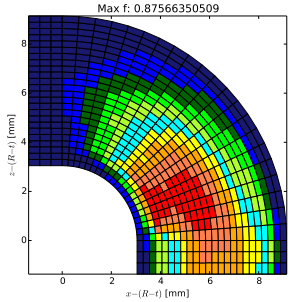

Figure C.22: Kim & Soni failure criterion distribution for the best stacking sequence due to in-plane loading, $R/t = 1$.

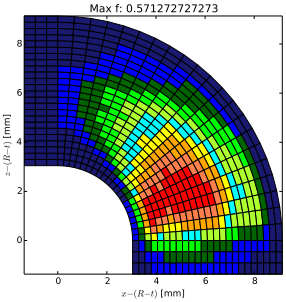

Figure C.23: S_{33} distribution for the best stacking sequence due to in-plane loading, $R/t = 1$.

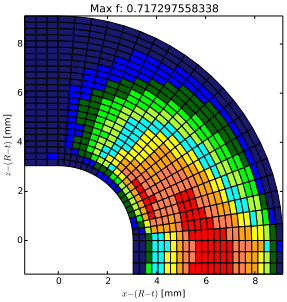

Figure C.24: S_{x3} distribution for the best stacking sequence due to in-plane loading, $R/t = 1$.

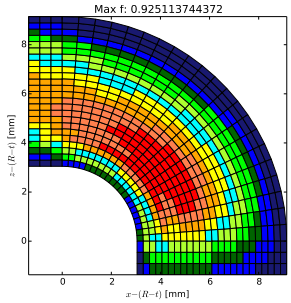

Figure C.25: Kim & Soni failure criterion distribution for best individual of the first generation due to out-of-plane loading, $R/t = 1$.

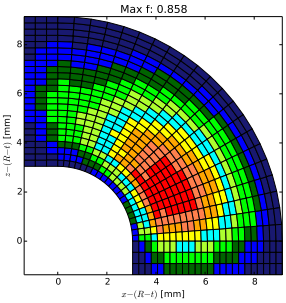

Figure C.26: S_{33} distribution for best individual of the first generation due to out-of-plane loading, $R/t = 1$.

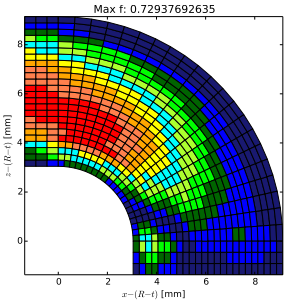

Figure C.27: S_{x3} distribution for best individual of the first generation due to out-of-plane loading, $R/t = 1$.

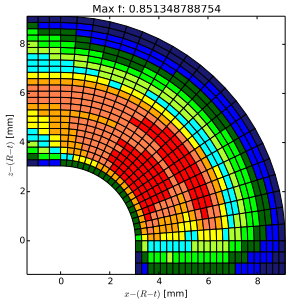

Figure C.28: Kim & Soni failure criterion distribution for the best stacking sequence due to out-of-plane loading, $R/t = 1$.

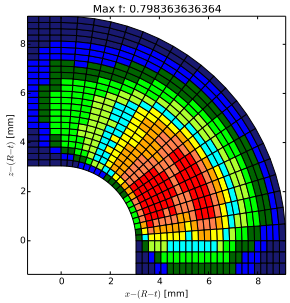

Figure C.29: S_{33} distribution for the best stacking sequence due to out-of-plane loading, $R/t = 1$.

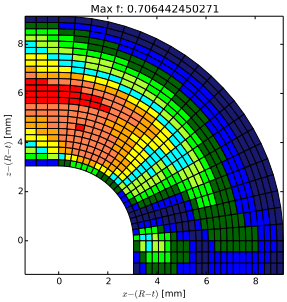

Figure C.30: S_{x3} distribution for the best stacking sequence due to out-of-plane loading, $R/t = 1$.

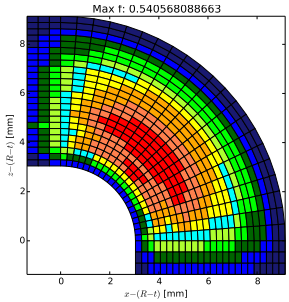

Figure C.31: Kim & Soni failure criterion distribution for best individual of the first generation due to an opening moment, $R/t = 1$.

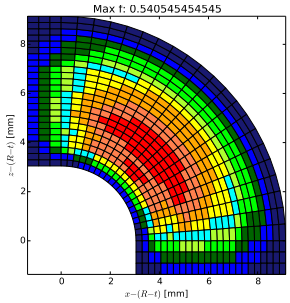

Figure C.32: S_{33} distribution for best individual of the first generation due to an opening moment, $R/t = 1$.

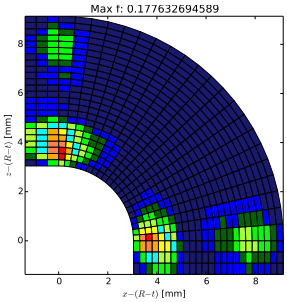

Figure C.33: S_{x3} distribution for best individual of the first generation due to an opening moment, $R/t = 1$.

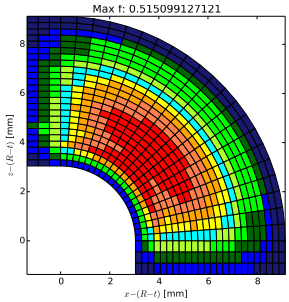

Figure C.34: Kim & Soni failure criterion distribution for the best stacking sequence due to an opening moment, $R/t = 1$.

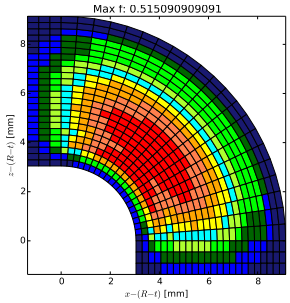

Figure C.35: S_{33} distribution for the best stacking sequence due to an opening moment, $R/t = 1$.

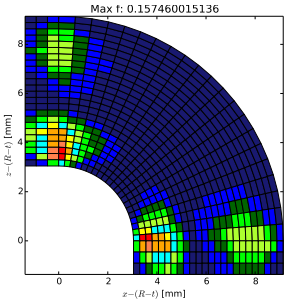

Figure C.36: S_{x3} distribution for the best stacking sequence due to an opening moment, $R/t = 1$.

D

Optimum Layup Combined Loading

Table D.1: Best stacking sequences of the standard GA optimisation for the symmetric cases due to combined loading

Case	R/t	Stacking Sequence	Kim & Soni
Loadcase 01	1	[45/-45/90/90/-45/90/45/-45/45/90/0/0/0/0/90/45/-45/45/90/-45/90/90/-45/45]s	0.945181504
	1.5	[45/-45/0/90/-45/45/90/-45/90/0/0/45/45/0/0/90/-45/90/45/-45/90/0/-45/45]s	0.957701437
	2	[45/-45/0/45/90/-45/90/45/-45/90/0/0/0/0/90/-45/45/90/-45/90/45/0/-45/45]s	0.962820283
	3	[45/-45/0/45/-45/90/45/90/-45/90/90/0/0/90/90/-45/90/45/90/-45/45/0/-45/45]s	0.96272206
	4	[45/-45/0/-45/45/-45/45/-45/90/45/90/0/0/90/45/90/-45/45/-45/45/-45/0/-45/45]s	0.963762467
	6	[45/-45/0/-45/45/-45/45/45/-45/90/90/0/0/90/90/-45/45/45/-45/45/-45/0/-45/45]s	0.956162665
	8	[45/-45/0/0/-45/45/-45/45/90/45/-45/90/90/-45/45/90/45/-45/45/-45/0/0/-45/45]s	0.984194541
Loadcase 02	1	[45/-45/0/90/45/-45/90/0/90/0/90/90/90/90/0/90/0/90/-45/45/90/0/-45/45]s	0.888372847
	1.5	[45/-45/0/90/45/90/-45/90/45/0/90/-45/-45/90/0/45/90/-45/90/45/90/0/-45/45]s	0.887795339
	2	[45/-45/0/90/-45/90/45/90/-45/90/0/45/45/0/90/-45/90/45/90/-45/90/0/-45/45]s	0.915142383
	3	[45/-45/0/-45/45/-45/90/45/90/90/90/0/0/90/90/90/45/90/-45/45/-45/0/-45/45]s	0.934564653
	4	[45/-45/0/-45/45/-45/45/-45/90/45/90/0/0/90/45/90/-45/45/-45/45/-45/0/-45/45]s	0.944858766
	6	[45/-45/0/-45/45/45/-45/-45/45/90/90/0/0/90/90/45/-45/-45/45/45/-45/0/-45/45]s	0.940882543
	8	[45/-45/0/-45/45/-45/45/45/-45/90/0/90/90/0/90/-45/45/45/-45/45/-45/0/-45/45]s	0.971301283
Loadcase 03	1	[45/-45/90/45/90/45/-45/90/-45/0/90/0/0/90/0/-45/90/-45/45/90/45/90/-45/45]s	0.9750594
	1.5	[45/-45/0/90/45/-45/90/90/0/90/0/90/90/0/90/0/90/90/-45/45/90/0/-45/45]s	0.986736494
	2	[45/-45/0/90/90/-45/90/45/-45/90/0/45/45/0/90/-45/45/90/-45/90/90/0/-45/45]s	0.988906331
	3	[45/-45/0/90/90/90/45/90/90/90/-45/0/0/-45/90/90/90/45/90/90/90/0/-45/45]s	0.984378042
	4	[45/-45/0/90/-45/90/45/90/90/90/90/0/0/90/90/90/90/45/90/-45/90/0/-45/45]s	0.992709938
	6	[45/-45/0/0/-45/-45/45/90/-45/45/90/45/45/90/45/-45/90/45/-45/-45/0/0/-45/45]s	1.005794978
	8	[45/-45/0/0/45/-45/45/45/90/-45/-45/90/90/-45/-45/90/45/45/-45/45/0/0/-45/45]s	0.997818522
Loadcase 04	1	[45/-45/0/45/-45/45/-45/-45/90/0/45/90/90/45/0/90/-45/-45/45/-45/45/0/-45/45]s	0.465457164
	1.5	[45/-45/0/-45/45/-45/45/90/90/90/90/0/0/90/90/90/90/45/-45/45/-45/0/-45/45]s	0.475634286
	2	[45/-45/0/-45/45/-45/45/45/-45/90/90/0/0/90/90/-45/45/45/-45/45/-45/0/-45/45]s	0.486542774
	3	[45/-45/45/-45/-45/45/-45/45/90/90/0/0/0/0/90/90/45/-45/45/-45/-45/45/-45/45]s	0.495133077
	4	[45/-45/-45/45/45/-45/-45/45/90/90/0/0/0/0/90/90/45/-45/-45/45/45/-45/-45/45]s	0.492890301
	6	[45/-45/-45/45/-45/45/45/-45/90/90/0/0/0/0/90/90/-45/45/45/-45/45/-45/-45/45]s	0.480718817
	8	[45/-45/-45/45/-45/45/45/-45/90/90/0/0/0/0/90/90/-45/45/45/-45/45/-45/-45/45]s	0.472070819
Loadcase 05	1	[45/-45/-45/45/45/-45/45/90/-45/90/0/0/0/0/90/-45/90/45/-45/45/45/-45/-45/45]s	0.477427874
	1.5	[45/-45/0/45/-45/-45/45/45/90/90/0/-45/-45/0/90/90/45/45/-45/-45/45/0/-45/45]s	0.513646851
	2	[45/-45/0/45/-45/-45/45/-45/45/90/90/0/0/90/90/45/-45/45/-45/-45/45/0/-45/45]s	0.503503664
	3	[45/-45/0/-45/45/-45/45/45/-45/90/90/0/0/90/90/-45/45/45/-45/45/-45/0/-45/45]s	0.527873963
	4	[45/-45/-45/45/45/-45/-45/45/90/90/0/0/0/0/90/90/45/-45/-45/45/45/-45/-45/45]s	0.492874511
	6	[45/-45/-45/45/-45/45/45/-45/90/90/0/0/0/0/90/90/-45/45/45/-45/45/-45/-45/45]s	0.492255732
	8	[45/-45/45/-45/-45/45/45/-45/90/90/0/0/0/0/90/90/-45/45/45/-45/-45/45/-45/45]s	0.495080504

Table D.2: Continued: Best stacking sequences of the standard GA optimisation for the symmetric cases due to combined loading

Case	R/t	Stacking Sequence	Kim & Soni
Loadcase 06	1	[45/-45/45/-45/45/45/-45/-45/90/90/0/0/0/0/90/90/-45/-45/45/45/-45/45/-45/45]	0.485839035
	1.5	[45/-45/0/45/-45/-45/45/90/90/0/45/-45/-45/45/0/90/90/45/-45/-45/45/0/-45/45]	0.505900927
	2	[45/-45/0/45/90/-45/45/90/-45/90/90/0/0/90/90/-45/90/45/-45/90/45/0/-45/45]	0.504076531
	3	[45/-45/0/45/45/-45/45/-45/90/-45/90/0/0/90/-45/90/-45/45/-45/45/45/0/-45/45]	0.501139969
	4	[45/-45/0/-45/45/-45/45/45/-45/90/90/0/0/90/90/-45/45/45/-45/45/-45/0/-45/45]	0.528971748
	6	[45/-45/0/-45/45/45/-45/-45/45/90/90/0/0/90/90/45/-45/-45/45/45/-45/0/-45/45]	0.546029972
	8	[45/-45/0/-45/45/45/-45/-45/45/90/90/0/0/90/90/45/-45/-45/45/45/-45/0/-45/45]	0.537716153
Loadcase 07	1	[45/-45/-45/45/-45/45/-45/45/90/90/0/0/0/0/90/90/45/-45/45/-45/45/-45/-45/45]	0.440589479
	1.5	[45/-45/-45/45/-45/45/45/-45/90/90/0/0/0/0/90/90/-45/45/45/-45/45/-45/-45/45]	0.493843576
	2	[45/-45/0/45/-45/-45/45/-45/45/90/90/0/0/90/90/45/-45/45/-45/-45/45/0/-45/45]	0.556348274
	3	[45/-45/0/45/-45/-45/45/45/-45/90/90/0/0/90/90/-45/45/45/-45/-45/45/0/-45/45]	0.585385545
	4	[45/-45/0/-45/45/45/-45/-45/45/90/90/0/0/90/90/45/-45/-45/45/45/-45/0/-45/45]	0.609692054
	6	[45/-45/0/-45/45/-45/45/45/-45/90/90/0/0/90/90/-45/45/45/-45/45/-45/0/-45/45]	0.644466064
	8	[45/-45/0/-45/45/45/-45/-45/45/90/90/0/0/90/90/45/-45/-45/45/45/-45/0/-45/45]	0.662988625
Loadcase 08	1	[45/-45/90/90/45/90/-45/-45/45/90/0/0/0/0/90/45/-45/-45/90/45/90/90/-45/45]	0.928711422
	1.5	[45/-45/0/90/45/90/-45/45/-45/0/90/90/90/90/0/-45/45/-45/90/45/90/0/-45/45]	0.929654043
	2	[45/-45/0/90/-45/90/45/90/-45/45/0/90/90/0/45/-45/90/45/90/-45/90/0/-45/45]	0.93806261
	3	[45/-45/0/90/-45/90/90/90/45/90/90/0/0/90/90/45/90/90/90/-45/90/0/-45/45]	0.949026712
	4	[45/-45/0/-45/45/45/45/-45/90/-45/90/0/0/90/-45/90/-45/45/45/45/-45/0/-45/45]	0.955920168
	6	[45/-45/0/-45/45/-45/45/45/-45/90/90/0/0/90/90/-45/45/45/-45/45/-45/0/-45/45]	0.95617589
	8	[45/-45/0/-45/45/-45/45/45/-45/90/90/0/0/90/90/-45/45/45/-45/45/-45/0/-45/45]	0.959255407
Loadcase 09	1	[45/-45/90/45/90/-45/45/90/0/-45/0/0/0/0/-45/0/90/45/-45/90/45/90/-45/45]	0.425643498
	1.5	[45/-45/90/90/90/45/90/-45/90/90/0/0/0/0/90/90/-45/90/45/90/90/90/-45/45]	0.426753232
	2	[45/-45/0/90/-45/90/45/45/90/0/-45/0/0/-45/0/90/45/45/90/-45/90/0/-45/45]	0.448237821
	3	[45/-45/0/90/90/45/90/-45/90/90/90/0/0/90/90/90/-45/90/45/90/90/0/-45/45]	0.434110414
	4	[45/-45/0/-45/45/-45/45/90/90/90/0/90/90/0/90/90/90/45/-45/45/-45/0/-45/45]	0.420448734
	6	[45/-45/0/-45/45/-45/45/-45/45/90/90/0/0/90/90/45/-45/45/-45/45/-45/0/-45/45]	0.408570628
	8	[45/-45/0/-45/45/45/-45/-45/45/90/90/0/0/90/90/45/-45/-45/45/45/-45/0/-45/45]	0.411000506
Loadcase 10	1	[45/-45/45/45/-45/45/-45/-45/90/0/0/90/90/0/0/90/-45/-45/45/-45/45/45/-45/45]	0.438000062
	1.5	[45/-45/-45/45/45/-45/-45/45/90/90/0/0/0/0/90/90/45/-45/-45/45/45/-45/-45/45]	0.423054131
	2	[45/-45/45/-45/-45/-45/45/45/90/90/0/0/0/0/90/90/45/45/-45/-45/-45/45/-45/45]	0.437983191
	3	[45/-45/45/-45/-45/-45/45/45/90/90/0/0/0/0/90/90/45/45/-45/-45/-45/45/-45/45]	0.480448208
	4	[45/-45/0/-45/-45/45/45/45/-45/90/90/0/0/90/90/-45/45/45/45/-45/-45/0/-45/45]	0.520098333
	6	[45/-45/45/-45/-45/-45/45/45/90/90/0/0/0/0/90/90/45/45/-45/-45/-45/45/-45/45]	0.498578817
	8	[45/-45/45/-45/-45/45/45/90/90/-45/0/0/0/0/-45/90/90/45/45/-45/-45/45/-45/45]	0.523213626
Loadcase 11	1	[45/-45/0/-45/45/45/-45/-45/45/90/0/90/90/0/90/45/-45/-45/45/45/-45/0/-45/45]	0.289678939
	1.5	[45/-45/0/-45/45/-45/45/-45/45/90/90/0/0/90/90/45/-45/45/-45/45/-45/0/-45/45]	0.317437249
	2	[45/-45/0/-45/45/-45/45/-45/45/90/90/0/0/90/90/45/-45/45/-45/45/-45/0/-45/45]	0.33774024
	3	[45/-45/0/-45/45/-45/45/45/-45/90/90/0/0/90/90/-45/45/45/-45/45/-45/0/-45/45]	0.374852155
	4	[45/-45/0/-45/45/-45/45/45/-45/90/90/0/0/90/90/-45/45/45/-45/45/-45/0/-45/45]	0.396113014
	6	[45/-45/0/-45/45/-45/45/45/-45/90/90/0/0/90/90/-45/45/45/-45/45/-45/0/-45/45]	0.419786811
	8	[45/-45/0/-45/45/-45/45/45/-45/90/90/0/0/90/90/-45/45/45/-45/45/-45/0/-45/45]	0.431218902

Bibliography

[1] J.C. Brewer and P.A. Lagace. Quadratic stress criterion for initiation of delamination. *Journal of Composite Materials*, 22:1141–1155, 1988.

[2] M. Ferdik. Layup optimization for strongly curved laminated shells. Master's thesis, Leopold-Franzens-Universität Innsbruck, 2014.

[3] D.E. Goldberg and R. Lingle. Alleles, loci and the traveling salesman problem. *Preceedings of an International Conference on Genetic Algorithms and their applications*, pages 154–159, 1985.

[4] *Advanced Composites Design Guide*. Grumman Corporation, January 1986.

[5] C. Kassapoglou. *Design and Analysis of Composite Structures*. John Wiley & Sons, Ltd, 2010.

[6] W.L. Ko and R.H. Jackson. Multilayer theory for delamination analysis of a composite curved bar subjected to end forces and end moments. Technical report, NASA, 1989.

[7] R.M. Koide, G. von Zeska de Franca, and M.A. Luersen. An ant colony algoritm applied to lay-up optimization of laminated composite plates. *Latin American Journal of Solids and Structures*, 10:491–504, 2013.

[8] S.G. Lekhnitskii. *Anisotropic Plates*. Gordon and Breach Science Publishers, 1968.

[9] A.E.H. Love. On the small free vibrations and ddeformation of elastic shells. *Philosphical trans. of the Royal Society (London)*, Vol. serie A(N° 17):491–549, 1888.

[10] S. McRobbie, A.J. Longuir, J.Wilcox, A.G. Gibson, and Chandler H.W. Through-thickness stress in curved laminates of single- and double-skinned construction. *Composites*, 26:339–45, 1995.

[11] R.D. Mindlin. Infshells of rotatory inertia and shear on flexural motions of isotropic, elastic plates. *ASME Journal of Applied Mechanics*, 18:31–38, 1951.

[12] A. Rama Mohan Rao and N. Arvind. Optimal stacking sequence design of laminate composite structures using tabu embedded simulated annealing. *Structeral Engineering and Mechanics*, 25(2):239–268, 2007.

[13] E. Reissner. The effect of transverse shear deformation on the bending of elastic plates. *ASME Journal of Applied Mechanics*, 12:A68–77, 1945.

[14] R. Roos, G. Kress, M. Barbezat, and P. Ermanni. Enhanced model for interlaminar normal stress in singly curved laminates. *Composite Structures*, 80:327–33, 2007.

[15] RA Shenoi and W. Wang. Through-thickness stresses in curved composite laminates and sandwich beams. *Composite Science and Technology*, 61:1501–12, 2001.